

**ENHANCING AERODYNAMIC PERFORMANCE ESTIMATION IN
SMALL AIRCRAFT DEVELOPMENT USING
OBJECT-ORIENTED TECHNIQUE**

KNUST

by

YESUENYEAGBE ATSU KWABLA FIAGBE

A thesis submitted to the Department of Mechanical Engineering,
Kwame Nkrumah University of Science and Technology, Kumasi in partial
fulfillment of the requirements for the Degree of

DOCTOR OF PHILOSOPHY

Faculty of Mechanical and Agricultural Engineering

College of Engineering

April 2010

ABSTRACT

Air transportation is expected to play a major role in global transportation systems in the future. A third world country like Ghana needs to prepare to leapfrog into the era of small aircraft in air transportation. As such, small aircraft design has to be approached in such a way as to derive optimum performance for any configuration that may be developed for given mission. Estimation of the aerodynamic forces developed by aircraft configuration forms a significant and challenging part of the design process. In practice, the aerodynamic performance is estimated from the coefficients obtained from the chosen wing profile. However, it can be envisioned that every section of the configuration could contribute to the aerodynamic forces. The goal of this work is to develop a technique or method that takes into account the contribution of all sections of the configuration with the aim of improving the accuracy of the evaluation of the aircraft performance.

The concept of the research is built on object oriented technique such that an object is defined as a function that accepts an input and results in an output. The input parameters comprise of two components, namely, fixed and design parameters. The output gives the geometry and performance characteristics of the aircraft. The performance is modelled as integral function over the surface and results in determination of Lift and Drag forces. The design parameters are used in creating the geometry such that with given set of parameters, unique and specific class of aircraft would be developed. The developed system and tools were validated and found to be satisfactory.

The lift performance of models with same wing profile indicated that fuselage components also contributed toward the overall lift force. The total lift and drag estimates of an aircraft using the developed system is more accurate than using estimates from the wing alone.

Further, results of the research show that for design of small aircraft, drag performance is optimum at angle of attack between 2° and 4° . Also, performance study shows that luggage cabin object significantly influences the drag performance such that, shorter portions perform better. It is recommended that the influence of the luggage cabin as observed be validated experimentally.

DEDICATION

This dissertation is dedicated to the Glory of
God and to the memory of my late parents
Rev. & Mrs. Andreas Kwaku Fiagbe

KNUST



ACKNOWLEDGEMENT

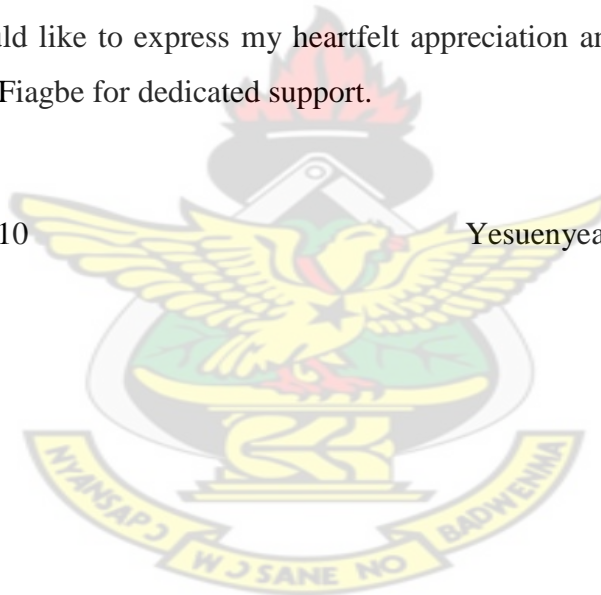
I am very grateful to God for His love and mercy and for the wisdom, direction and protection for me in completing this research successfully. I would like to express my sincere gratitude and indebtedness to my sponsors: North Carolina A&T State University (NCAT), KNUST and German Academic Exchange Service (DAAD) for their support.

I am very grateful to Dr. L.E. Ansong for his supervisory role and support. My sincere gratitude to Prof. F. Ferguson of Department of Mechanical Engineering, NCAT, USA for his encouragement and advice during the course of the research. I wish to thank Prof. S. Owusu-Ofori for his contribution in various ways toward the success of the work. My thanks go to the staff of the Department of Mechanical Engineering, KNUST for their contribution and support in various ways.

Finally, I would like to express my heartfelt appreciation and love to my wife Mrs. Edith Esinam Fiagbe for dedicated support.

April 2010

Yesueneagbe A.K. FIAGBE



LIST OF CONTENTS

ABSTRACT	iii
DEDICATION	iv
ACKNOWLEDGEMENT	v
LIST OF CONTENTS	vi
LIST OF FIGURES	ix
LIST OF TABLES	xiii
NOMENCLATURE	xiv
ABBREVIATIONS	xvi
CHAPTER ONE: OVERVIEW OF RESEARCH	
1.0 INTRODUCTION	1
1.1 BACKGROUND OF STUDY	1
1.2 STATEMENT OF PROBLEM	2
1.3 RESEARCH GOAL AND OBJECTIVES	4
1.4 RESEARCH METHODOLOGY	4
1.5 SIGNIFICANCE OF THE RESEARCH	5
1.6 STRUCTURE OF THE THESIS	6
CHAPTER TWO: REVIEW OF AIRCRAFT DESIGN AND PERFORMANCE	
2.0 INTRODUCTION	7
2.1 AIRCRAFT DESIGN PROCESS	7
2.2 AIRCRAFT ESSENTIAL PARTS	11
2.2.1 Important Geometric Parameters of a Wing	12
2.3 AERODYNAMIC FORCES	13
2.3.1 The Lift	13

2.3.2	The Drag	14
2.4	OTHER FORCES ACTING ON AN AIRCRAFT	18
2.4.1	Thrust	18
2.4.2	The Weight	20
2.5	AIRCRAFT PERFORMANCE	20
2.6	AIRCRAFT GEOMETRY DEVELOPMENT	22
2.7	OBJECT ORIENTED PROGRAMMING	23
CHAPTER THREE: GOVERNING AND RELATED EQUATIONS FOR AERODYNAMIC ANALYSIS		
3.0	INTRODUCTION	25
3.1	POSSIBLE SOLUTION/ANALYSIS METHODS	25
3.2	NAVIER-STOKES EQUATION	25
3.3	EULER AND BOUNDARY LAYER EQUATIONS	27
3.3.1	Inviscid Flow Portion	28
3.3.2	Pressure Distribution and Pressure Coefficient	31
3.3.3	Boundary Layer Portion	32
3.3.4	Shear Stress	34
3.3.5	Blasius Solution of the Boundary layer equations on a flat plate	35
3.4	AERODYNAMIC FORCE ANALYSIS	36
3.4.1	The Mean Value Theorem	37
3.4.2	Projected and Wetted Areas	38
3.4.3	Lift, Drag, and Side Forces	40
3.5	SOLUTION TO THE POTENTIAL FLOW EQUATION	40
3.5.1	Grid Transformation	41
3.5.2	Governing Equation	42

CHAPTER FOUR: DESIGN CONCEPT AND DEVELOPMENT

4.0	INTRODUCTION	46
4.1	AIRCRAFT DESIGN CONCEPT	46
4.2	AIRCRAFT GEOMETRY DESIGN AND DEVELOPMENT	47
4.2.1	Mapping Aircraft Reality into Object-Oriented Programming Environment	48
4.2.2	Design Parameters	55
4.2.2	Sample Aircraft Geometry	60
4.3	AERODYNAMICS ANALYSIS	62
4.3.1	Numerical Wind Tunnel Development	62
4.3.2	Flow Field Generation	63
4.3.3	Numerical Wing Tunnel Code Validation	67
4.4	THE PRESSURE DISTRIBUTION	71
4.5	THE SHEAR STRESS	72
4.6	SURFACE/WETTED AND PROJECTED AREAS	74
4.7	AERODYNAMIC FORCE ESTIMATION	81
CHAPTER FIVE: PERFORMANCE ANALYSIS AND RESULTS		
5.0	INTRODUCTION	82
5.1	AERODYNAMIC PERFORMANCE	82
5.2	SAMPLE RESULTS WITH ANGLE OF ATTACK VARIATION	82
5.3	DESIGN PARAMETRIC STUDY	95
5.3.1	Luggage Cabin Influence	98
CHAPTER SIX: CONCLUSION AND RECOMMENDATION		
6.1	CONCLUSION	101
6.2	RECOMMENDATION	103
REFERENCES		104
APPENDICES		107

LIST OF FIGURES

Figure 2.1 Basic Airplane Components	11
Figure 2.2 Airfoil Shape	12
Figure 2.3 Illustration of Aerodynamic Forces on airfoil	15
Figure 2.4 Pressure distribution over an airfoil	15
Figure 2.5 Illustration of boundary layer structure and growth over flat plate	16
Figure 2.6 Power Plant	19
Figure 2.7 Bernoulli Theory	19
Figure 2.8 Newton's Theory	20
Figure 2.9 Illustration of Performance Parameters	21
Figure 3.1 Illustration of Inviscid and boundary layer portions of flow	28
Figure 3.2 Illustration of Projected surface Areas	37
Figure 3.3 Sample Triangular Element	39
Figure 3.4 Illustration of the Physical plane	44
Figure 3.5 Illustration of the Computational Plane	44
Figure 3.6 Physical plane of Generated Grid system	45
Figure 4.1 Illustration of Research Concept	47
Figure 4.2 Decomposed aircraft into Components	49
Figure 4.3 Schematic illustration of aircraft Components	49
Figure 4.4 General System Design Flowchart	51
Figure 4.5 Fuselage Component Design Flowchart	52
Figure 4.6 Wing Component Design Flowchart	54
Figure 4.7 Empennage Component Design Flowchart	55
Figure 4.8 Schematic Drawing of the Nose	56
Figure 4.9 Schematic Drawing of the Nose-Cabin Intercept	56

Figure 4.10 Schematic Drawing of the Cabin	57
Figure 4.11 Schematic Drawing of the Luggage Cabin	57
Figure 4.12 Schematic Drawing of the Tail boom	57
Figure 4.13 Schematic Drawing of the Wing or Horizontal Tail	58
Figure 4.14 Schematic Drawing of the Vertical Tail	58
Figure 4.15 Aircraft Geometry Sample #1	61
Figure 4.16 Aircraft Geometry Sample #2	61
Figure 4.17 Aircraft Geometry Sample #3	61
Figure 4.18 Aircraft Geometry Sample #4	61
Figure 4.19 Aircraft Geometry Sample #5	61
Figure 4.20 Aircraft Geometry Sample #6	61
Figure 4.21 Sample generated physical Plane with Grid	64
Figure 4.22 Stream line plot for wing section (NACA 2412) at AoA = 0.0	65
Figure 4.23 Stream line plot for wing section (NACA 2412) at AoA = 3.0	65
Figure 4.24 Stream line plot for Fuselage section at AoA = 0.0	66
Figure 4.25 Stream line plot for Fuselage section at AoA = 3.0	66
Figure 4.26 NACA 0010 at AoA = 0.0 Compared with Reference data	68
Figure 4.27 NACA 0012 at AoA = 0.0 Compared with Reference data	68
Figure 4.28 NACA 0024 at AoA = 0.0 Compared with Reference data	69
Figure 4.29 Typical velocity distribution over NACA 2412 at AoA = 0.0	69
Figure 4.30 Typical velocity distribution over NACA 2412 at AoA = 3.0	70
Figure 4.31 Typical velocity distribution over fuselage profile at AoA = 0.0	70
Figure 4.32 Typical velocity distribution over fuselage profile at AoA = 3.0	71
Figure 4.33 Illustration of elemental surface area	75
Figure 5.1 Lift Performance with different wing profiles	85
Figure 5.2 Drag Performance with different wing profiles	85

Figure 5.3 Lift Performance with the same wing profile	. . .	87
Figure 5.4 Drag Performance with the same wing profile	. . .	87
Figure 5.5 Object Lift Performance for Sample #1	. . .	88
Figure 5.6 Object Drag Performance for Sample #1	. . .	89
Figure 5.7 Sample #1 Configuration	. . .	89
Figure 5.8 Object Lift Performance for Sample #2	. . .	90
Figure 5.9 Object Drag Performance for Sample #2	. . .	90
Figure 5.10 Sample #2 Configuration	. . .	91
Figure 5.11 Sample #3 Configuration	. . .	91
Figure 5.12 Sample #4 Configuration	. . .	91
Figure 5.13 Sample #5 Configuration	. . .	92
Figure 5.14 Object Lift Performance for Sample #6	. . .	92
Figure 5.15 Object Drag Performance for Sample #6	. . .	92
Figure 5.16 Sample #6 Configuration	. . .	93
Figure 5.17 Object Lift Performance for Sample #7	. . .	93
Figure 5.18 Object Drag Performance for Sample #7	. . .	93
Figure 5.19 Sample #7 Configuration	. . .	94
Figure 5.20 Sample #8 Configuration	. . .	94
Figure 5.21 Sample #9 Configuration	. . .	94
Figure 5.22 Sample #10 Configuration	. . .	95
Figure 5.23 Lift Performance for Nose-Cabin Offset height variation	. . .	96
Figure 5.24 Drag Performance for Nose-Cabin Offset height variation	. . .	96
Figure 5.25 Fuselage profile indicating the variation of Cabin height	. . .	96
Figure 5.26 Lift Performance for Luggage-cabin end diameter variation	. . .	97
Figure 5.27 Drag Performance for Luggage-cabin end diameter variation	. . .	97
Figure 5.28 Fuselage profile indicating the variation of Luggage Cabin diameter	. . .	98

Figure 5.29 Drag Performance for Luggage-cabin length variation	99
Figure 5.30 Luggage-cabin length variation	100

KNUST



LIST OF TABLES

Table 4.1 Fixed and Design Variables	59
Table 4.2 Sample Design parameters for illustration in figures 4.16 to 4.21	60
Table 4.3 Validation of surface Integration Routine (Quarter Cylinder)	77
Table 4.4 Validation of surface Integration Routine (Quarter Truncated Cone)	78
Table 4.5 Validation of surface Integration Routine (Quarter Cone)	79
Table 4.6 Validation of surface Integration Routine (Semi Cylinder)	80
Table 5.1 Sample Design Parameters for samples #1 - #5	84
Table 5.2 Sample Design Parameters for samples #6 - #10	86



NOMENCLATURE

x, y, z	-	Cartesian coordinate
u, v, w	-	velocity components in x, y, z directions respectively
V	-	velocity of moving fluid
ρ	-	fluid density
t	-	time
p, P	-	pressure
\mathbf{f}, f	-	body force per unit mass
e	-	internal energy per unit mass
q	-	volumetric rate of heat addition per unit mass (J/s.kg)
Q_{viscous}	-	rate of heat addition due to viscous effect
W_{viscous}	-	rate of work done due to viscous effect
F	-	surface force due to viscous stresses
ψ	-	Stream function
C_p	-	pressure coefficient
C_L	-	global lift coefficient
C_D	-	global drag coefficient
C_l	-	local lift coefficient
C_d	-	local drag coefficient
C_f	-	friction coefficient
μ	-	dynamic viscosity
τ	-	shear stress
Re	-	Reynolds number
S	-	surface area

L - Lift force

D - Drag force

J - Jacobian

Subscript ∞ - free stream property

KNUST



ABBREVIATIONS

NACA	-	National Advisory Committee for Aeronautics
NASA	-	National Aeronautics and Space Administration
NCAM	-	National Consortium for Aviation Mobility
SATS	-	Small Air Transportation Systems
MOGA	-	Multi-Objective Genetic Algorithm
MOD	-	Multidisciplinary Optimization
VLJ	-	Very Light Jet
UAV	-	Unmanned Aerial Vehicles
OOP	-	Object-Oriented Programming
COTS	-	Commercial Off-The-Self
AOA	-	Angle of Attack
CAD	-	Computer Aided Design
RAGE	-	Rapid Geometric Engine
CFD	-	Computational Fluid Dynamics
PDE	-	Partial Differential Equation

CHAPTER ONE

OVERVIEW OF RESEARCH

1.0 INTRODUCTION

This chapter is the introduction to the thesis and contains the background of the research, statement of the problem, research methodology, objectives, and structure of the thesis.

1.1 BACKGROUND OF STUDY

Since the successful flight of aircraft by the Wright brothers, air transportation has seen tremendous revolution and has become very important means of transportation. In order to further promote air transportation, Small Air Transportation Systems (SATS) project was conducted by National Aeronautics and Space Administration (NASA) and partners in the National Consortium for Aviation Mobility (NCAM) to ascertain viability of developing small aircrafts. SATS proved the viability and technical capabilities in the following four areas: 1. High-volume operations at airports without control towers or terminal radar facilities, 2. Technologies enabling safe landings at more airports in almost all weather conditions, 3. Integration of SATS aircrafts into a higher capacity air traffic control system, with complex flows and slower aircraft and 4. Improved single-pilot ability to function competently in evolving, complex national airspace.

In third-world countries, a tremendous leapfrog in the air transportation can be anticipated in the near future. Encouraging design and production of small aircrafts

will go a long way to promote air transportation in Ghana. Small aircrafts may be in the form of personal, remote or radio controlled aircrafts. These usually operate at low speed and are used for different kinds of activities. Air vehicle design requires a multidisciplinary perspective and involves knowledge in a wide range of subjects such as aerodynamics, engineering structures, propulsion, control systems, and materials. The process of aircraft design according to Raymer (1995), can be structured into three major phases. These are conceptual design, preliminary design, and detailed design phases. Each phase has a different set of goals and objectives. The design process associated with each phase is quite different from the other phases. In the conceptual design phase, configuration, size, weight, and performance parameters are determined. According to Stinton, (1998), the configuration or shape is influenced by the aerodynamics, propulsion and structural design.

The aerodynamic performance of the aircraft is estimated from the lift and drag coefficients obtained as a result of the selected airfoil of the wing geometry. These coefficients are used together with other derived coefficients in the estimation of the lift and drag developed by the aircraft.

1.2 STATEMENT OF PROBLEM

Development of a flight vehicle configuration is a complex and time consuming process. Estimation of the aerodynamic forces developed by the configuration forms a significant and challenging part of the design process. Over the years, a number of researchers have developed systems to aid the design process and to better predict the aerodynamic forces. The lift, aerodynamic force normal to the direction of free-stream flow, is typically estimated from parameters associated with pre-determined

wing geometry. This is because the wing is considered to be the main contributor to lift. Thus the aerodynamic performance of the aircraft is estimated from the lift and drag coefficients obtained due to the selected airfoil of the wing geometry. In practice, the aerodynamic performance is estimated from the coefficients obtained as a result of the chosen wing profile. However, it can be envisioned that every section of the configuration could contribute to the aerodynamic forces. The goal of this work is to develop a technique or method that takes into account the contribution of all sections of the configuration with the aim of improving the accuracy of the evaluation of the aircraft performance.

Labrujere and Slooff (1993) used the inverse design approach for the aerodynamic design of the aircraft. The approach was mainly for the wing design and employed computational methods. Turevskiy et al, (1999) used a combination of free and commercial off-the-shelf (COTS) modelling and simulation software to simplify and improve the flight vehicle design process. Raymer (2002), in his doctoral thesis, used Multidisciplinary Optimization (MDO) technique to enhance the conceptual design process of the aircraft design. He employed various techniques such as orthogonal steepest descent (full factorial stepping search), Monte Carlo and mutation-based evolutionary option to develop a design code. Neufeld et al (2007) developed Multi-Objective Genetic Algorithm (MOGA) optimizer to assist in the design process for very light jet (VLJ) and an Unmanned Aerial Vehicles (UAVs). In all these cases, the aerodynamic analysis was based on the wing geometry and coefficients to determine the lift and drag. The total lift was projected from the wing geometry.

In practice, during the design process, the aerodynamic performance is projected from the coefficients obtained as a result of the chosen wing profile. Every section or part of the configuration, however, contributes to the aerodynamic forces. As such a

technique or method that considers the contribution from all surfaces of the configuration would improve the accuracy and the evaluation of the performance.

1.3 RESEARCH GOAL AND OBJECTIVES

The goal of the research is to develop subsonic aircraft configurations with optimal performance capability for a given mission using object-oriented technique and to improve the estimation of the aerodynamic performance parameters by considering the contribution of all surfaces.

The goal will be achieved through the following objectives:

1. Develop subsonic aircraft design concept.
2. Identify and exploit engineering design parameters to construct aircraft configurations with optimal capability.
3. Develop an object oriented program/code to implements aircraft design concept.
4. Develop aerodynamic analysis tools to evaluate integrated aircraft configurations.
5. Validate aircraft subsystems and tools.

1.4 RESEARCH METHODOLOGY

The research has been undertaken by an initial review and development of design scheme. The aircraft configuration was decomposed into components referred to as objects. Development of the design parameters was carried out to completely describe the aircraft geometry. These parameters were expected to independently

describe various objects. For the purpose of aerodynamic analysis, numerical wind tunnel has been developed based on 2D incompressible approximation to system of Navier-Stokes equations for fluid flow. Aerodynamic analysis was conducted in the numerical wind tunnel. The result of the numerical wind tunnel tests was used in estimating the aerodynamic performance of the aircraft. Finally, parametric studies are conducted on the defined objects using the design parameters.

1.5 SIGNIFICANCE OF THE RESEARCH

Creating a new or modifying an existing flight vehicle is a complex and time consuming process and estimation of the aerodynamic forces developed by the configuration is a significant challenge. Over the years, the lift estimation of an aircraft has been a projection from the wing as it is the main contributor. However, aerodynamic forces, which result in Lift and Drag, are developed by every surface of the flight vehicle. It is therefore, prudent to determine the contribution of every part of the aircraft configuration toward lift and drag.

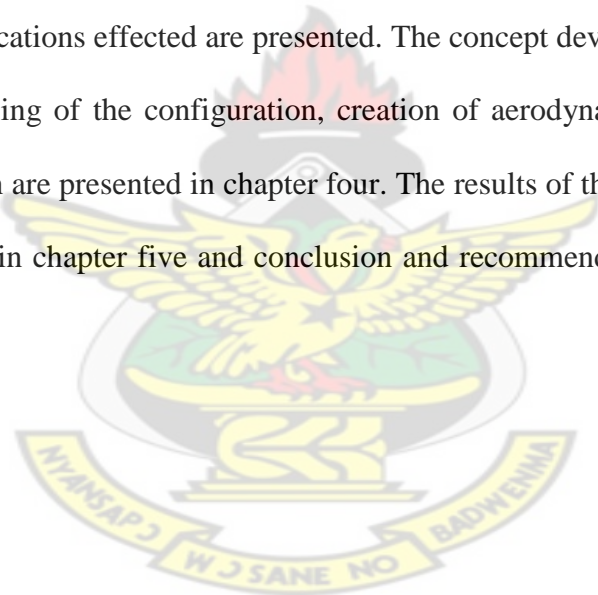
The estimation of the aerodynamic performance in the design of the aircraft is very significant process and good estimate is essential and contribute a lot in the overall weight limit and selection of power plant. This research seeks to employ object-oriented technique in the development of aircraft configuration and determine performance of each object of the configuration leading to the overall aerodynamic performance.

The results of the research are expected to lead to more accurate performance estimation which will help in choosing an optimum power plant and better design for

maximum payload. Also, the research result can enhance the design and production of small aircrafts and promote air transportation in future.

1.6 STRUCTURE OF THE THESIS

The thesis consists of an abstract and six chapters. Chapter one is the introductory part and contains statement of the problem, research methodology, and objectives. Literature review of aircraft design and means of performance estimation are presented in chapter two. Chapter three provides the governing equations of fluid flow relevant to the research. It also discusses how and why these relations are used and the modifications effected are presented. The concept development of the aircraft design, modelling of the configuration, creation of aerodynamic analysis tools and their validation are presented in chapter four. The results of the research are analyzed and presented in chapter five and conclusion and recommendations are presented in chapter six.



CHAPTER TWO

REVIEW OF AIRCRAFT DESIGN AND PERFORMANCE

2.0 INTRODUCTION

This chapter provides review of aircraft design process and description of the major essential components of aircrafts which will form the basis of the object oriented programming to be used in the total evaluation of aircraft performance. Definition of aerodynamic forces and explanation of other forces that act on the aircraft are provided. Information on development or generation of the configuration of aircraft is provided.

2.1 AIRCRAFT DESIGN PROCESS

Aircraft development started significantly after the Wright brothers' successful first controlled, sustained, powered, heavier than air and manned flight in 1903 in North Carolina, United States of America. Aircraft is a complex system and multidisciplinary in design. The main disciplines involved in aircraft design are Aerodynamics, Structural Mechanics, Propulsion, System Controls, and Materials Engineering. These disciplines work together to create the ultimate design of an aircraft.

The aircraft design process is structured into three phases, namely: conceptual design; preliminary design; and detail design phases, (Raymer, 1995). Each of these design phases has different tasks and objectives and, also, the design process within each phase is quite unique from other phases. The Conceptual Design phase is the

first phase. During this phase some basic questions of configuration, size, weight, power required and performance are answered. At the Preliminary Design phase, specialists in areas such as structural mechanics, landing gear, and control systems, design and analyze aircraft portions of interest. Detail Design phase is the last stage when actual pieces to be fabricated are designed.

In the conceptual design phase, the design requirements are used to guide and evaluate the development of the overall aircraft configuration. The level of detail in the configuration design is not very deep, but the interactions among all different components are so crucial that it may require years of experience to create a good conceptual design. The question that arises is, can this process be shortened? Outcome of this work shows that using the object oriented approach suggested later, the conceptual design stage process can be enhanced. During the conceptual design phase, a number of alternative designs are studied to determine which design approach is preferred.

The preliminary design phase is said to begin when the major configurations have been established. During the preliminary design minor changes in the configuration may result as specialists of various disciplines are involved. The end of preliminary design usually involves a full-scale development proposal.

Detailed design phase begins with the assumption that favourable decision for entering full-scale development is reached. This phase involves the design of actual pieces to be fabricated. This phase is the most expensive part of the aircraft design process and is characterized by a large number of designers preparing detailed drawings or CAD files with specifications of actual fabrication geometry and dimensions.

The aerodynamic design which is one of the first steps during the conceptual design phase is one of the crucial processes to ensure overall good aircraft performance. This research considers a further development of the method of estimating aerodynamics performance by including contributions of aerodynamic forces from all surfaces of the aircraft.

According to Stinton, (1998) an aircraft may be considered as having three separate contributory factors in determining its final configuration or shape, which are: aerodynamic; propulsion and structure. This implies that the final configuration of an aircraft will be obtained only after satisfying aerodynamic performance requirements, structural soundness and provision of adequate power. However, Stinton's stipulation omitted the role of the mission in the determination of the shape or configuration.

During the conceptual design phase, estimation of the aerodynamic forces developed by the configuration is a significant and challenging part of the process. Over the years, a number of researchers have developed systems to aid the process and to better predict the aerodynamic forces. A number of researchers tried to develop systems to enhance either conceptual design phase or some process of the aircraft design. In almost all cases, the estimation of the aerodynamic forces, lift and drag, is based only on the wing geometry and other coefficients.

The aerodynamic design of aircraft that mostly results in the streamline shape has posed challenges to designers and developers. Some researchers like Labrujere, and Slooff (1993) use the inverse design approach for the aerodynamic design of the aircraft. Computational methods were employed for the wing design. Raymer (2002) in his doctoral thesis used Multidisciplinary Optimization (MDO) technique to

enhance the conceptual design process of the aircraft. He employed various techniques such as orthogonal steepest descent (full factorial stepping search), Monte Carlo, a mutation-based evolutionary options with his design code called RDS. Neufeld, D. et al (2007) developed Multi-Objective Genetic Algorithm (MOGA) optimizer to assist in the design process and it is limited to very light jet (VLJ) and an Unmanned Aerial Vehicle (UAV). The total lift was projected from the wing geometry.

In another thinking, Turevskiy et al, (1999) used a combination of free and commercial off-the-shelf (COTS) modeling and simulation software to simplify and accelerate flight vehicle design process. Determination of the geometry of the aircraft was not clearly spelt out and they concentrated on the controls by using Digital Datcom. The aerodynamic coefficient and parameters were obtained from output file of Digital Datcom. In all these cases, the aerodynamic analysis is based on the wing geometry and coefficients to determine the projected lift and drag. Trevor S. Ferguson, (2007) in his master thesis used Microsoft Excel spreadsheet to create a numerical RC design tool. Ferguson's work actually serves as a motivation to this dissertation.

The lift, aerodynamic force normal to the direction of free-stream flow, is estimated by the use of equation 2.1 (presented later) with the lift and drag coefficients obtained from catalogue. Since the wing of an aircraft is considered to be main provider of lift, researchers have catalogued performance coefficients of wing profiles that are made available to designers and developers. The lift and drag estimation with the projection from the coefficients that are based on the airfoil profile selected for the wing geometry are less accurate since they directly ignore the contribution from all surfaces and rather use the derived coefficients to account for

the contribution from some of the surfaces. This research will consider the contribution of all surfaces in estimating the aerodynamic performance parameters such as lift and drag; this will provide more accurate estimation.

2.2 AIRCRAFT ESSENTIAL PARTS

In general, every aircraft can be identified with some essential or major components. Figure 2.1 illustrates some of these major components. Every aircraft requires a power plant component for the production of thrust to sustain flight. For instance, the space shuttle uses rockets as the power plant, fighter jets use turbines, and most small aircrafts use either an internal combustion engine or an electric motor that rotates a propeller. The second, and arguably the most important component, is the wing. This is the main component of the airplane that produces the lift force. The landing gear, empennage, and fuselage make up one body. This body acts as the third component and is largely responsible for the production of the drag force.

Due to the large contribution of the wing to the performance of the aircraft, there is the need to highlight the important parameters associated with it. They will find application later in this work.

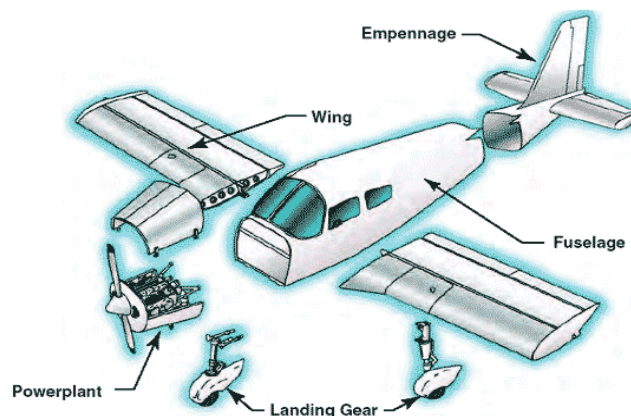


Figure 2.1: Basic Airplane Component.

2.2.1 Important Geometric Parameters of a Wing

The surfaces that support the aircraft by means of the dynamic reaction of the ambient air are called wings. An aircraft may have several wings which may be either fixed with respect to the fuselage or have any of several motions as in the case of helicopters or ornithopters.

A cross section of the wing takes the shape of an airfoil (Figure 2.2) and has a number of characteristic parameters associated with it. These are: 1. *mean camber line* – a line drawn midway between the upper and lower surfaces. 2. The *chord line* – a straight line connecting the leading and trailing edges of the airfoil, at the ends of the mean camber line. 3. The *chord* – the length of the chord line and is the characteristic dimension of the airfoil section. 4. The *maximum thickness* and the *location of maximum thickness* are expressed as a percentage of the chord. For symmetrical airfoils both *mean camber line* and *chord line* pass through centre of gravity of the airfoil and they touch at leading and trailing edge of the airfoil. 5. The *aerodynamic center* is the chord wise length about which the pitching moment is independent of the lift coefficient and the angle of attack. And 6. The *center of pressure* is the chord wise location about which the pitching moment is zero.

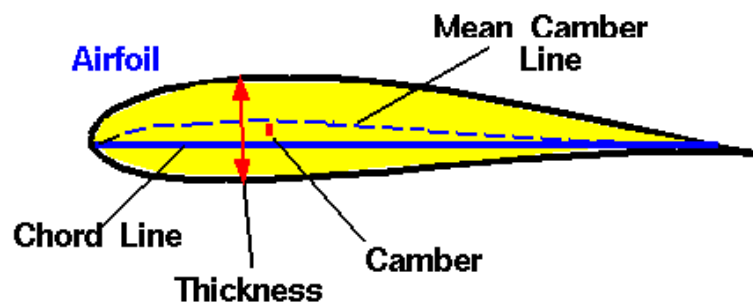


Figure 2.2: Airfoil Shape.

2.3 AERODYNAMIC FORCES

Aerodynamic forces are forces developed as a result of the interaction between the object and the surrounding air. The aerodynamic forces arise from two basic sources: 1) Pressure distribution over the body surface and 2) Shear stress distribution over the body surface (Anderson, 2005). The net effect of the pressure and shear stress distributions integrated over the complete body surface gives the resultant aerodynamic force and moment on the body. The resultant force, in Cartesian coordinate system can be split into components as lift, drag and 'side force'. Due to the symmetric nature of aircraft, the side force usually cancels out and does not play significant role in the performance of the aircraft.

2.3.1 The Lift

The lift is aerodynamic force component acting perpendicular to free airstream direction. The molecules of a fluid are free to move about the surfaces of an object with a relative velocity. Because of the physical properties of air, mainly its viscous characteristic, air moves slower when closer to the surface of the object, and forms a boundary layer. The generation of lift can be explained from the point of view of rate of change of momentum. As the fluid comes into contact with an airfoil surface, there is momentum change leading to change in velocity in such a way that at a given angle of attack, there is lower flow below the airfoil compared to the upper side. This variance in velocity causes a pressure difference over the surface of the object. The pressure differential between the upper and lower surfaces of the wing, results in the lift force that supports the aircraft. This is accomplished by the wing's angle of attack and/or wing camber.

It is important to note, that with an interaction of two solid bodies there is a single point of contact by which force is transmitted. Adversely, when a solid body interacts with a fluid, contact is at every point on the surface of the body. During the interaction of a solid body and fluid, the transmitted force is a pressure force that acts normal to the surface of the object. This pressure force changes in direction and magnitude at different points on the object surface. To determine the net force acting on the entire body, the pressure forces from each point of contact are summed. The resultant force that occurs is the aerodynamic force. This net resultant force can be resolved into two components, the component perpendicular to the object surface which is the lift force, and the component parallel to the body which is the drag force. Figure 2.4 provides a visual model for the net resultant force and the two resolved components.

2.3.2 The Drag

The drag is aerodynamic force component in free airstream direction. The drag form mostly used is the profile drag which comprises two components: surface friction drag and normal pressure drag (form drag). The drag force that represents the streamwise component of the pressure force integrated over the entire configuration is known as Pressure or Form drag. The drag force that is obtained by integrating the streamwise component of the shear force over the vehicle is termed skin friction drag. The drag is generated by every part of the airplane. The total aerodynamic force on an aircraft is determined by resolving the aerodynamic force into two components. The component parallel to the object body is the drag force (Figure 2.3).

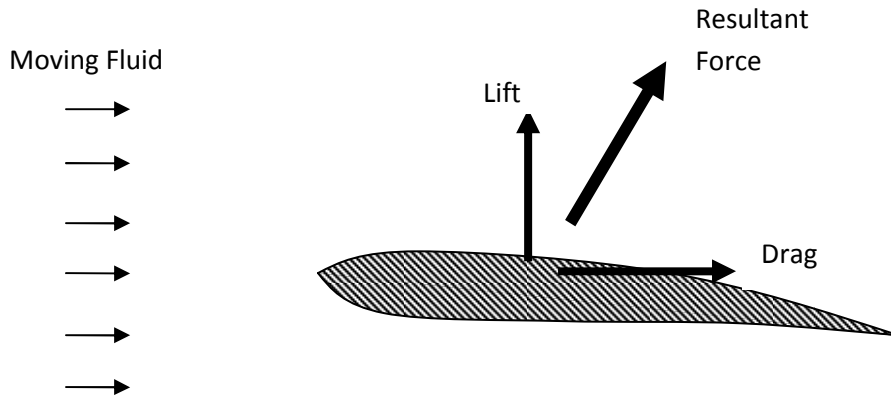


Figure 2.3 Illustration of Aerodynamic Forces on airfoil.

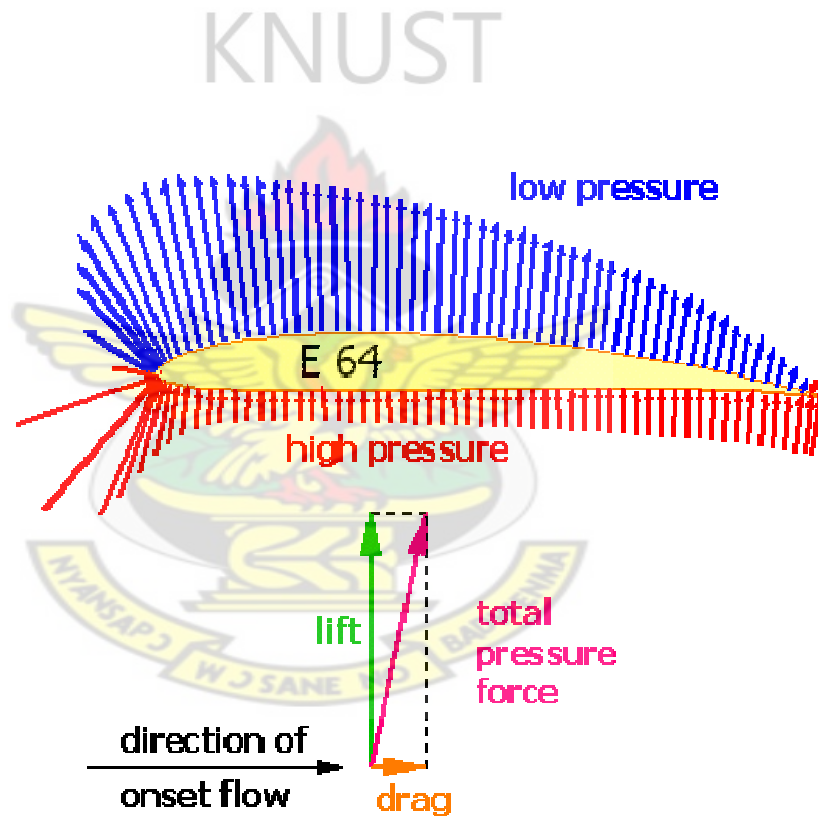


Figure 2.4 Pressure distributions over an airfoil.

Surface Friction Drag: The Surface Friction Drag arises from the tangential stresses due to the viscosity or "stickiness" of the air. When air flows over any part of an aircraft there exists, immediately adjacent to the surface, a thin layer of air called the

boundary layer, within which the air slows from its high velocity at the edge of the layer to zero at the surface itself. Surface friction drag depends upon the rate of change of velocity through the boundary layer, i.e. the velocity gradient. There are two types of boundary layers, laminar and turbulent illustrated in Figure 2.5. Although all aircraft surfaces develop a laminar boundary layer to start with, this rapidly becomes turbulent within a few per cent of the length of the surface. This leaves most of the aircraft immersed in a turbulent boundary layer, the thickness of which increases with length along the surface.

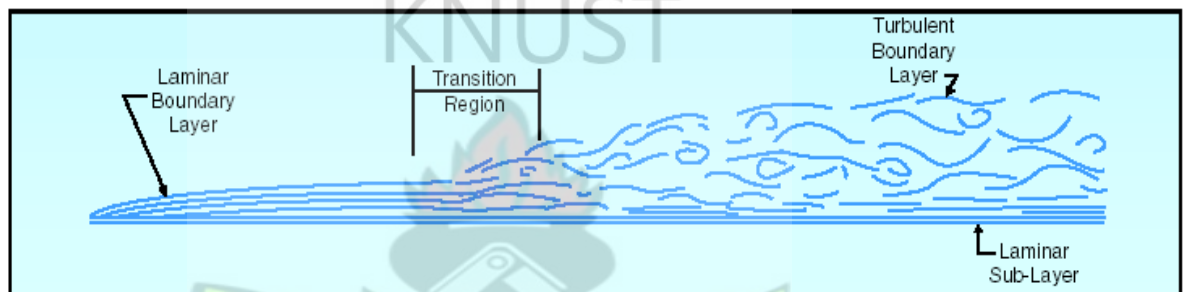


Figure 2.5 Illustration of boundary layer structure and growth over flat plates.

Normal Pressure Drag (form drag): The Normal Pressure Drag also depends upon the viscosity of the air and is related to flow separation. It is best explained by considering a typical pressure distribution over a wing section, as shown in Figure 2.4. At low angle of attack the high pressures near the leading edge produce a component of force in the rearward (i.e. drag) direction, while the low pressures ahead of the maximum thickness point tend to suck the wing section forward, giving a thrust effect. The low pressures aft of the maximum thickness point tend to suck the wing rearwards, since they act on rearward-facing surfaces. Without the influence of the boundary layer, the normal pressure forces due to the above drag and thrust components would exactly cancel.

There is a favorable pressure gradient up to the minimum pressure point, with the pressure falling in the direction of flow. This helps to stabilize the boundary layer. Downstream of the minimum pressure point, however, the thickening boundary layer has to flow against an adverse pressure gradient. Viscous effects reduce momentum within the boundary layer, and the thickness of the layer further increases so that the external flow "sees" a body which does not appear too close to a point at the trailing edge. A narrow wake is formed as the boundary layer streams off the section. This prevents the pressures on the aft-facing surface of the wing section from recovering to the high value obtaining near the stagnation point on the leading edge, as they would have done if a boundary layer had not formed. There is thus a lower than expected pressure acting on the aft facing surface, giving rise to normal pressure drag. In the low-angle-of- attack case this component is small, most of the profile drag being made up of surface friction drag.

As the angle-of-attack (AOA) of the wing section is increased, the point of minimum pressure moves towards the leading edge, with increasingly high suction being achieved. This means that the pressure then has to rise by a greater extent downstream of the minimum pressure point and that the length of wing surface exposed to the rising pressure is increased. The resulting adverse pressure gradient becomes more severe as AOA is increased. This has serious implications for the boundary layer, which is always likely to separate from the wing surface under such conditions.

According to Bernoulli's equation, the total pressure (static plus dynamic) along a subsonic streamline remains constant. If the local air velocity increases, the dynamic pressure has increased so the static pressure must decrease. Similarly, a reduction in local air velocity leads to an increase in static pressure. Thus, the passage of the

aircraft creates varying pressures around it, which pushes on the skin as shown in Figure 2.4.

Development in aerodynamics has increased exponentially since the breakthrough of the Wright brothers. Research in the areas of aircraft design and its performance estimation has also seen significant progress. An area that has contributed and promoted flight development is the development of aerodynamic coefficients such as lift and drag coefficients. These became conventions for expressing aerodynamic forces as:

$$\begin{aligned} L &= \frac{1}{2} \rho_{\infty} V_{\infty}^2 S C_L \\ D &= \frac{1}{2} \rho_{\infty} V_{\infty}^2 S C_D \end{aligned} \quad (2.1)$$

where L and D are lift and drag respectively, C_L and C_D are the lift coefficient and drag coefficient respectively, ρ_{∞} is the free-stream density, V_{∞} is the free-stream velocity and S is the platform area (Anderson, 2005). The aerodynamic performance of an aircraft is, generally, estimated from the lift and drag coefficients obtained as a result of the selected airfoil for the wing geometry. These coefficients are used together with other derived coefficients.

2.4 OTHER FORCES ACTING ON AN AIRCRAFT

2.4.1 Thrust

The power plant component produces the thrust force that is required to propel the airplane through the air. Figure 2.6 shows a typical setup of the power plant component.

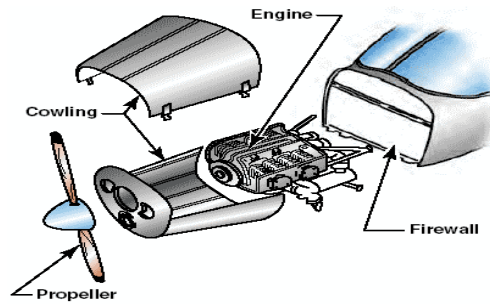


Figure 2.6: Power Plant.

Thrust is typically generated by accelerating a mass of air. A typical aircraft may have an internal combustion engine which is connected to a propeller. The cross section of the propeller takes the shape of an airfoil. This shape accelerates a mass of air to the back of the propeller as it rotates. Based on Bernoulli's theory, because of this change in velocity, a pressure difference occurs between the front and behind the propeller. This causes a suction force and pulls the airplane forward. This is illustrated in Figure 2.7.

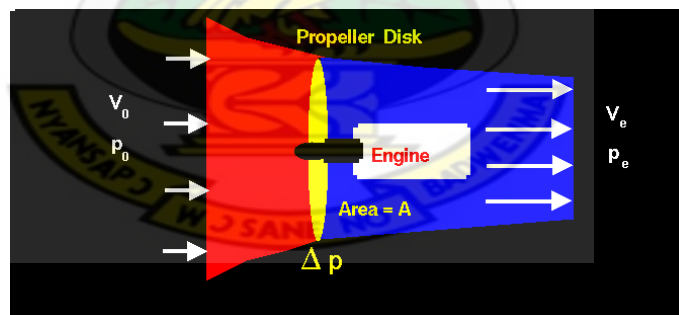


Figure 2.7: Bernoulli Theory.

It is also argued that the thrust force created is due to Newton's third law which states, "For every action there is an equal and opposite reaction". However, both theories provide a sound explanation of how thrust is developed. Newton's explanation on the production of thrust is illustrated in Figure 2.8.

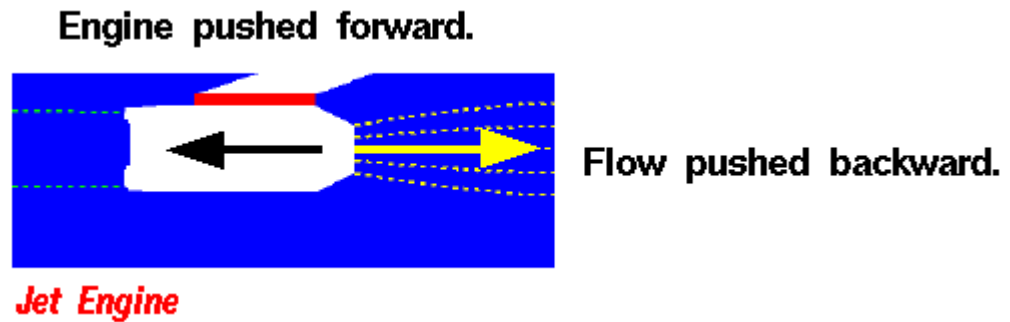


Figure 2.8: Newton's Theory.

Having a power plant for an airplane to sustain flight and obtain motion from the thrust force is just as important as having a wing to produce lift. This is because a wing cannot produce lift without motion.

2.4.2 The Weight

The total weight of the airplane is the penalty for having all the necessary components to sustain flight. Each component has a weight and the component weight summed up to the total weight of the aircraft and this must be balanced by the lift force.

2.5 AIRCRAFT PERFORMANCE

At this point, all of the forces that act on an airplane while in flight have been discussed. It is now important to determine how these forces interact and counter each other in flight. At level flight when an aircraft maintains constant velocity and altitude the thrust force is equal to the drag force and the lift force is equal to the weight. This relationship is illustrated in Figure 2.9. Moreover, the moment around the center of gravity of the airplane must also be zero. Control surfaces are designed

to give the aircraft its necessary maneuvering capabilities and increase or decrease in deflection for lift and descent.

The mention of performance of an aircraft may bring to the fore the following questions:

- How fast can the aircraft fly?
- How high can the aircraft fly?
- How much (weight or perhaps volume) can the aircraft carry?
- How far can the aircraft go without refueling?
- How steep (or perhaps how quickly) can the aircraft climb?

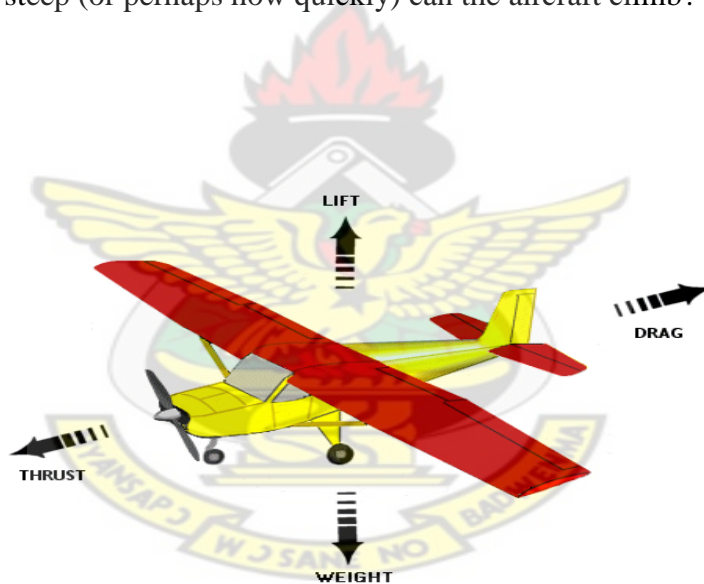


Figure 2.9: Illustration of Performance Parameters.

Aircraft performance may be attributed to a number of parameters. However, most of these parameters are based on the aerodynamic forces developed by the aircraft. These aerodynamics forces are the lift and drag. The equations that are used to determine the forces that act on an airplane are developed and presented in chapter three.

2.6 AIRCRAFT GEOMETRY DEVELOPMENT

One of the initial significant processes in aircraft design is the development or generation of the configuration. Presently, geometry generation methods usually involve the use of computer-aided design (CAD) software, although there are some examples of parametric geometry tools such as Boeing's proprietary tool, GGG1,2 (General Geometry Generator), NASA's RAM3,4 (Rapid Aircraft Modeler) tool (Gloude-mans et al, 1996), and Avid's PAGE5 (Parametric Aircraft Geometry Engine) application. Unfortunately, CAD-based modeling can be detrimental to efficiency as geometry must usually be generated manually and then converted to something usable by an analysis method. Generating the initial geometry model in CAD can be tedious and time-consuming.

Perhaps a better method for creating geometry models is to use the actual parameters that define the aircraft design in the first place. Parametric geometry generation is the process of creating an aircraft model entirely from the set of defining parameters. For example, simple straight tapered wing geometry can be generated from a very simple set of parameters: the root and tip chords, the wing sweep and span, and an airfoil definition. This parameter set is near the bare minimum required and of course more parameters can always be included; the twist distribution can be specified, for example. Rodriguez and Sturdza (2006) developed the Rapid Geometric Engine (RAGE) using some defined parameter. RAGE is good for shapes operating at Mach numbers above 0.5.

2.7 OBJECT-ORIENTED TECHNIQUE (PROGRAMMING)

Object-oriented programming (OOP) is a programming paradigm that uses "objects" and their interactions to design applications and computer programs. The methodology focuses on data rather than processes, with programmes composed of self-sufficient modules (objects) each containing all the information needed to manipulate its own data structure. This is in contrast to the modular programming method which had been dominant for many years that focused on the *function* of a module, rather than specifically the data, but equally provided for code reuse, and self-sufficient reusable units of programming logic, enabling collaboration through the use of linked modules (subroutines). This more conventional approach, which still persists, tends to consider data and behavior separately.

An object-oriented program may be viewed as a collection of cooperating *objects*, as opposed to the conventional model, in which a program is seen as a list of tasks (subroutines) to perform. In OOP, each object is capable of receiving messages, processing data, and sending messages to other objects and can be viewed as an independent 'machine' with a distinct role or responsibility.

The principal advantages of OOP are: 1. Through inheritance, redundant code can be eliminated and use of existing classes can be extended. 2. Programmes can be built from the standard working modules that communicate with one another, rather than having to start writing the code from scratch. This leads to saving of development time and higher productivity. 3. The principle of data hiding helps the programmer to build secure programmes that cannot be invaded by code in other parts of the programme. Also, it is possible to have multiple instances of an object to coexist without any interference. It is possible to map objects in the problem domain to those

in the program. It is easy to partition the work in a project based on objects. The data-centered design approach enables the programmer to capture more details of a model in implementable form. Object-oriented systems can easily be upgraded from small to large systems. Message passing techniques for communication between objects makes the interface descriptions with external systems much simpler.

The advantages make the technique amendable to the concept being developed for the small aircraft design.



CHAPTER THREE

GOVERNING AND RELATED EQUATIONS FOR AERODYNAMIC ANALYSIS

3.0 INTRODUCTION

This chapter provides the Governing equations of fluid flow relevant to the research. It also discusses how and why these relations are used and modifications that are applied to them are presented.

3.1 POSSIBLE SOLUTION/ANALYSIS METHODS

Aerodynamic analysis can be performed on objects moving in a fluid by using different methods. Available methods include the solution of the full Navier-Stokes Equation using Computational Fluid Dynamics (CFD) or Commercial off-the-shelve (COTS) software and tools. This usually gives the best and most accurate result. Next to it is the coupled 3D Euler and boundary analysis tools that give an approximate solution. Coupled 2D Euler and boundary analysis tool is one of the good approximate methods that can be applied to incompressible flows.

3.2 NAVIER-STOKES EQUATION

The most comprehensive and general fluid flow equation is the system of Navier-Stokes Equation. The System of Navier-Stokes equation is described by the Mass conservation, Momentum conservation and Energy conservation equations in Cartesian coordinates as (Anderson, 1995):

Mass Conservation Equation:

$$\frac{\partial \rho}{\partial t} + \nabla \cdot (\rho \mathbf{V}) = 0 \quad (3.1)$$

Momentum Conservation Equation (Navier-Stokes equation):

$$\begin{aligned} \frac{\partial(\rho u)}{\partial t} + \nabla \cdot (\rho u \mathbf{V}) &= -\frac{\partial p}{\partial x} + \rho f_x + (F_x)_{viscous} \\ \frac{\partial(\rho v)}{\partial t} + \nabla \cdot (\rho v \mathbf{V}) &= -\frac{\partial p}{\partial y} + \rho f_y + (F_y)_{viscous} \\ \frac{\partial(\rho w)}{\partial t} + \nabla \cdot (\rho w \mathbf{V}) &= -\frac{\partial p}{\partial z} + \rho f_z + (F_z)_{viscous} \end{aligned} \quad (3.2)$$

Energy Conservation Equation:

$$\frac{\partial}{\partial t} \left[\rho \left(e + \frac{V^2}{2} \right) \right] + \nabla \cdot \left[\rho \left(e + \frac{V^2}{2} \right) \mathbf{V} \right] = \rho \dot{q} - \nabla \cdot (p \mathbf{V}) + \rho (\mathbf{f} \cdot \mathbf{V}) + \dot{Q}_{viscous} + \dot{W}_{viscous} \quad (3.3)$$

where

u, v, w – velocity components in x, y, z directions respectively

\mathbf{V} – velocity of moving fluid

ρ – fluid density

t – time

p – pressure

\mathbf{f}, f – body force per unit mass

f_x, f_y, f_z – components of body forces in x, y, z directions

e – internal energy per unit mass

q – volumetric rate of heat addition per unit mass (J/s.kg)

Q_{viscous} – rate of heat addition due to viscous effect

W_{viscous} – rate of work done due to viscous effect

F – surface force due to viscous stresses

Due to the mathematical complexity of the system of Navier Stokes equation, they cannot be solved analytically except in few cases of practical interest. Various simplifications have been adopted in modelling flows. In this research, reduction of the equation to Euler equation and application of boundary layer simplification assumptions are considered.

KNUST

3.3 EULER AND BOUNDARY LAYER EQUATIONS

The application of the boundary layer approximation to fluid flow equations is one of the significant simplifications of the Navier-Stokes' equation. The deduction of the boundary layer equations by Prandtl was one of the most important advances in fluid dynamics. Using an order of magnitude analysis, the well-known governing Navier–Stokes equations of viscous fluid flow can be greatly simplified within the boundary layer. Notably, the partial differential equations (PDE) become parabolic, rather than the elliptical form of the full system of Navier–Stokes equation. This greatly simplifies the solution of the equations. By using the boundary layer approximation, the flow is divided into an inviscid portion (which can be solved by a number of methods) and the boundary layer, which is governed by an easier to solve PDE (Figure 3.1).

The approximation is that, for a sufficiently high Reynolds number the flow over a surface can be divided into an outer region of inviscid flow unaffected by viscosity

(the greater portion of the flow), and a region close to the surface where viscosity influence dominate (the boundary layer).

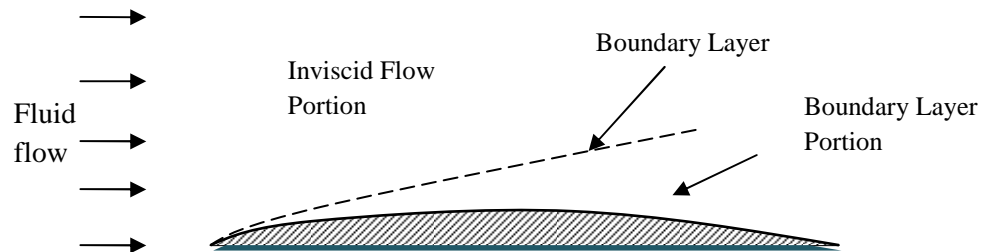


Figure 3.1 Illustration of Inviscid and boundary layer portions of flow.

3.3.1 Inviscid Flow Portion

The inviscid flow portion of the approximation can be expressed generally by the Euler equation as Anderson, 1995):

Mass conservation equation:

$$\frac{\partial \rho}{\partial t} + \nabla \cdot (\rho \mathbf{V}) = 0 \quad (3.4)$$

Momentum Conservation (Euler) Equation:

$$\begin{aligned} \frac{\partial(\rho u)}{\partial t} + \nabla \cdot (\rho u \mathbf{V}) &= -\frac{\partial p}{\partial x} + \rho f_x \\ \frac{\partial(\rho v)}{\partial t} + \nabla \cdot (\rho v \mathbf{V}) &= -\frac{\partial p}{\partial y} + \rho f_y \\ \frac{\partial(\rho w)}{\partial t} + \nabla \cdot (\rho w \mathbf{V}) &= -\frac{\partial p}{\partial z} + \rho f_z \end{aligned} \quad (3.5)$$

Energy conservation equation:

$$\frac{\partial}{\partial t} \left[\rho \left(e + \frac{V^2}{2} \right) \right] + \nabla \cdot \left[\rho \left(e + \frac{V^2}{2} \right) \mathbf{V} \right] = \rho \dot{q} - \nabla \cdot (p \mathbf{V}) + \rho (\mathbf{f} \cdot \mathbf{V}) \quad (3.6)$$

The equations apply to incompressible flow or constant density flow which is valid for most liquids and can be extended to low flow velocities for gases (Mach numbers less than 0.3). Assuming irrotational steady flow condition, the Euler equation reduces to:

Mass conservation Equation:

$$\nabla \cdot \mathbf{V} = 0 \quad (3.7)$$

Momentum Conservation Equation:

$$\nabla \times \mathbf{V} = 0 \quad (3.8)$$

Energy Equation:

$$\frac{\partial}{\partial t} \left[\rho \left(e + \frac{V^2}{2} \right) \right] + \nabla \cdot \left[\rho \left(e + \frac{V^2}{2} \right) \mathbf{V} \right] = \rho \dot{q} - \nabla \cdot (p \mathbf{V}) + \rho (\mathbf{f} \cdot \mathbf{V}) \quad (3.9)$$

At this point the Energy equation is decoupled from the Mass and Momentum equations. The Mass and Momentum equations can, therefore, be solved for the velocity which is of interest. At the flow regime under consideration the temperature change is insignificant and can therefore be assumed to be zero (the process is assumed to be isothermal). As such the solution to the energy equation is insignificant and can be ignored.

Defining the stream function, ψ , the mass and momentum equations (equations 3.7 and 3.8) can further be reduced to a single Laplace equation given by

$$\nabla^2 \psi = 0 \quad (3.10)$$

Or in two dimensional Cartesian coordinates form

$$\frac{\partial^2 \psi}{\partial x^2} + \frac{\partial^2 \psi}{\partial y^2} = 0 \quad (3.11)$$

For some given boundary conditions that completely define the problem, the solution for the streamline could be obtained.

For a stream function $\psi(x, y) = \text{Constant}$

$$d\psi = \frac{\partial \psi}{\partial x} dx + \frac{\partial \psi}{\partial y} dy = 0 \quad (3.12)$$

But by definition

$$\frac{\partial \psi}{\partial x} = -v \quad (3.13)$$

and $\frac{\partial \psi}{\partial y} = u \quad (3.14)$

The velocity, V , at a point on the surface is

$$V = \sqrt{u^2 + v^2} \quad (3.15)$$

Also equation 3.12 becomes

$$d\psi = -v dx + u dy = 0 \quad (3.16)$$

$$\left(\frac{dy}{dx} \right)_{\psi=\text{Const}} = \frac{v}{u} \quad (3.17)$$

3.3.2 Pressure Distribution and Pressure Coefficient

The solution to the Inviscid Flow portion approximation to Navier-Stokes equation results in the velocity of the fluid flow along the object boundary. For incompressible flow, pressure coefficient, C_p , can be expressed in terms of the velocity only. By Bernoulli's equation

$$P - P_\infty = \frac{\rho(V_\infty^2 - V^2)}{2}$$

or
$$P - P_\infty = \frac{1}{2} \rho V_\infty^2 \left(1 - \frac{V^2}{V_\infty^2} \right)$$
 (3.18)

where V is the velocity on the object boundary and V_∞ is the free stream velocity of flow.

The Pressure coefficient, C_p , is given by
$$C_p = \frac{P - P_\infty}{q_\infty}$$
 (3.19)

where q_∞ is the dynamic pressure and
$$q_\infty = \frac{\rho_\infty V_\infty^2}{2}$$
 (3.20)

$$C_p = \frac{P - P_\infty}{q_\infty} = \frac{\frac{1}{2} \rho (V_\infty^2 - V^2)}{\frac{1}{2} \rho_\infty V_\infty^2}$$

$$C_p = 1 - \left(\frac{V}{V_\infty} \right)^2$$

(3.21)

Therefore

$$P = \frac{1}{2} \rho V_\infty^2 C_p + P_\infty$$
 (3.22)

Average Pressure is evaluated as

$$P_{avg} = \frac{\sum_{i=1}^N P_i}{\text{Number of points}(N)} \quad (3.23)$$

where $i = 1, 2, \dots, N$

3.3.3 Boundary Layer Portion

The Navier–Stokes equations for a two-dimensional steady incompressible flow in Cartesian coordinates are given by (Houghton and Carpenter, 2003):

$$\frac{\partial u}{\partial x} + \frac{\partial v}{\partial y} = 0 \quad (3.24)$$

$$u \frac{\partial u}{\partial x} + v \frac{\partial u}{\partial y} = -\frac{1}{\rho} \frac{\partial p}{\partial x} + \nu \left(\frac{\partial^2 u}{\partial x^2} + \frac{\partial^2 u}{\partial y^2} \right) \quad (3.25)$$

$$u \frac{\partial v}{\partial x} + v \frac{\partial v}{\partial y} = -\frac{1}{\rho} \frac{\partial p}{\partial y} + \nu \left(\frac{\partial^2 v}{\partial x^2} + \frac{\partial^2 v}{\partial y^2} \right) \quad (3.26)$$

where u and v are the velocity components, ρ is the density, p is the pressure, and ν is the kinematic viscosity of the fluid at a point.

Let u and v be streamwise and transverse (wall normal) velocities respectively inside the boundary layer. Using asymptotic analysis, it can be shown that the above equations of motion reduce within the boundary layer to become

$$\frac{\partial u}{\partial x} + \frac{\partial v}{\partial y} = 0 \quad (3.27)$$

$$u \frac{\partial u}{\partial x} + v \frac{\partial u}{\partial y} = -\frac{1}{\rho} \frac{\partial p}{\partial x} + \nu \frac{\partial^2 u}{\partial y^2} \quad (3.28)$$

and if the fluid is incompressible as is applicable to liquids under standard conditions and for air at Mach numbers less than 0.3:

$$\frac{1}{\rho} \frac{\partial p}{\partial y} = 0 \quad (3.29)$$

The asymptotic analysis also shows that v , the wall normal velocity, is small compared with u the streamwise velocity, and that variations in properties in the streamwise direction are generally much lower than those in the wall normal direction.

Since the static pressure p is independent of y , then pressure at the edge of the boundary layer is the pressure throughout the boundary layer at a given streamwise position. The external pressure may be obtained through an application of Bernoulli's Equation. Let u_0 be the fluid velocity outside the boundary layer, where u and u_0 are both parallel. This gives upon substituting for p the following result

$$u \frac{\partial u}{\partial x} + v \frac{\partial u}{\partial y} = u_0 \frac{\partial u_0}{\partial x} + \nu \frac{\partial^2 u}{\partial y^2} \quad (3.30)$$

With the continuity equation

$$\frac{\partial u}{\partial x} + \frac{\partial v}{\partial y} = 0 \quad (3.31)$$

For a flow in which the static pressure p also does not change in the direction of the flow then

$$\frac{\partial p}{\partial x} = 0 \quad (3.32)$$

so u_0 remains constant.

Therefore, the equation of motion (3.28) simplifies to become

$$u \frac{\partial u}{\partial x} + v \frac{\partial u}{\partial y} = \nu \frac{\partial^2 u}{\partial y^2} \quad (3.33)$$

These approximations are used in a variety of practical flow problems of scientific and engineering interest. The above analysis is for any instantaneous laminar or turbulent boundary layer, but is used mainly in laminar flow studies since the mean flow is also the instantaneous flow because there are no velocity fluctuations present.

3.3.4 Shear Stress

A viscous, Newtonian fluid (including air and water) moving along a solid boundary will incur a shear stress on that boundary. The no-slip condition dictates that the speed of the fluid at the boundary (relative to the boundary) is zero, but at some distance from the boundary the flow speed must equal that of the free stream. The region between these two points is called the boundary layer. The boundary layer is that layer of fluid in the immediate vicinity of a bounding surface. The shear stress is imparted onto the boundary as a result of this loss of velocity and can be expressed as

$$\tau_{wall} = \mu \left. \frac{du}{dy} \right|_{y=0} \quad (3.34)$$

where μ is the dynamic viscosity of the fluid,

u is the velocity of the fluid along the boundary, and

y is the height of the boundary.

3.3.5 Blasius Solution of the Boundary layer equations on a flat plate

Blasius investigated the shear stress on a plate, and computed for drag forces on flat plate. His result yielded the friction coefficient as function of the Reynolds Number, Re .

$$C_f = f(Re) \quad (3.35)$$

The skin friction coefficient is the non-dimensional wall parameter defined as:

$$C_f = \frac{\tau_{wall}}{\frac{1}{2}\rho V^2} \quad (3.36)$$

Local Skin Friction Coefficient and Shear Stress

The skin friction coefficient distribution along the streamlines that form the airfoil or fuselage configuration is evaluated using approximation to a flat plate solution of the boundary layer equation known as Blasius solution as stated above. For laminar flow, the local skin friction is given by (Anderson, 2005) :

$$c_f = \frac{0.664}{\sqrt{Re_s}} \quad (3.37)$$

where Re_s is the local Reynolds number defined as:

$$Re_s = \frac{\rho_\infty v_\infty s}{\mu_\infty} \quad (3.38)$$

where v_∞ , μ_∞ and ρ_∞ are freestream quantities and s is the local distance measured from the leading edge.

In the case of turbulent flow, the local skin friction is evaluated in accordance with the relationship given as (Houghton and Carpenter, 2003):

$$c_f = \frac{0.0592}{(\text{Re}_s)^{0.2}} \quad (3.39)$$

The local shear stress is found to be a function of the skin friction coefficient and is calculated with the equation:

$$\tau = C_f \times q_E \quad (3.40)$$

where q_E is the dynamic pressure at the edge, defined by:

$$q_E = \frac{1}{2} \rho \times V^2 \quad (3.41)$$

3.4 AERODYNAMIC FORCE ANALYSIS

With the aircraft configuration/shape developed, it is possible to perform an aerodynamic analysis which is very important and will result in the aerodynamic parameters in the form of lift and drag. Aerodynamic forces are calculated by numerically integrating the local pressures and shear stresses acting on the wetted surfaces. The mean value theorem is used to evaluate all surface integration routines.

3.4.1 The Mean Value Theorem

The evaluation of the inviscid force on a given aircraft configuration involves the evaluation of the following expressions as they are applied to the upper and lower geometric surfaces,

$$\vec{F}_p = \oint\oint_{\text{Aircraft}} P d\vec{S} \quad (3.42)$$

and
$$\vec{F}_p = D_p \vec{i} + G_p \vec{j} + L_p \vec{k} \quad (3.43)$$

where L_p , D_p , and G_p are the Lift, Drag, and Slip forces due to pressure respectively and dS (elementary surface area) is defined as:

$$d\vec{S} = dS_x \vec{i} + dS_y \vec{j} + dS_z \vec{k} \quad (3.44)$$

with S_x , S_y , and S_z being the area projections onto the yz , xz , and xy planes respectively, as shown in Figure 3.2.

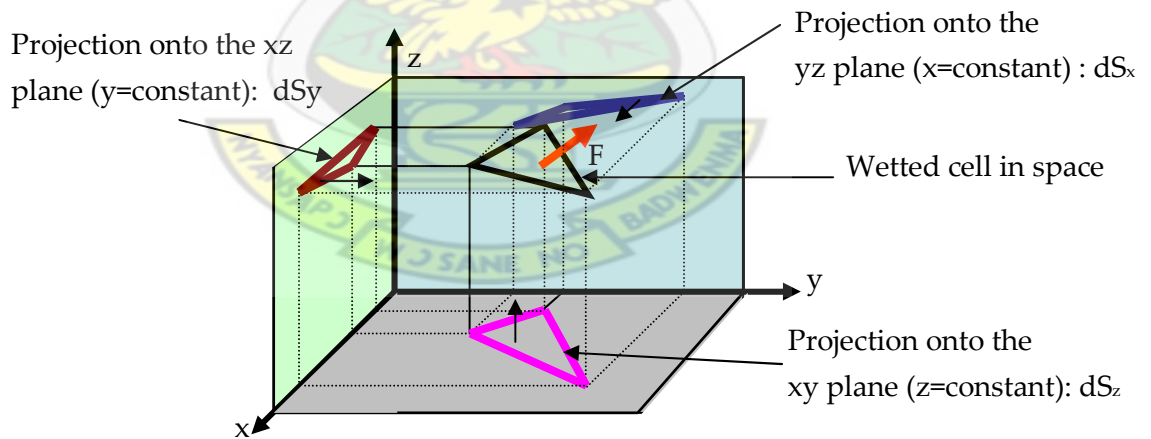


Figure 3.2: Illustration of Projected surface Areas.

Similarly, the force due to shear stress is evaluated with the following expressions,

$$\vec{F}_\tau = \oint\oint_{\text{Aircraft}} \tau d\vec{S} \quad (3.45)$$

$$\text{and} \quad \vec{F}_\tau = D_\tau \vec{i} + L_\tau \vec{j} + G_\tau \vec{k} \quad (3.46)$$

where L_τ , D_τ , and G_τ are the Lift, Drag, and Slip forces due to shear respectively.

Using the mean value theorem, equations 3.42 and 3.45 become:

$$\begin{aligned} \vec{F}_p &= \iint_{\text{Aircraft}} p d\vec{S} = p_{avg} \iint_{\text{Aircraft}} d\vec{S} = p_{avg} \iint_{\text{Aircraft}} (dS_x \vec{i} + dS_y \vec{j} + dS_z \vec{k}) \\ \vec{F}_\tau &= \iint_{\text{Aircraft}} \tau d\vec{S} = \tau_{avg} \iint_{\text{Aircraft}} d\vec{S} = \tau_{avg} \iint_{\text{Aircraft}} (dS_x \vec{i} + dS_y \vec{j} + dS_z \vec{k}) \end{aligned} \quad (3.47)$$

The average Pressure P_{avg} and shear stress τ_{avg} are as evaluated from equation 3.23.

KNUST

3.4.2 Projected and Wetted Areas

In order to evaluate equation 3.47, first the area projections must be calculated. The aircraft shapes are often not shapes whose area can easily be calculated. The surface is divided into small rectangular units with known coordinate points. Each rectangular unit consists of triangular units. Triangulation method, therefore, is used in evaluating the surface area. Figure 3.3 shows sample single triangular element ABC.

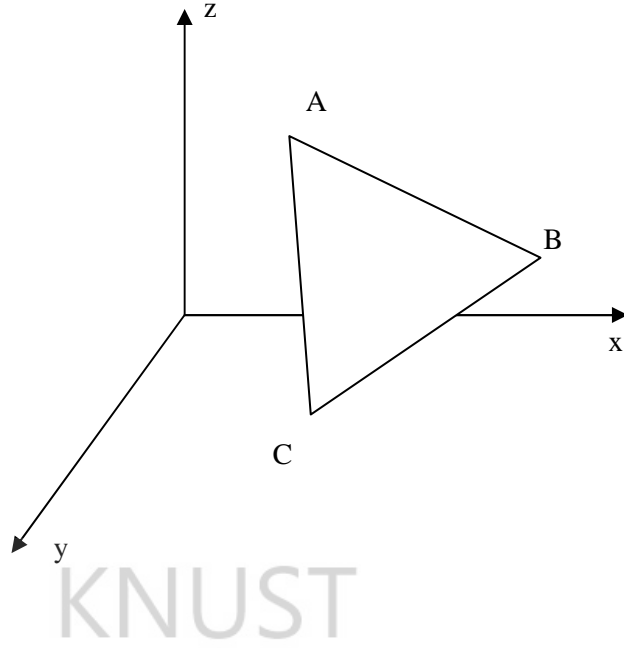


Figure 3.3: Sample Triangular Element.

The sides of the element are calculated as follows:

$$\begin{aligned}
 AB &= \left[\lambda_m (X_A - X_B)^2 + \lambda_m (Y_A - Y_B)^2 + \lambda_m (Z_A - Z_B)^2 \right]^{0.5} \\
 AC &= \left[\lambda_m (X_A - X_C)^2 + \lambda_m (Y_A - Y_C)^2 + \lambda_m (Z_A - Z_C)^2 \right]^{0.5} \\
 BC &= \left[\lambda_m (X_B - X_C)^2 + \lambda_m (Y_B - Y_C)^2 + \lambda_m (Z_B - Z_C)^2 \right]^{0.5}
 \end{aligned} \tag{3.48}$$

where λ_m equals 1, or 0 if the projection is in the m direction. The projected area is calculated using Heron's formula for area of a triangle given as

$$\begin{aligned}
 A_{element} &= \left[t \times (t - AB) \times (t - BC) \times (t - AC) \right]^{0.5} \\
 t &= (AB + BC + AC) / 2
 \end{aligned} \tag{3.49}$$

$$S_m = \sum A_{element}$$

3.4.3 Lift, Drag, and Side Forces

Each variable in equations 3.47 is now known and thus the aerodynamic forces on the aircraft can be evaluated. Keeping in mind that the Lift is the k component, the Drag the i component, and Side Force the j component, these forces are evaluated as

$$L = P_{avg} A_{xy} + \tau_{avg} A_{yz} + \tau_{avg} A_{xz} \quad (3.50)$$

$$D = P_{avg} A_{yz} + \tau_{avg} A_{xy} + \tau_{avg} A_{xz}$$

Where A_{xy} , A_{xz} and A_{yz} are projected areas in the x-y, x-z and y-z planes respectively. Due to the symmetrical design of the aircraft, which causes the Side Forces to cancel each other out the Side Force is neglected. Other aerodynamic properties, Lift and drag coefficient (C_L and C_D) are found as:

$$C_L = \frac{L}{q_{\infty} A_{Plan}} \quad (3.51)$$

$$C_D = \frac{D}{q_{\infty} A_{Plan}} \quad (3.52)$$

3.5 SOLUTION TO THE POTENTIAL FLOW EQUATION

The solution to fluid flow problems given by equation 3.10 or 3.11 can be obtained numerically with given boundary conditions.

$$\nabla^2 \psi = 0 \quad (3.53)$$

or in two dimensional Cartesian coordinate form

$$\frac{\partial^2 \psi}{\partial x^2} + \frac{\partial^2 \psi}{\partial y^2} = 0 \quad (3.54)$$

Solving for the streamline will lead to the velocity distribution along the boundary of the object in the flow field. The stream function equation described by the Laplace equation is an elliptic partial differential equation and any available method for the elliptic equation solution may be applicable. Using curvilinear boundary fitting technique, the physical elliptic grid is transformed into a rectangular grid with square grid spacing.

3.5.1 Grid Transformation

The physical plane (x, y) boundary is a complex boundary system and has higher level of difficulty in handling the boundary condition when using numerical methods. The system can be simplified by transforming into rectangular system which acquires simple boundary conditions. General transformation from the physical plane (x, y) to transform plane (η, ξ) is given by $\xi = \xi(x, y)$, $\eta = \eta(x, y)$. Likewise the inverse transformation is $x = x(\xi, \eta)$ and $y = y(\xi, \eta)$.

Using the Laplace equation with the coordinate variable (ξ, η) on the transformed or computational grid and (x, y) on the physical grid. We have the Laplace equations as

$$\frac{\partial^2 \xi}{\partial x^2} + \frac{\partial^2 \xi}{\partial y^2} = 0$$

$$\frac{\partial^2 \eta}{\partial x^2} + \frac{\partial^2 \eta}{\partial y^2} = 0 \tag{3.55}$$

Interchanging the independent and dependent variable, the transformed elliptic equation is given by Thompson et al, (1974) as

$$\alpha \frac{\partial^2 x}{\partial \xi^2} - 2\beta \frac{\partial^2 x}{\partial \xi \partial \eta} + \gamma \frac{\partial^2 x}{\partial \eta^2} = 0$$

$$\alpha \frac{\partial^2 y}{\partial \xi^2} - 2\beta \frac{\partial^2 y}{\partial \xi \partial \eta} + \gamma \frac{\partial^2 y}{\partial \eta^2} = 0 \quad (3.56)$$

where

$$\alpha = \left(\frac{\partial x}{\partial \eta} \right)^2 + \left(\frac{\partial y}{\partial \eta} \right)^2$$

$$\beta = \left(\frac{\partial x}{\partial \xi} \right) \left(\frac{\partial x}{\partial \eta} \right) + \left(\frac{\partial y}{\partial \xi} \right) \left(\frac{\partial y}{\partial \eta} \right)$$

$$\gamma = \left(\frac{\partial x}{\partial \xi} \right)^2 + \left(\frac{\partial y}{\partial \xi} \right)^2 \quad (3.57)$$

The transformed equations allow the calculation of the (x, y) coordinates of the grid points in the physical plane as a function of the (η , ξ) locations of the same grid points in the computational plane.

3.5.2 Governing Equation

The Governing Equation of interest $\nabla^2 \psi = 0$ is accordingly transformed as

$$\alpha \frac{\partial^2 \psi}{\partial \xi^2} - 2\beta \frac{\partial^2 \psi}{\partial \xi \partial \eta} + \gamma \frac{\partial^2 \psi}{\partial \eta^2} = 0 \quad (3.58)$$

The boundary conditions are given according to Thompson et al (1974) as

$$\psi(\xi, \eta) = 0 \quad \text{at the object boundary}$$

$$\psi(\xi, \eta) = U_{\infty} y(\xi, \eta) \cos \theta - U_{\infty} x(\xi, \eta) \sin \theta \quad \text{at far field boundary}$$

where θ is the angle of attack.

The normal derivative at the boundary is given as

$$\frac{\partial f}{\partial n} = \frac{1}{J(1+(g')^2)^{1/2}} \left[\frac{\partial f}{\partial \xi} \left(g' \frac{\partial y}{\partial \eta} + \frac{\partial x}{\partial \eta} \right) - \frac{\partial f}{\partial \eta} \left(g' \frac{\partial y}{\partial \xi} + \frac{\partial x}{\partial \xi} \right) \right] \quad (3.59)$$

Where f is the function of interest

$$g' = \frac{dy}{dx} \text{ at the boundary}$$

J is the Jacobian

n indicates directional normal

The velocity at the boundary is evaluated from

$$V = \frac{\partial \psi}{\partial n} = \frac{1}{J(1+(g')^2)^{1/2}} \left[\frac{\partial \psi}{\partial \xi} \left(g' \frac{\partial y}{\partial \eta} + \frac{\partial x}{\partial \eta} \right) - \frac{\partial \psi}{\partial \eta} \left(g' \frac{\partial y}{\partial \xi} + \frac{\partial x}{\partial \xi} \right) \right] \quad (3.60)$$

Figure 3.4 is a schematic of the physical plane and figure 3.5 is the equivalent computational plane. The transformation is such that, the object boundary 1 in the physical plane is boundary AA^1 in the computational plane. The cutting plane AB in the physical plane (Figure 3.4) transform into boundaries AB and A^1B^1 (boundary 3 and 4) in the computational plane (Figure 3.5). Each grid point in the physical plane has the corresponding point in the computational plane. Figure 3.6 is an illustration of the physical plane with grid system.

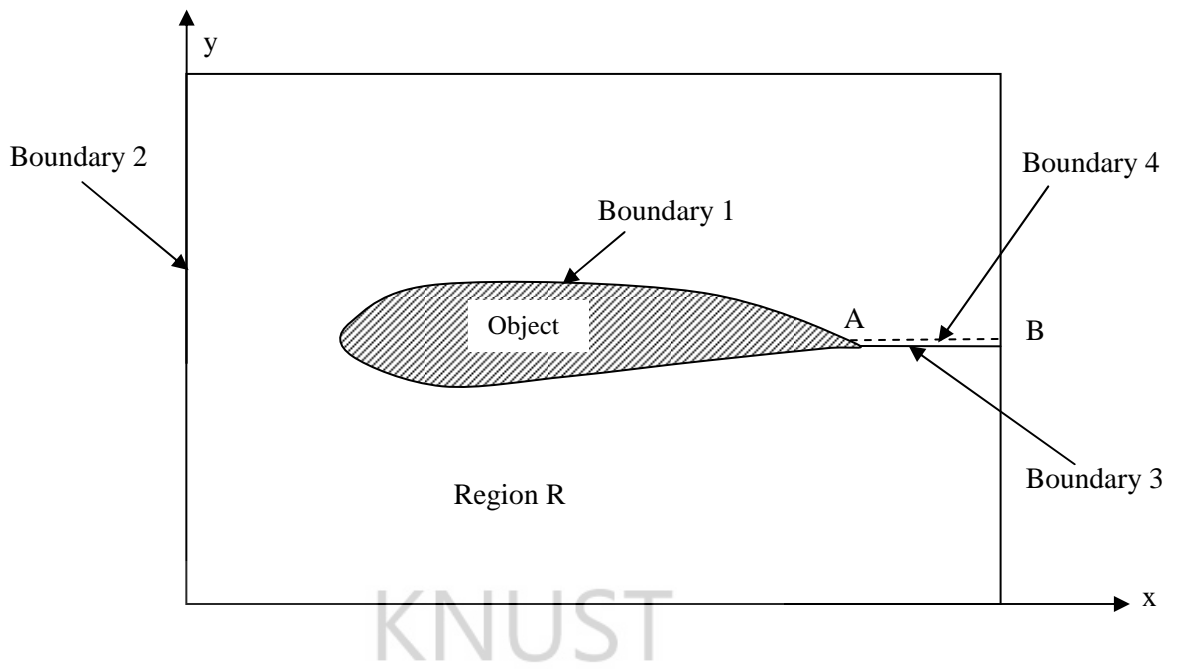


Figure 3.4. Illustration of the Physical plane.

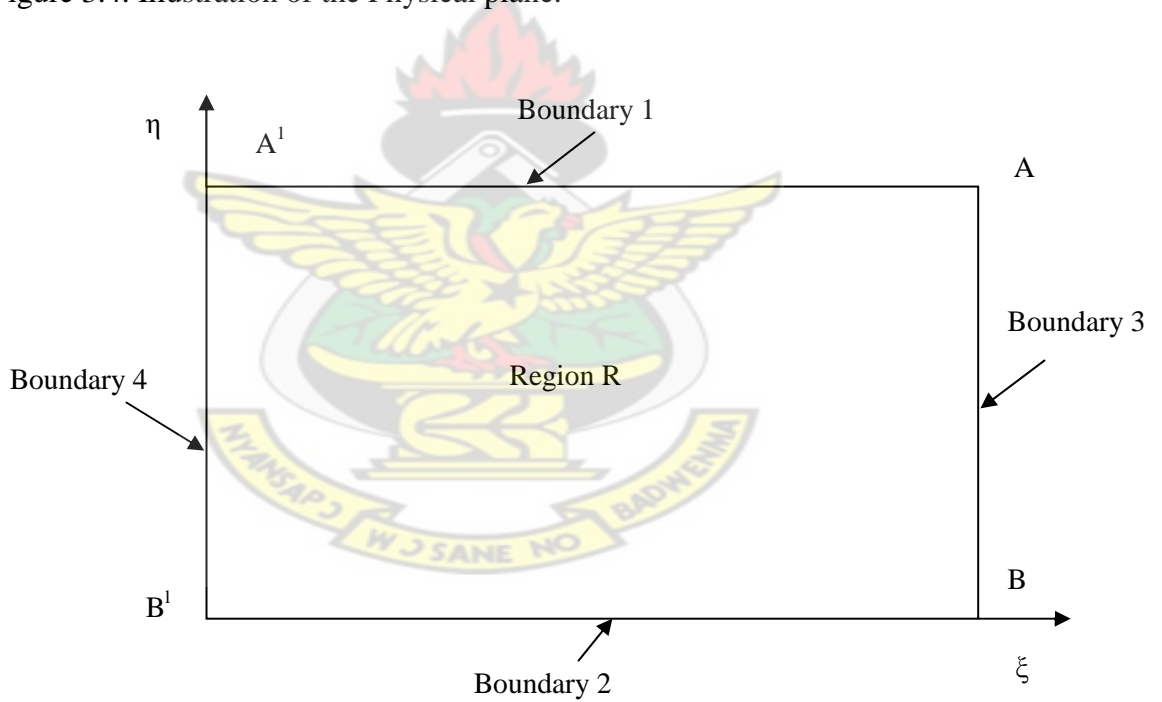


Figure 3.5 Illustration of the Computational Plane.

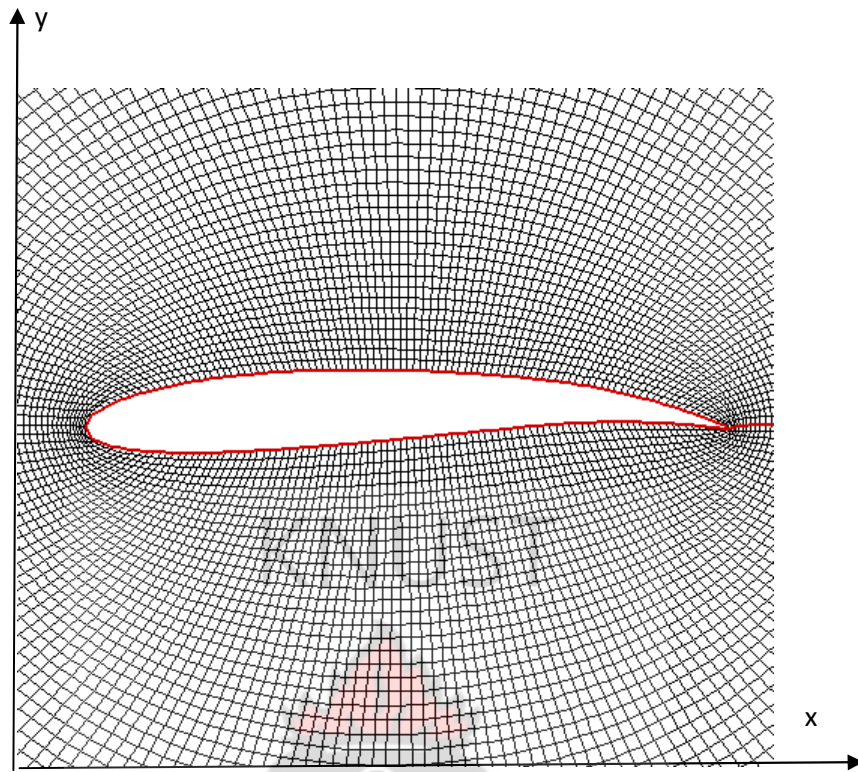
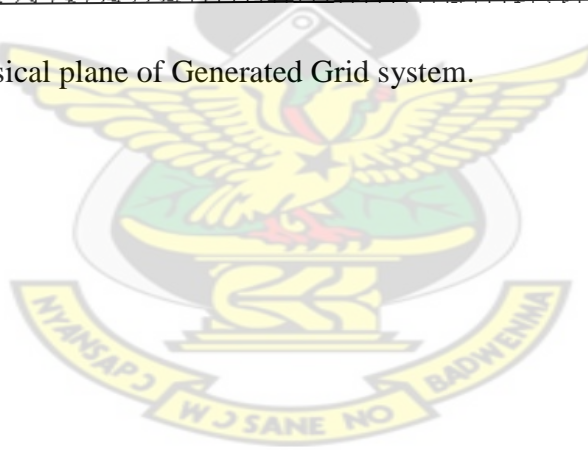


Figure 3.6 Physical plane of Generated Grid system.



CHAPTER FOUR

DESIGN CONCEPT AND DEVELOPMENT

4.0 INTRODUCTION

The Aircraft design concept is presented in this chapter. The design and development of the aircraft geometry, numerical wing tunnel and its validation are explained. The sample generated aircraft configurations with varying design parameters are also illustrated in this chapter.

KNUST

4.1 AIRCRAFT DESIGN CONCEPT

The concept of the research is built on object oriented technique such that an object is defined as a function that accepts an input parameter and results in an output. As an illustration of the concept, the aircraft aerodynamic performance is defined analogous to a function $F = f(x)$, where the output, F , involves the geometry and performance of the aircraft. The input parameter, x , is made of two components, fixed and design parameters. Figure 4.1 is an illustration of the research concept. The performance, F , which is a vector quantity, is modeled as integral function over the surface and its components (D_i , L_j and S_k) respectively result into drag, lift and slip force. The function f , under the integration represents the surface properties: pressure P , and shear stress τ , distributed over the surface S .

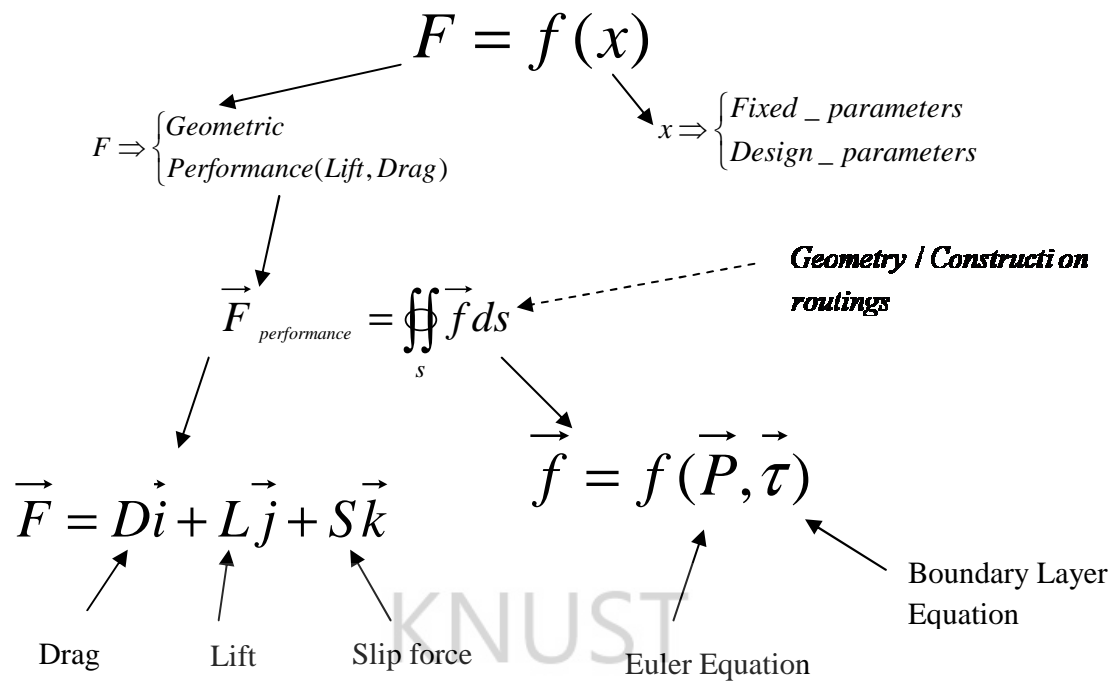


Figure 4.1 Illustration of Research Concept.

4.2 AIRCRAFT GEOMETRY DESIGN AND DEVELOPMENT

One of the initial significant processes in the aircraft design process is the development or generation of the configuration. To simplify and be more generic in the configuration design, the configuration of the aircraft is decomposed or disintegrated into components or objects, which are defined by some design parameters. The components identified are: Fuselage (Nose, Nose-cabin interface, Cabin, Luggage-cabin, Tail-Boom), Empennage (Horizontal tail, Vertical Tail), Wing, Landing gear and Power plant. Figure 4.2 is sample illustration of the components of the aircraft. The components are defined by design parameters such that a change in a value may change the configuration. Other kinds of parameters used to describe a component are fixed parameters. A fixed parameter is such that for a given desired configuration, its value remains constant while the design parameters

may be varied. Examples of the fixed parameters are the nose tip diameter for the nose, dihedral and sweep angles for the wing and the angle of attack.

Parametric geometry generation is the process of creating a physical model entirely from a set of defining parameters. The actual design parameters are used in creating the geometry models such that with a given parameter, unique and specific class of aircraft could be generated.

4.2.1 Mapping Aircraft Reality into Object-Oriented Programming

Environment

The physical aircraft is mapped into Object-Oriented Programming (OOP) Environment to enable creation of the various objects that will be needed for the configuration design. The aircraft is, first, decomposed into wing, fuselage and empennage. The fuselage is further broken down into nose, nose-cabin-interface, cabin, luggage-cabin and tailboom. The empennage consists of horizontal tail and vertical tail objects. Figure 4.2 is an illustration of the physical aircraft divided into components and figures 4.3 shows relational break down of the aircraft components.

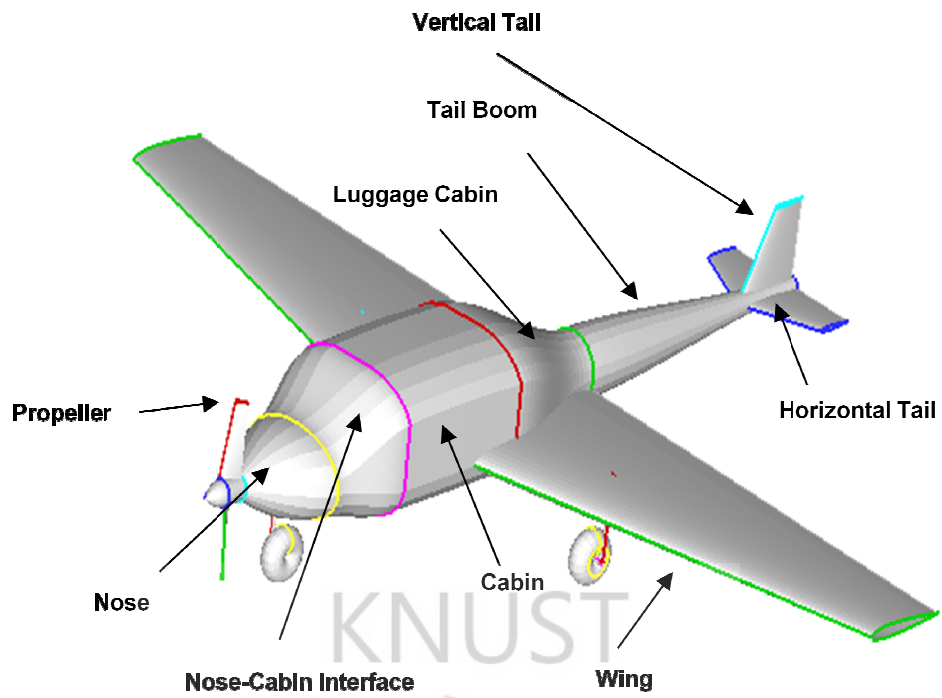


Figure 4.2 Decomposed aircraft into Components.

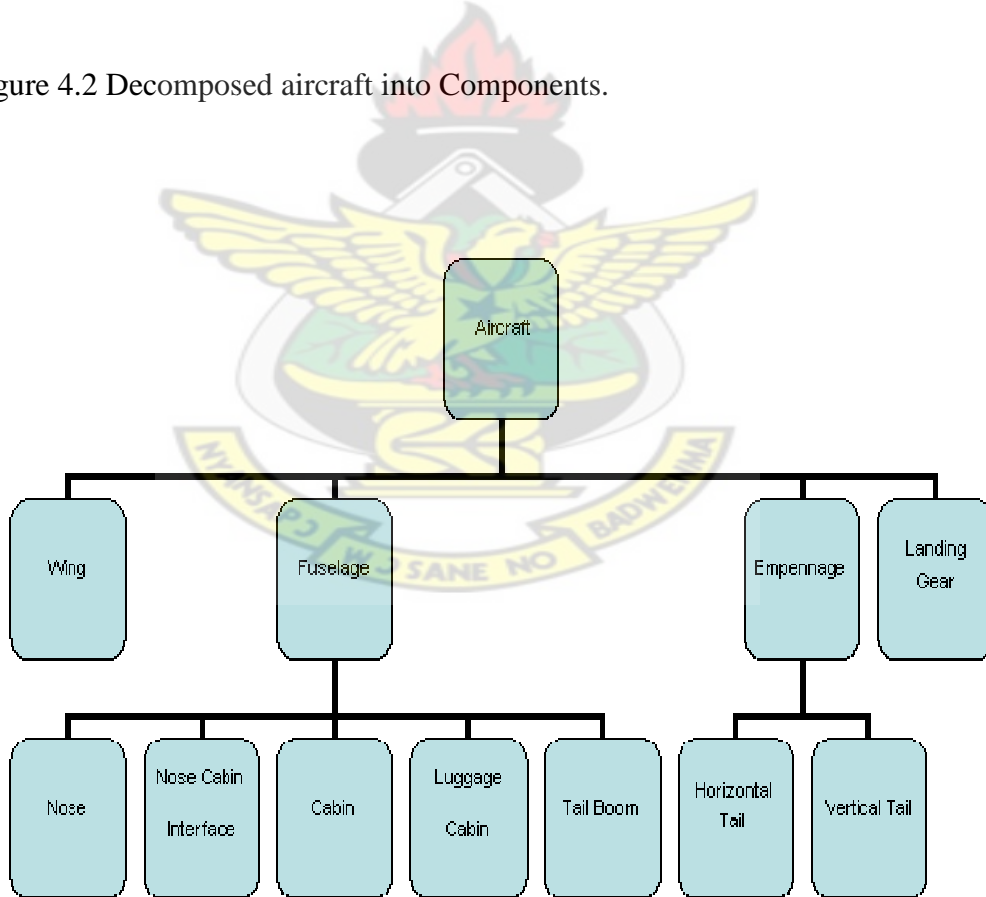


Figure 4.3 Schematic illustrations of aircraft Components.

In the Object Oriented environment, an algorithm is developed. Generally, the system accepts the input parameters. These parameters are allocated to various routines to be used by objects in creating the aircraft configuration. Figures 4.4 to 4.7 are the flowcharts illustrating the nature of the interaction between system components or objects. Figure 4.4 is the overview of system design flow chart. The system consists of three major parts namely wing, empennage and fuselage. The system takes the design variables and distributed them to respective parts. Other distinct parts of the system are numerical wind tunnel and surface integrator. The numerical wind tunnel components is used to for estimating the surface properties and the surface integrator used for evaluating surface and projected areas of aircraft components. Lift and drag performance is determined for each component and these are then summed to obtained the aircraft lift and drag performance. Components of fuselage as illustrated in figure 4.5 are independently created but are joined to create fuselage profile before wind tunnel experiment. After the wind tunnel experiment, the surface properties of each component are respectively assigned.

The design system is developed using FORTRAN 95 programming language. By Object-Oriented Programming technique, fundamental primitives such as 'point', 'line', 'curve', 'circle' and others have been defined with required input parameters. The simple fundamental objects are used in various combinations to create complex objects. Sample code is provided in appendix A. The results of objects created are visualized using TECPLOT which is post data processing software.

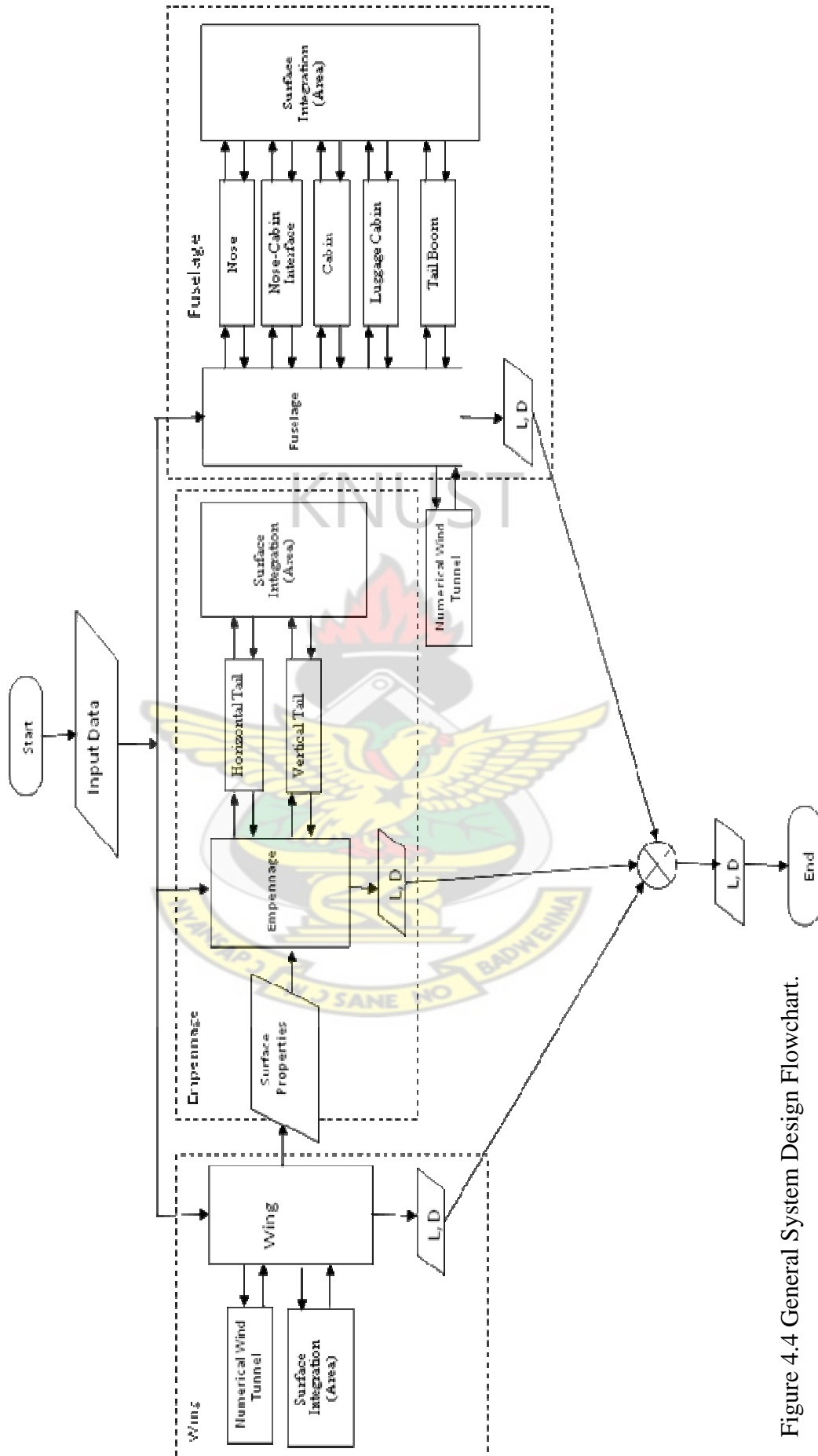


Figure 4.4 General System Design Flowchart.

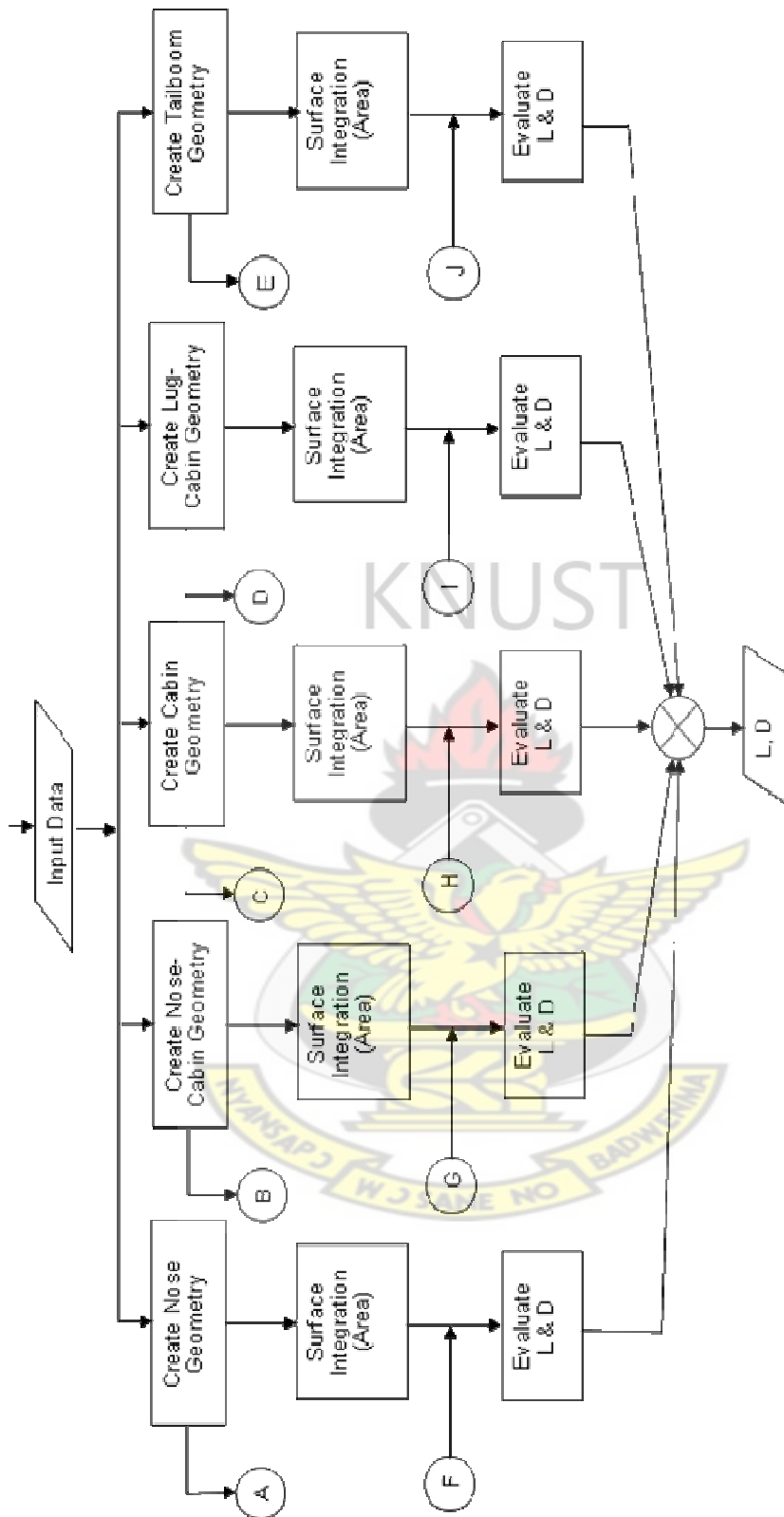


Figure 4.5 Fuselage Component Design Flowchart.

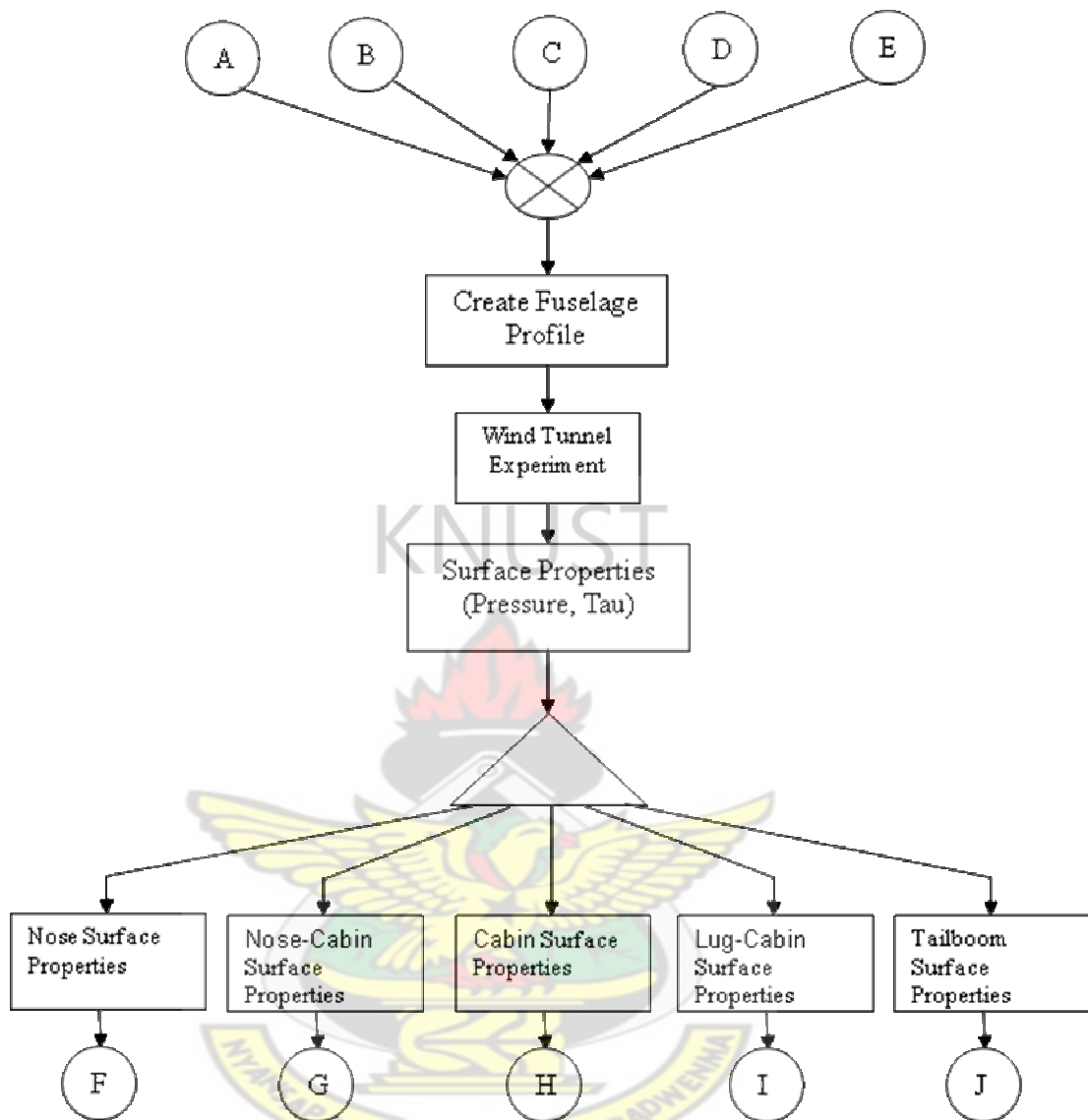


Figure 4.5 Fuselage component Design Flowchart (cont.).

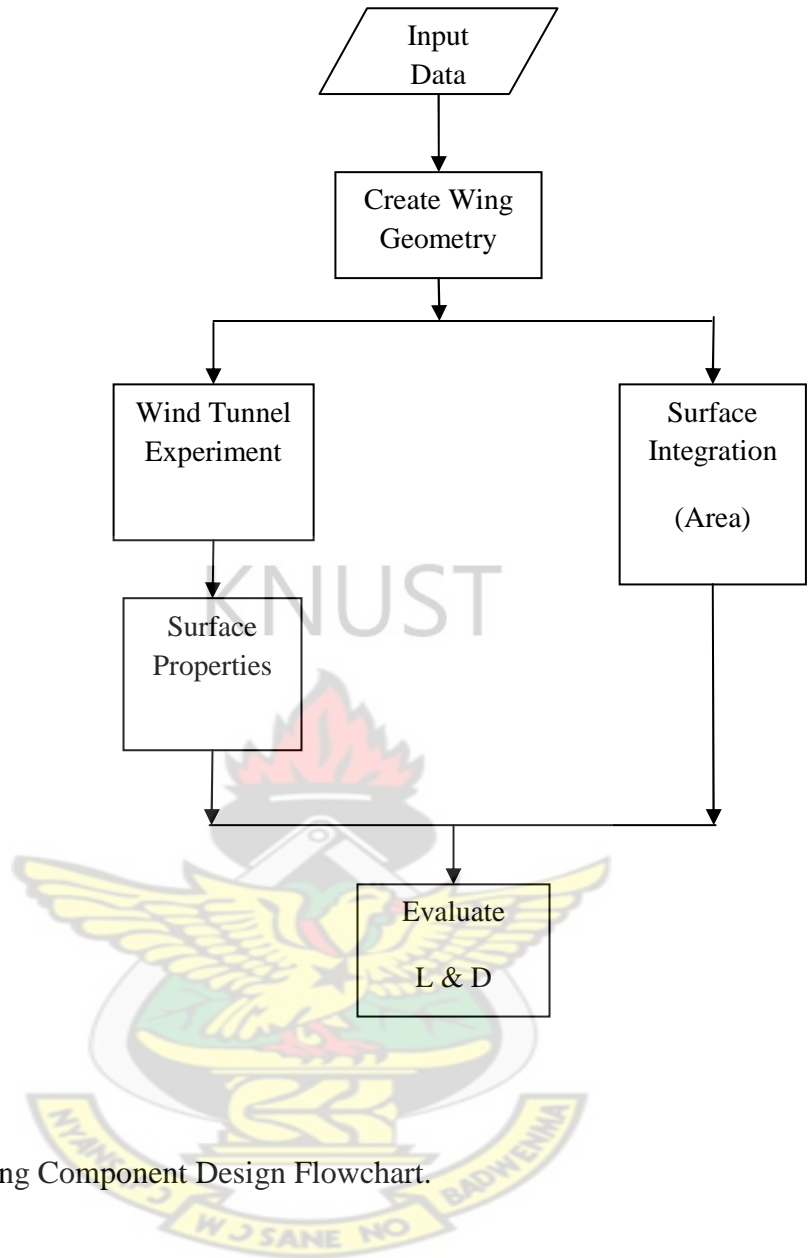


Figure 4.6 Wing Component Design Flowchart.

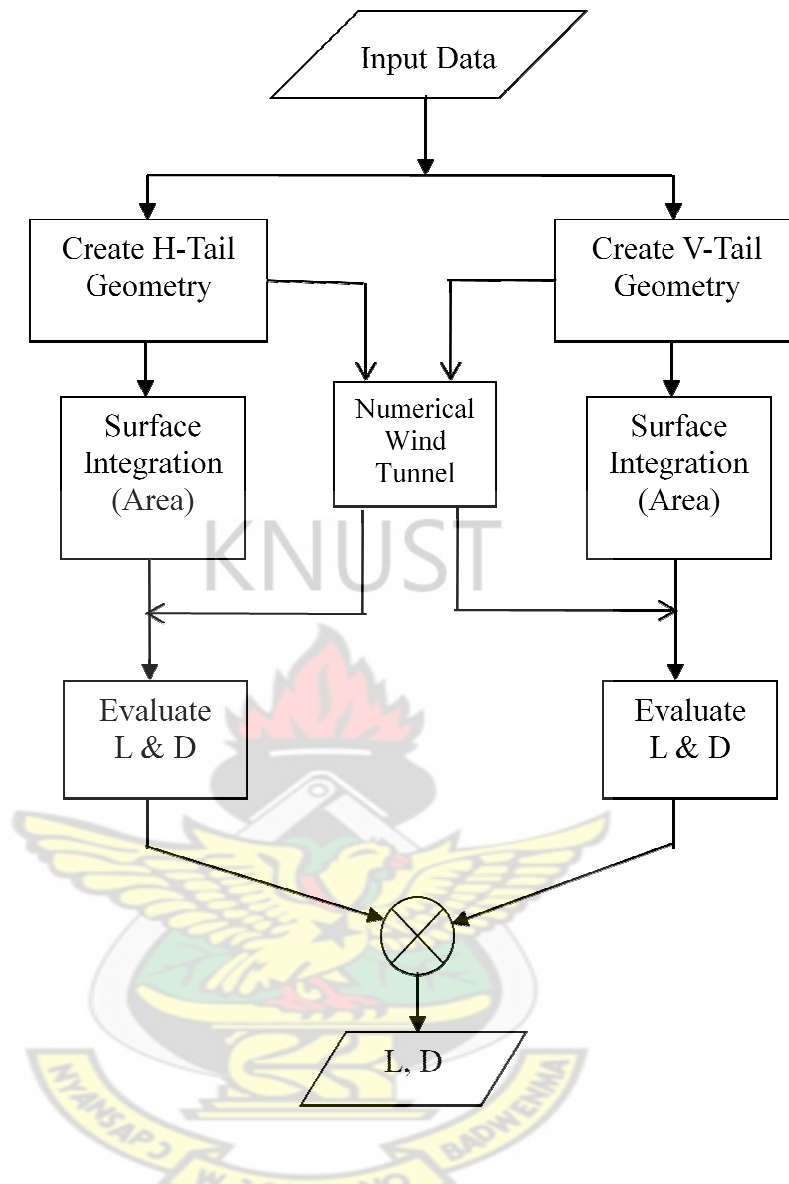


Figure 4.7 Empennage Component Design Flowchart.

4.2.2 Design Parameters

The design parameters are the parameters which when specified completely describe the shape and size of the aircraft configuration. The design parameters, α , are defined as ratios of various geometric lengths to aircraft length. For the fuselage, the nose is completely described by one fixed parameter three and design parameters α_1 , α_2 and

α_3 , and variation of the design parameters may change the configuration. The nose-cabin interface is defined by three parameter; the cabin by one parameter; the luggage cabin is defined by two parameters and the tail-boom by one parameter. The components of the wing and the empennage are defined by three design parameters each. Figures 4.8 to 4.14 illustrate the design parameters as applied to the components and Table 1 is a list and range of the parameters. It should be noted that each object is defined by both design parameters as indicated on the figures and fixed parameters. As an example, the nose-cabin interface has fixed parameter taken from the nose parameters and the cabin object obtained its fixed parameter from the nose-cabin interface object.

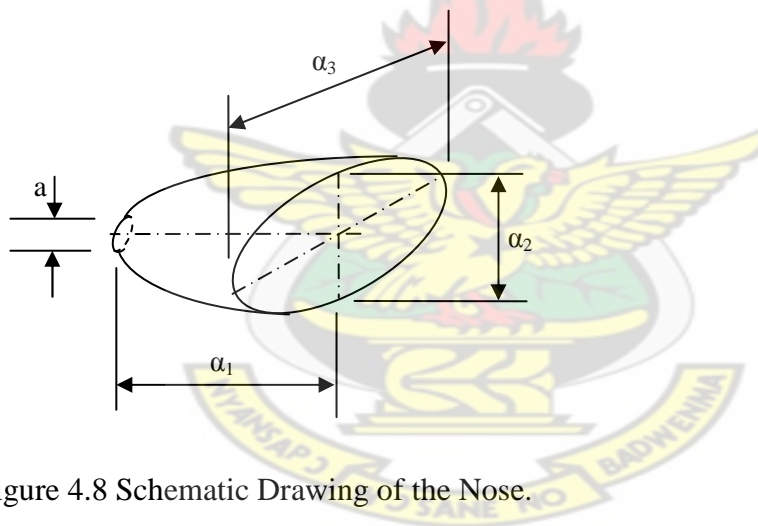


Figure 4.8 Schematic Drawing of the Nose.

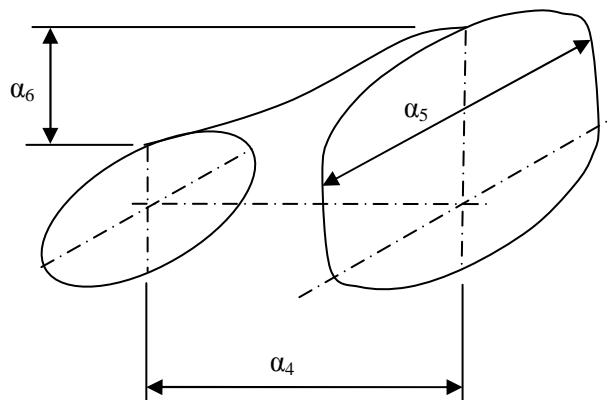


Figure 4.9 Schematic Drawing of the Nose-Cabin Intercept.

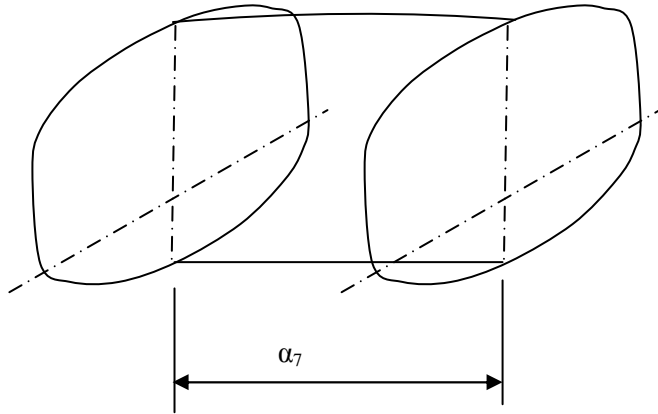


Figure 4.10 Schematic Drawing of the Cabin.

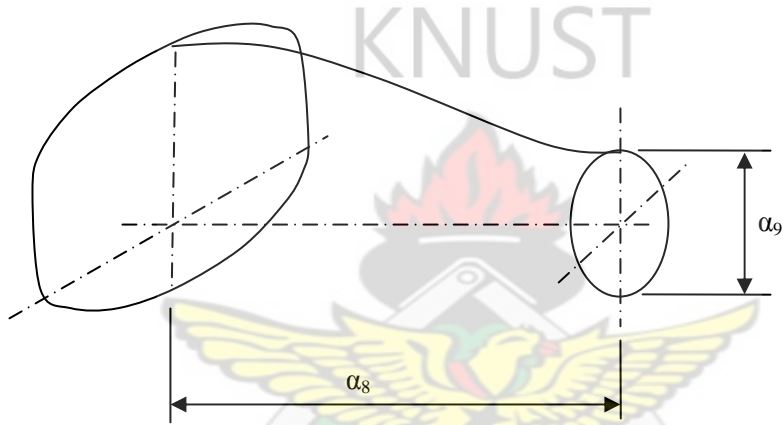


Figure 4.11 Schematic Drawing of the Luggage Cabin.

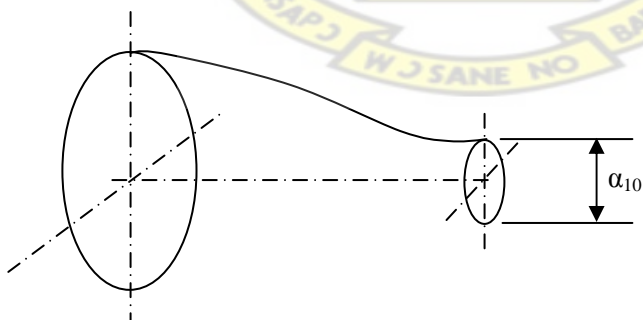


Figure 4.12 Schematic Drawing of the Tail boom.

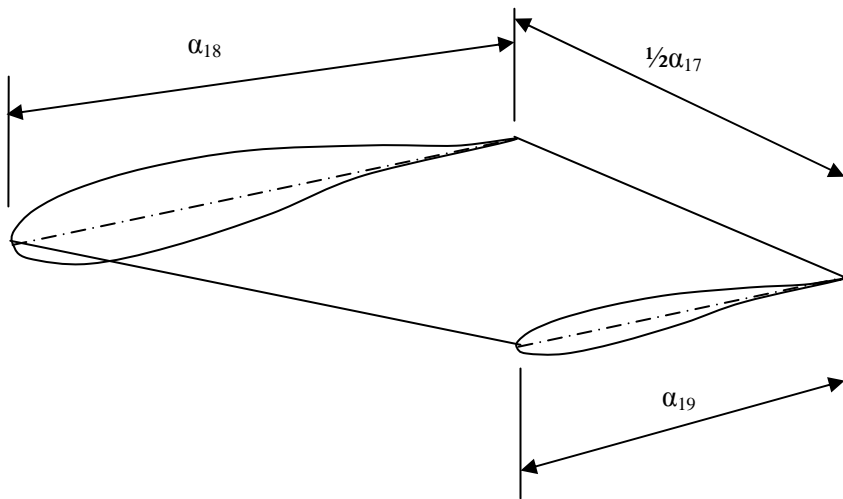


Figure 4.13 Schematic Drawing of the Wing or Horizontal Tail.

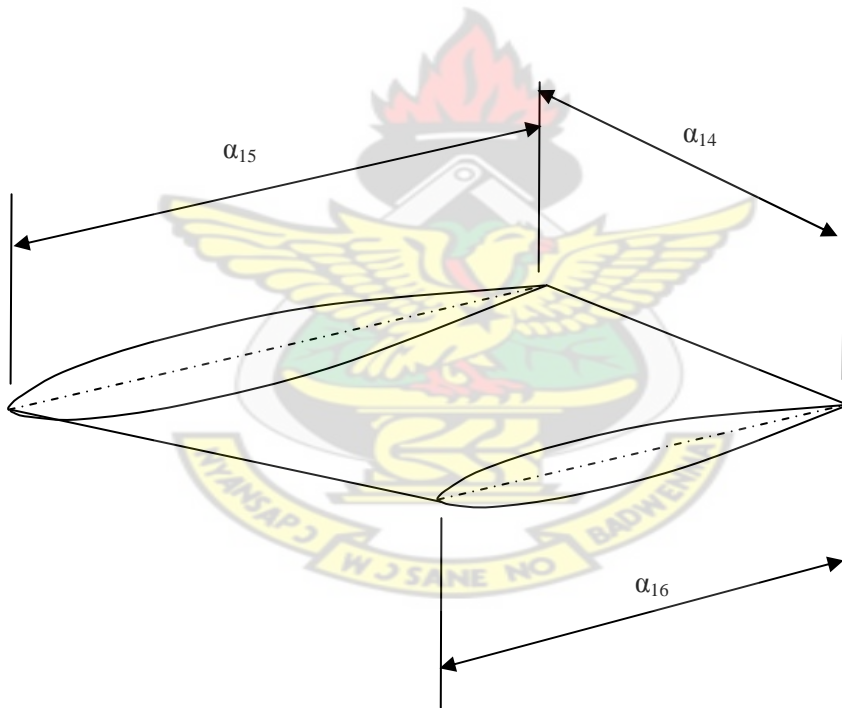


Figure 4.14 Schematic Drawing of the Vertical Tail.

Table 4.1: Fixed and Design Variables.

Component	Fixed Parameter	Controlling Dimension	Design Parameter	Symbol	Range
Aircraft	Length			L	
	Mach Number			M	0.10 – 0.30
	Altitude			A	
Nose	Nose tip diameter	Nose Length	Nose Length to Plane Length ratio	α_1	0.05 – 0.30
	Location	End Height	End Height to Plane Length ratio	α_2	0.05 – 0.20
		End Width	End Width to Plane Length ratio	α_3	1.00 – 2.50
Nose Cabin Interface	Start coordinates (from Nose)	Length	Length to Plane-Length ratio	α_4	0.02 – 0.15
		Width	Height to Width ratio	α_5	1.00 – 3.00
		Offset Height	Offset Height to Length ratio	α_6	0.00 – 0.20
Cabin	Start coordinates (from Nose-Cabin Interface)	Length	Length to Plane- Length ratio	α_7	0.10 – 0.40
Luggage Cabin	Start coordinates (from Cabin)	Length	Length to Plane-Length ratio	α_8	0.1 – 0.25
		End Diameter	End Diameter to Plane-Length ratio	α_9	0.05 – 0.20
Tail	Start coordinates (from Luggage Cabin)	End Diameter	End Diameter to Plane-Length ratio	α_{10}	0.01 – 0.05
Horizontal Tail	Profile	Span	Span to Plane-Length ratio	α_{11}	0.15 – 0.50
	Angle of Attack	Root Chord	Root-Chord to Plane-Length ratio	α_{12}	0.05 – 0.15
	Sweep angle	Tip Chord	Tip Chord to Root-Chord ratio	α_{13}	0.25 – 1.00
	Dihedral angle				
Vertical Tail	Profile	Span	Span to Plane-Length ratio	α_{14}	0.07 – 0.25
	Angle of Attack	Root Chord	Root-Chord to Plane-Length ratio	α_{15}	0.05 – 0.15
	Sweep angle	Tip Chord	Tip Chord to Root-Chord ratio	α_{16}	0.25 – 1.00
	Dihedral angle				
Wing	Profile	Span	Span to Plane-Length ratio	α_{17}	0.50 – 2.00
	Angle of Attack	Root Chord	Root-Chord to Plane-Length ratio	α_{18}	0.10 – 0.25
	Sweep angle	Tip Chord	Tip Chord to Root-Chord ratio	α_{19}	0.25 – 1.00
	Dihedral angle				

4.2.3 Sample Aircraft Geometry

The design parameters selected are used to generate sample plane geometries as illustrated in figures 4.15 to 4.20.

Table 4.2 Sample Design parameters for illustration in figures 4.15 to 4.20.

Sample	#1	#2	#3	#4	#5	#6
Nose Length to Plane Length ratio	0.100	0.100	0.100	0.100	0.100	0.100
Nose End Height to Plane Length ratio	0.100	0.100	0.100	0.150	0.120	0.100
Nose End Width Plane Length Ratio	0.120	0.120	0.100	0.150	0.130	0.120
Nose Cabin Length to Plane Length Ratio	0.100	0.100	0.100	0.100	0.150	0.100
NoseCabin Offset Height to Length Ratio	0.030	0.010	0.000	0.000	0.060	0.035
Nose Cabin End Width to Plane Length Ratio	0.140	0.140	0.100	0.150	0.150	0.140
Cabin Length to Plane Length Ratio	0.250	0.250	0.250	0.400	0.300	0.250
Luggage Cabin Length to Plane Length Ratio	0.300	0.200	0.200	0.200	0.100	0.400
Luggage Cabin End Diameter to Plane Length Ratio	0.060	0.020	0.060	0.150	0.050	0.120
Tailboom End Diameter to Plane Length Ratio	0.010	0.010	0.010	0.010	0.010	0.010
Horizontal tail Root Chord to Plane Length Ratio	0.100	0.100	0.100	0.100	0.100	0.100
Horizontal tail Tip To Root Chord Ratio	0.500	0.500	0.500	0.500	0.500	0.500
Horizontal Tail Span To Plane Length Ratio	0.200	0.200	0.200	0.200	0.300	0.200
Vertical Tail Root Chord to Plane Length Ratio	0.100	0.100	0.100	0.100	0.100	0.100
Vertical tail Tip To Root Chord Ratio	0.500	0.500	0.500	0.500	0.500	0.500
Vertical tail Span To Plane Length Ratio	0.100	0.100	0.100	0.100	0.100	0.100
Wing Root Chord Plane Length Ratio	0.200	0.300	0.300	0.300	0.300	0.200
Wing Tip To Root Chord Ratio	0.500	0.700	1.000	0.300	0.300	0.500
Wing Span To Plane Length Ratio	1.500	1.500	1.500	1.500	1.500	1.500
Wing Profile	NACA 1412	NACA 2412	NACA 2424	NACA 2410	NACA 2410	NACA 0024

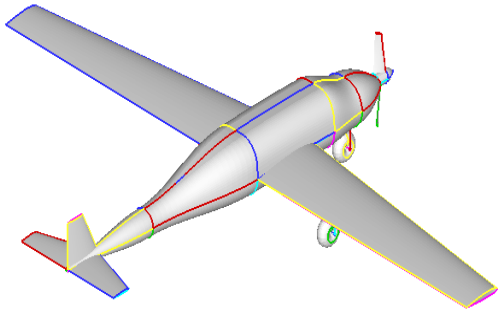


Figure 4.15 Aircraft Geometry Sample #1

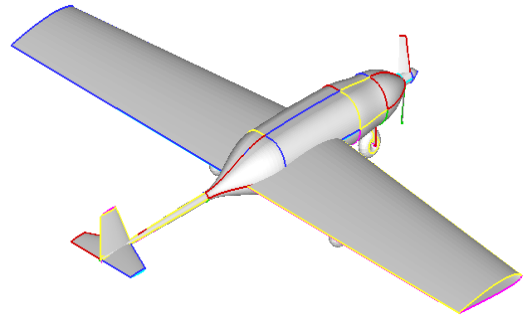


Figure 4.16 Aircraft Geometry Sample #2

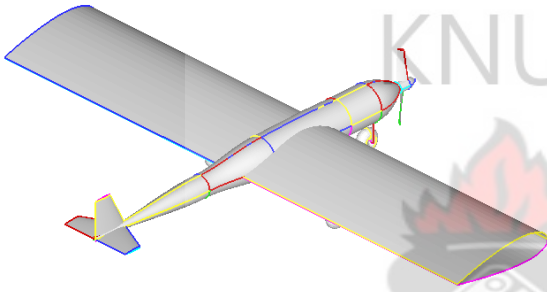


Figure 4.17 Aircraft Geometry Sample #3

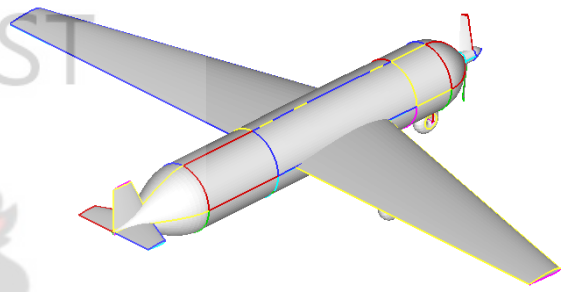


Figure 4.18 Aircraft Geometry Sample #4

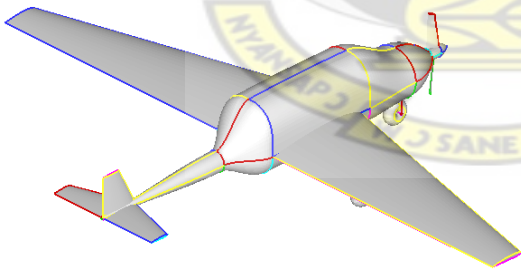


Figure 4.19 Aircraft Geometry Sample #5

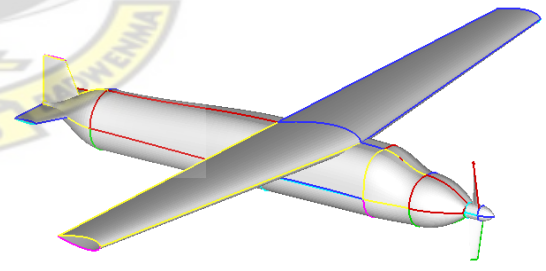


Figure 4.20 Aircraft Geometry Sample #6

4.3 AERODYNAMICS ANALYSIS

With the development of the geometric configuration or shape of the aircraft, aerodynamic analysis can be performed. Aerodynamics analysis is the process of determining the properties of the flow around an object. These properties may include the velocity and pressure. The final results of the aerodynamic analysis may be the aerodynamic forces.

The aerodynamic analysis undertaken in this research is achieved by first developing a numerical wind tunnel which is used as an experimental tool to determine the velocity distribution over the surface of the object. With appropriate equations, pressures acting on the surfaces are computed, leading to the lift and drag force determination.

4.3.1 Numerical Wind Tunnel Development

A wind tunnel is a research tool developed to assist in studying the effects of air moving over or around solid objects. In aerodynamic studies, most experiments are conducted in wind tunnels to determine the performance characteristics. The lift and drag characteristics of airfoil are determined experimentally using wind tunnel experiments. In like manner, the numerical wind tunnel is developed mainly to determine the velocity or pressure distribution around the object surface. This is, however, valid for incompressible flow regime. The Laplace equation is employed.

The Laplace equation for two dimensional flows is given by

$$\nabla^2\psi = 0 \quad \text{or} \quad \frac{\partial\psi^2}{\partial x^2} + \frac{\partial\psi^2}{\partial y^2} = 0 \quad (4.1)$$

Boundary conditions:

$$\text{Outer boundary: } \Psi(x, y) = f(x, y) = \text{Constant} \quad (4.2)$$

$$\text{Inner boundary: } \Psi(x, y) = 0.0 \quad (4.3)$$

A well posed partial differential equation as presented can be solved by numerical methods. A method presented by Thompson et al, (1974) is employed to determine the velocity distribution over the prescribed object boundary.

4.3.2 Flow Field Generation

An integral part of the aerodynamic analysis involves the flow field generation. The stream function described by the Laplace equation is an elliptic partial differential equation and any available method for solving the elliptic equation may be applicable.

Using curvilinear boundary fitting technique developed by Thompson et al, (1974), the physical elliptic grid (Figure 3.5) is transformed into a rectangular grid (Figure 3.6) with square grid spacing. Figure 4.21 is sample generated physical grid system.

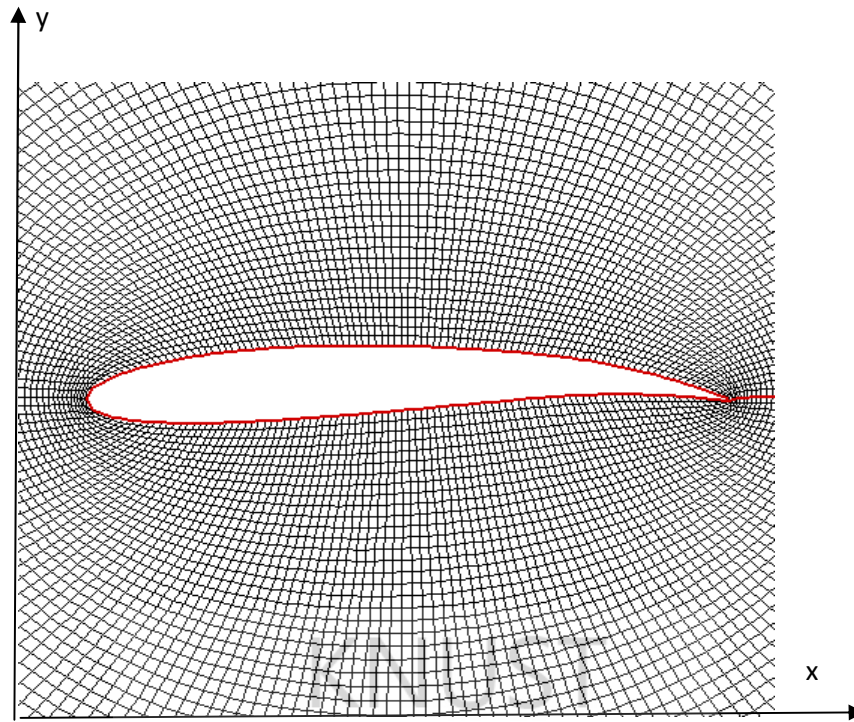


Figure 4.21 Sample generated physical Plane with Grid.

The Governing Equation of interest $\nabla^2\psi = 0$ is transformed into

$$\alpha \frac{\partial^2 \psi}{\partial \xi^2} - 2\beta \frac{\partial^2 \psi}{\partial \xi \partial \eta} + \gamma \frac{\partial^2 \psi}{\partial \eta^2} = 0 \quad (4.4)$$

The boundary conditions are given according to Thompson et al (1974) as

$$\psi(\xi, \eta) = 0 \quad (4.5)$$

at the object or inner boundary, and as

$$\psi(\xi, \eta) = U_{\infty} y(\xi, \eta) \cos \theta - U_{\infty} x(\xi, \eta) \sin \theta \quad (4.6)$$

at far field or outer boundary

Figures 4.22 - 4.25 are illustrations of the solution to the stream function equation as applied to airfoil and fuselage profiles respectively.

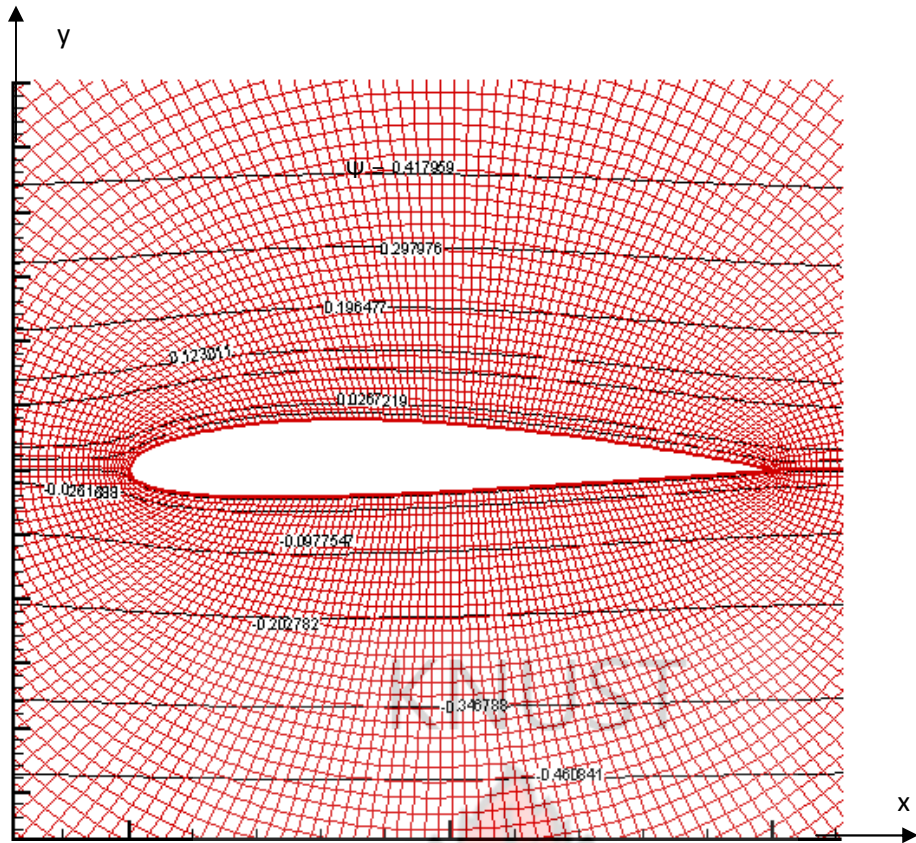


Figure 4.22 Stream line plot for wing section (NACA 2412) at AoA = 0.0.

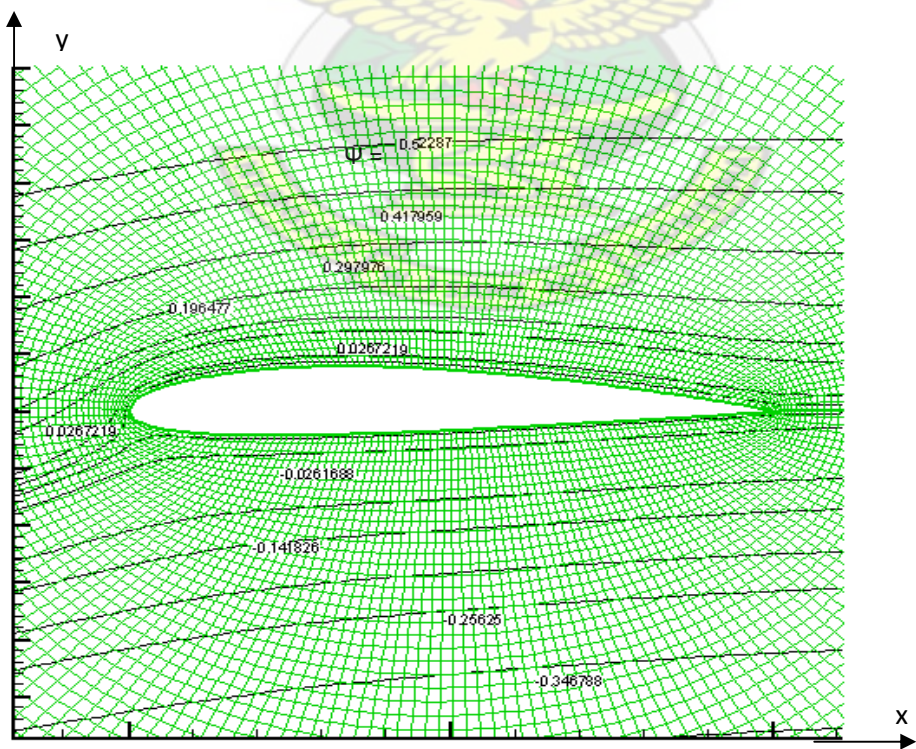


Figure 4.23 Stream line plot for wing section (NACA 2412) at AoA = 3.0.

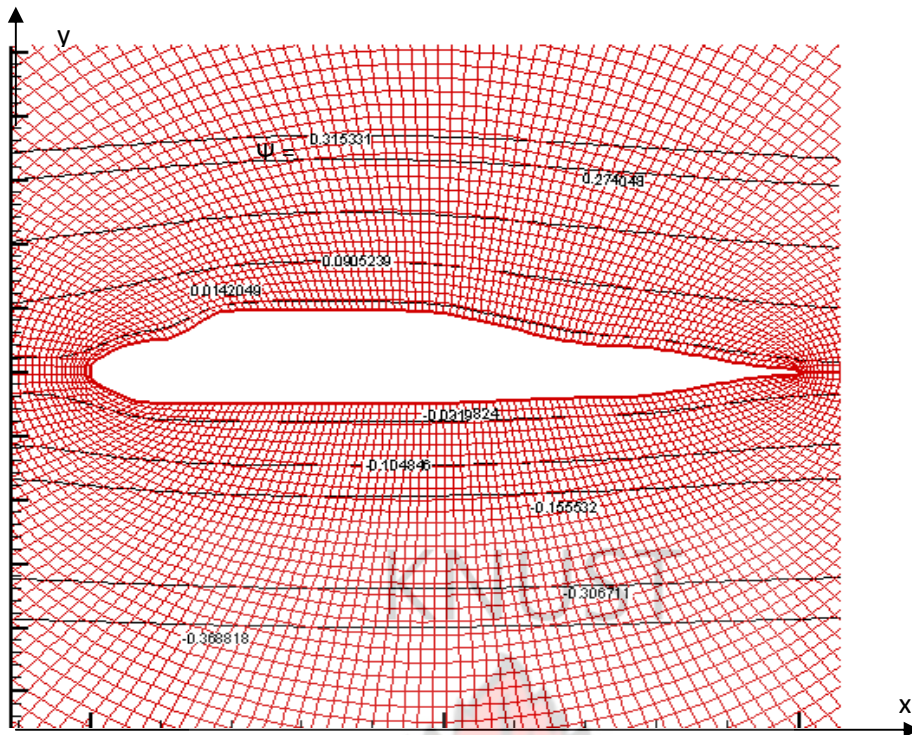


Figure 4.24 Stream line plot for Fuselage section at AoA = 0.0.

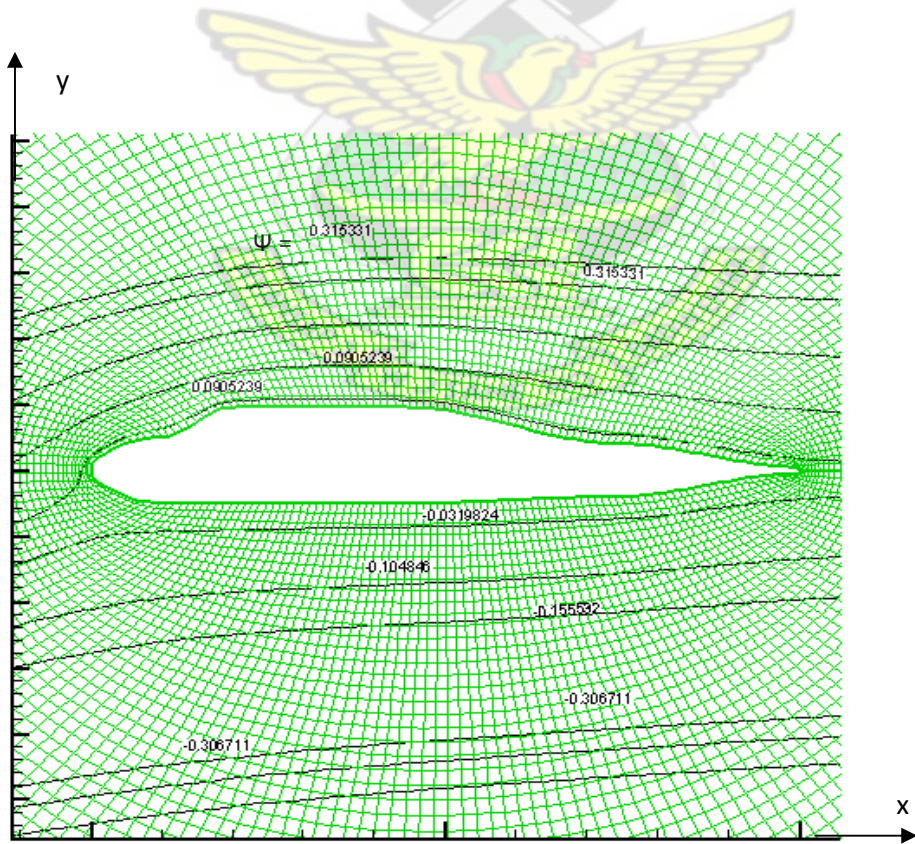


Figure 4.25 Stream line plot for Fuselage section at AoA = 3.0.

Computation of the velocity distribution over the boundary surface is achieved by considering the normal derivative at the boundary as

$$\frac{\partial f}{\partial n} = \frac{1}{J(1+(g')^2)^{1/2}} \left[\frac{\partial f}{\partial \xi} \left(g' \frac{\partial y}{\partial \eta} + \frac{\partial x}{\partial \eta} \right) - \frac{\partial f}{\partial \eta} \left(g' \frac{\partial y}{\partial \xi} + \frac{\partial x}{\partial \xi} \right) \right] \quad (4.7)$$

Where $g' = \frac{dy}{dx}$ at the object boundary and J is Jacobian.

The velocity at the boundary is therefore evaluated by

$$V = \frac{\partial \psi}{\partial n} = \frac{1}{J(1+(g')^2)^{1/2}} \left[\frac{\partial \psi}{\partial \xi} \left(g' \frac{\partial y}{\partial \eta} + \frac{\partial x}{\partial \eta} \right) - \frac{\partial \psi}{\partial \eta} \left(g' \frac{\partial y}{\partial \xi} + \frac{\partial x}{\partial \xi} \right) \right] \quad (4.8)$$

4.3.3 Numerical Wing Tunnel Code Validation

In order to be sure of the validity of the results obtained from the code, it should be validated. The validation is done by comparing the results with similar independent results or established data. The velocity distribution result in the form $(v/v_0)^2$ is compared with that from wing profile catalog (Abbott and Von Doenhoff, 1959). The result shows a satisfactory comparison as illustrated in Figures 4.26 to 4.28. Figures 4.29 to 4.32 are typical results of airfoil profile and fuselage profile at indicated angle of attack obtained from the code.

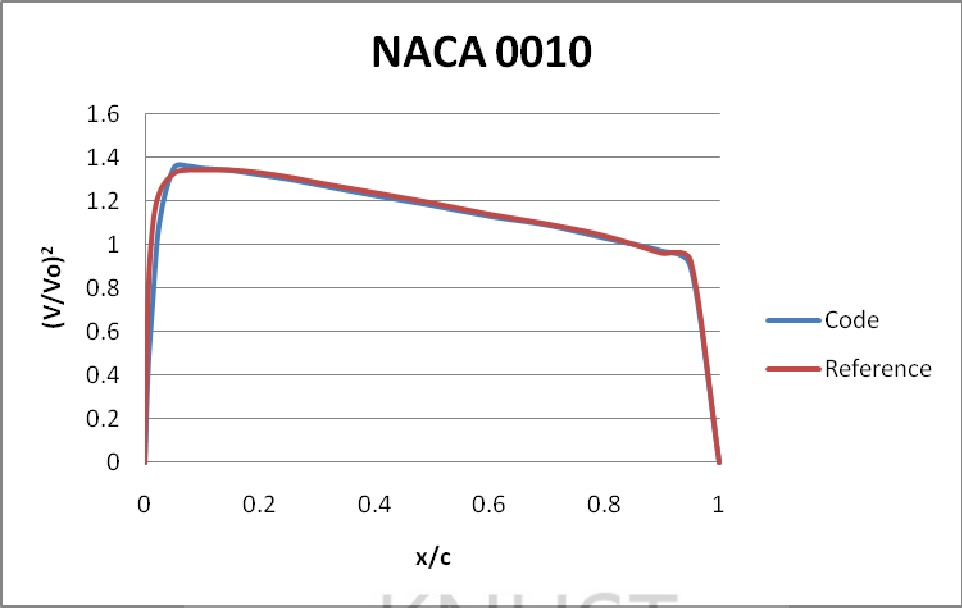


Figure 4.26 NACA 0010 at AoA = 0.0 Compared with Reference data.

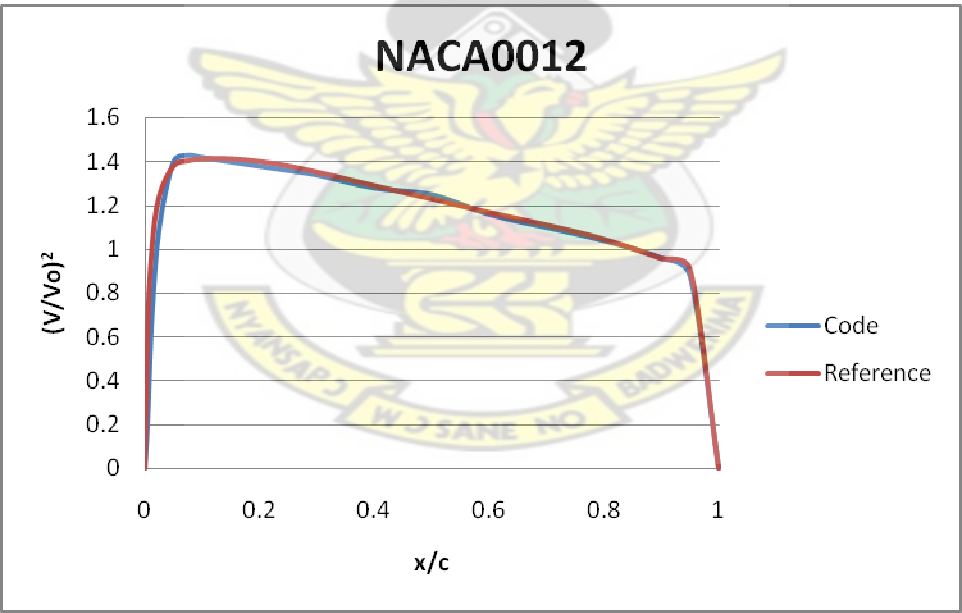


Figure 4.27 NACA 0012 at AoA = 0.0 Compared with Reference data.

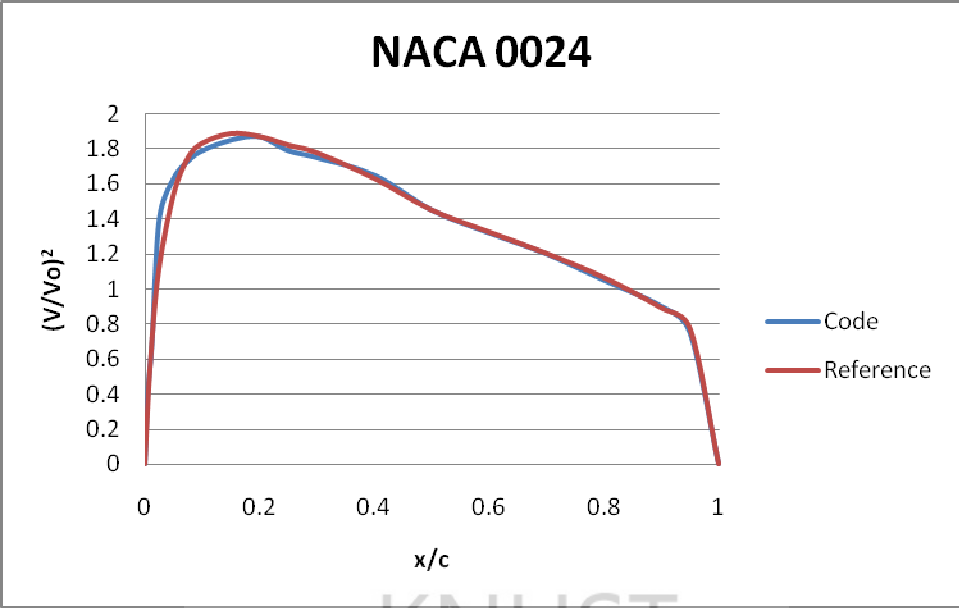


Figure 4.28 NACA 0024 at AoA = 0.0 Compared with reference data.

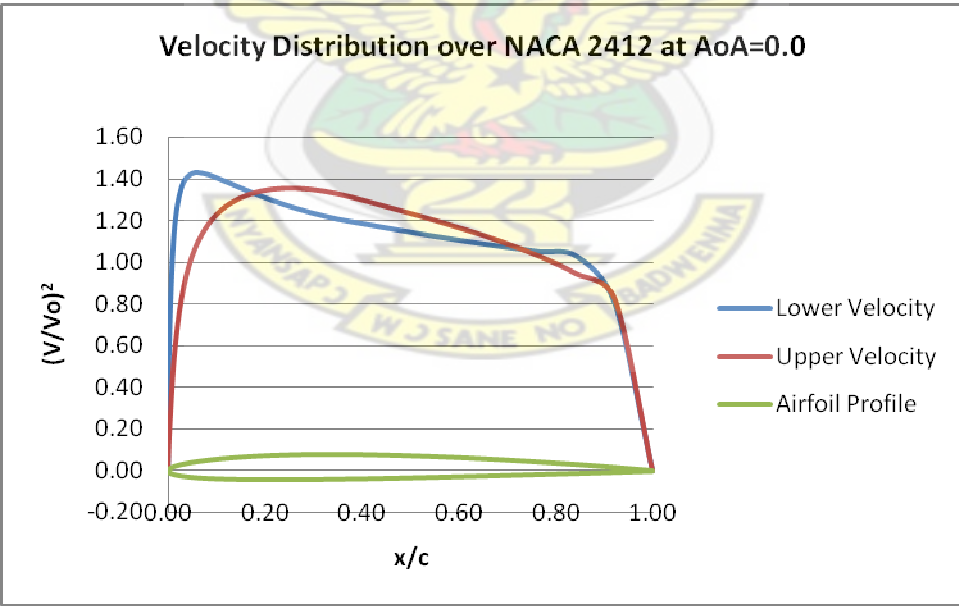


Figure 4.29 Typical velocity distribution over NACA 2412 at AoA = 0.0.

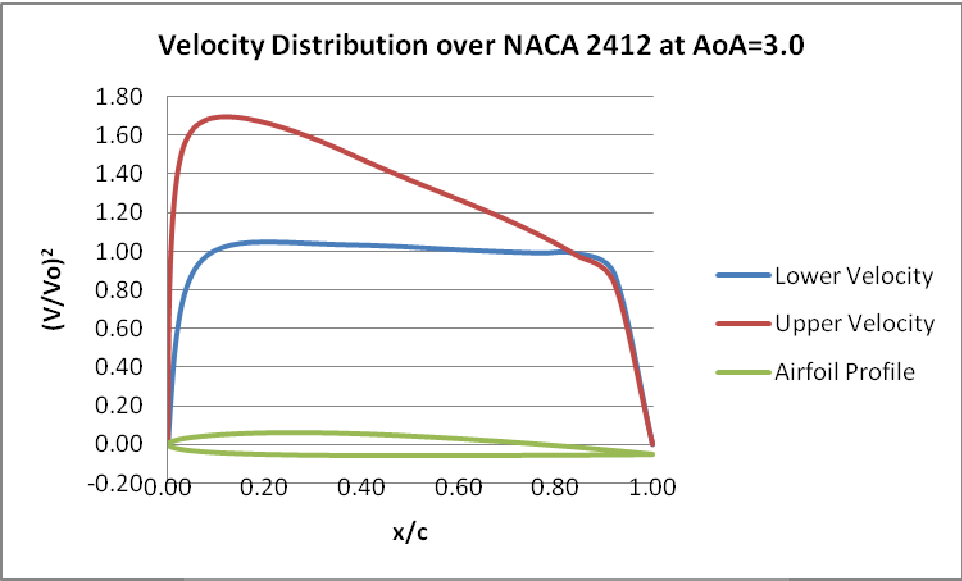


Figure 4.30 Typical velocity distribution over NACA 2412 at AoA = 3.0.

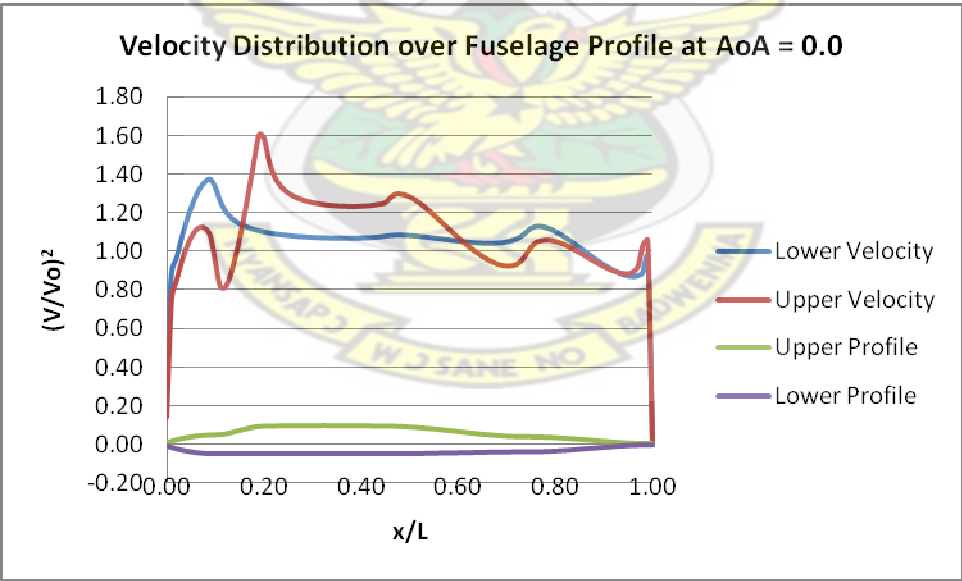


Figure 4.31 Typical velocity distribution over fuselage profile at AoA = 0.0.

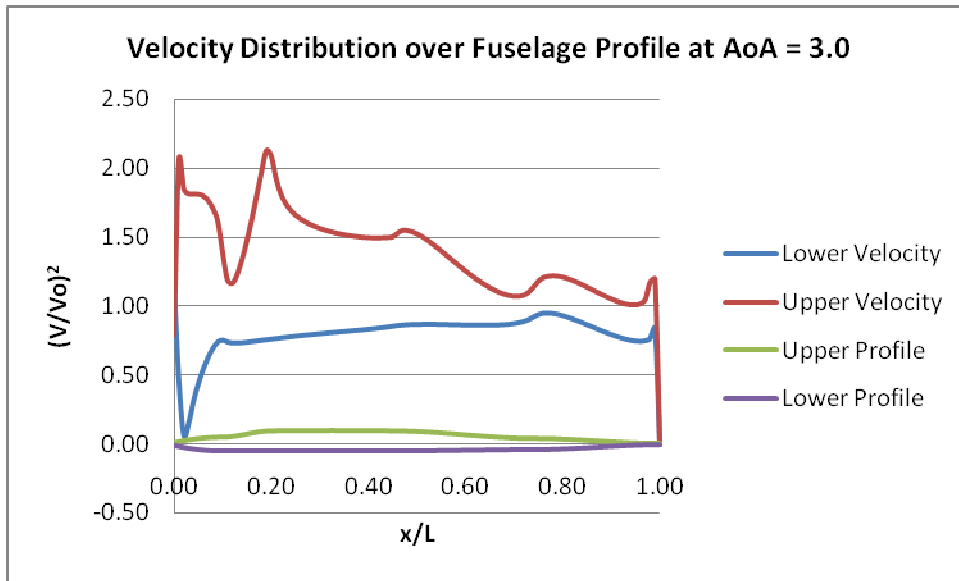


Figure 4.32 Typical velocity distribution over fuselage profile at AoA = 3.0.

4.4 THE PRESSURE DISTRIBUTION

The development of force resulting in lift and drag experienced by an object moving through the air is mainly from associated pressure imparted on the object through the interaction between the fluid flow and the object. The aerodynamic pressure developed by fluid flow is related to the flow velocity. With the velocity distribution obtained, the pressure coefficient and/or pressure distribution over the object surface could be evaluated. The Pressure coefficient, C_p , is given by

$$C_p = \frac{P - P_\infty}{q_\infty} \quad (4.9)$$

Where q_∞ is the dynamic pressure and

$$q_\infty = \frac{\rho_\infty V_\infty^2}{2} \quad (4.10)$$

For incompressible flow, C_p can be expressed in terms of the velocity only. By

$$\text{Bernoulli's equation } P - P_\infty = \frac{\rho(V_\infty^2 - V^2)}{2}$$

$$C_p = \frac{P - P_\infty}{q_\infty} = \frac{\frac{1}{2}\rho(V_\infty^2 - V^2)}{\frac{1}{2}\rho V_\infty^2} \quad (4.11)$$

$$C_p = 1 - \left(\frac{V}{V_\infty}\right)^2$$

$$\text{Also } P - P_\infty = \frac{1}{2}\rho V_\infty^2 \left(1 - \frac{V^2}{V_\infty^2}\right) \quad (4.12)$$

It should be noted that the expression of C_p was used for validation in figures 4.26 to 4.28.

4.5 THE SHEAR STRESS

The shear stress is developed as a result of boundary layer effect on bounding or wall surfaces. By applying the boundary layer approximation, the flow is considered to be of two portions, an inviscid portion (which is easy to solve by a number of methods) and the boundary layer portion (which is governed by an easier to solve partial differential equation. Blasius Solution of the Boundary layer equations on a flat plate could be used for boundary layer portion of the flow.

The skin friction coefficient is the non-dimensional wall shear expressed as

$$C_f = \frac{\tau_{wall}}{\frac{1}{2}\rho V_\infty^2}$$

$$\text{Therefore } \tau_{wall} = \frac{\rho V_\infty^2}{2} C_f \quad (4.13)$$

$$c_f = f(\text{Re})$$

$$\tau = \frac{\rho V_\infty^2}{2} c_f$$

The skin friction coefficient C_f distribution along the streamlines that form the aircraft configuration is evaluated using the reference temperature method. For laminar flow, the local skin friction is given by:

$$c_f = \frac{0.664}{\sqrt{\text{Re}}} \left(\frac{T'}{T_\infty} \right)^{(\omega-1)/2} \quad (4.14)$$

where Re is the local Reynolds number defined as:

$$\text{Re} = \frac{\rho_\infty v_\infty s}{\mu_\infty}$$

where v_∞ , μ_∞ and ρ_∞ are freestream quantities and s is the local distance measured from the leading edge. T' is some reference temperature which is however, same as freestream temperature, T_∞ , at the conditions of interest (isothermal condition).

Equation 4.15 therefore become

$$C_f = \frac{0.664}{\sqrt{\text{Re}}} \quad (4.15)$$

In the case of turbulent flow, the local skin friction is evaluated in accordance with the relationship:

$$C_f = \frac{0.0592}{\text{Re}^{0.2}} \quad (4.16)$$

4.6 SURFACE/WETTED AND PROJECTED AREA

Pressure is defined as the force per unit area acting normal to the surface. The various computations yield the pressure of the fluid acting on the given surface. The resulting force in the form of Lift and Drag can now be obtained as a result of the product of the experienced pressure and the surface area. The aircraft shapes are often not shapes of which the area can be easily calculated. As such an integral part of the aerodynamic analysis involves the evaluation of the surface area. This involves the estimation of the projected platform area, frontal and side areas. The surface area is determined numerically using Heron's formula for area of a triangle given in equation 4.18. The Surface area, A , is computed through surface integration.

$$\Delta_{area} = \sqrt{S(S - ab)(S - bc)(S - ac)} \quad (4.17)$$

Where ab , bc , and ac are the side lengths of the triangle and S is the semi-perimeter. The area A is the sum of elementary areas dA as

$$A = \sum_i dA \quad (4.18)$$

In evaluating the area of an arbitrary elementary surface, four grid points A , B , C , and D , located on the surface are considered. The approximate area enclosed by these four surface points can be considered as the sum of the areas generated by the two triangles, Δ_1 and Δ_2 , also formed by these points. The perimeter of the two triangles Δ_1 and Δ_2 , are considered to be S_1 and S_2 given by the following expressions.

$$S_1 = \frac{1}{2}(AB + BC + AC)$$

and

$$S_2 = \frac{1}{2}(AD + CD + AC) \quad (4.19)$$

Where AB , BC , AC are the lengths of the sides of the triangle Δ_1 and AD , CD , AC are the lengths of the sides of the triangle Δ_2 .

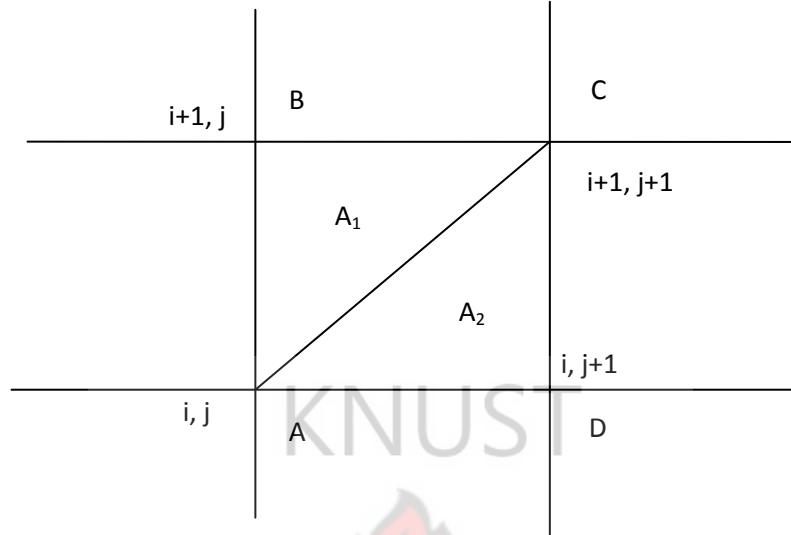


Figure 4.33 Illustration of elemental surface area.

With the given coordinates, the lengths of the sides can be calculated as follow (Figure 4.33):

$$|AB| = \sqrt{(x_{i+1,j} - x_{i,j})^2 + (y_{i+1,j} - y_{i,j})^2 + (z_{i+1,j} - z_{i,j})^2} \quad (4.20)$$

$$|AD| = \sqrt{(x_{i,j+1} - x_{i,j})^2 + (y_{i,j+1} - y_{i,j})^2 + (z_{i,j+1} - z_{i,j})^2} \quad (4.21)$$

$$|AC| = \sqrt{(x_{i+1,j+1} - x_{i,j})^2 + (y_{i+1,j+1} - y_{i,j})^2 + (z_{i+1,j+1} - z_{i,j})^2} \quad (4.22)$$

$$|CD| = \sqrt{(x_{i,j+1} - x_{i+1,j+1})^2 + (y_{i,j+1} - y_{i+1,j+1})^2 + (z_{i,j+1} - z_{i+1,j+1})^2} \quad (4.23)$$

$$|BC| = \sqrt{(x_{i+1,j+1} - x_{i+1,j})^2 + (y_{i+1,j+1} - y_{i+1,j})^2 + (z_{i+1,j+1} - z_{i+1,j})^2} \quad (4.24)$$

The area of the triangles can be evaluated using the trigonometric expressions

$$A_1 = \sqrt{S_1(S_1 - AB)(S_1 - BC)(S_1 - AC)} \quad (4.25)$$

And

$$A_2 = \sqrt{S_2(S_2 - AD)(S_2 - CD)(S_2 - AC)} \quad (4.26)$$

Where A_1 and A_2 are area of triangle Δ_1 and Δ_2 , respectively. The area of the surface element $dA = A_1 + A_2$

The total surface area A is computed as the sum of elemental areas (Figure 4.34). In order to validate the result of the surface integration routine, known simple shape surfaces like quarter cylinder, semi cylinder, quarter cone and quarter truncated cone are created. The routine is used to evaluate the surface and projected areas. This is compared with result from known relations. The maximum error from this is 0.003236 (0.103%) with semi cylindrical surface. Tables 4.3 to 4.6 show the surface integration validation results for Quarter Cylinder, Quarter Truncated Cone, Quarter Cone and Semi Cylinder respectively.

Table 4.3 Validation of surface Integration Routine (Quarter Cylinder).

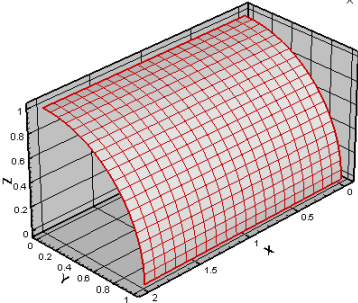
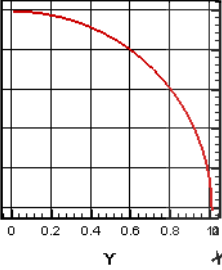
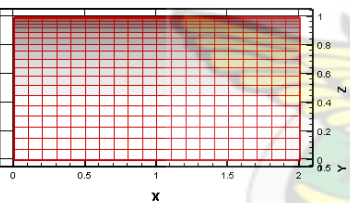
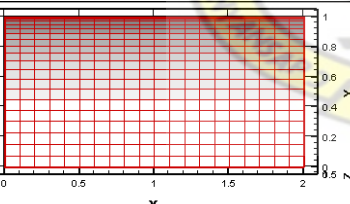
Surface	Plane	Area (Integration)	Area (Exact)	Error
	Surface	3.140791	$A = 2\pi rh/4$ $= 2\pi$ $(1.0)(2.0)/(4.0)$ $= \pi$ $= 3.141592$	0.00081 (0.0258%)
	Y-Z	0.0	0.0	0.0 (0.0%)
	X-Z	2.000004	Rectangular $A = LB$ $= (2.0)(1.0)$ $= 2.0$	0.000004 (0.0002%)
	X-Y	1.999998	Rectangular $A = LB$ $= (2.0)(1.0)$ $= 2.0$	0.000002 (0.0001%)

Table 4.4 Validation of surface Integration Routine (Quarter Truncated Cone).

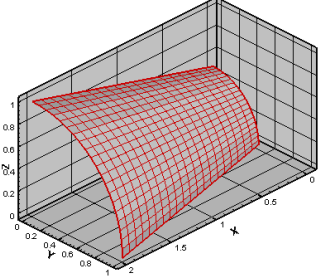
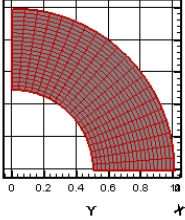
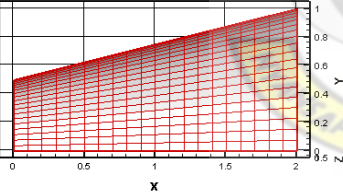
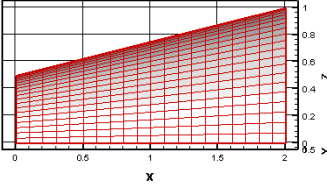
Surface	Plane	Area (Integration)	Area (Exact)	Error
	Surface	2.427975	Truncated Cone $A = ((C_1 + C_2)s/2)/4$ $A = \pi(r_1+r_2)((r_1-r_2)^2+h^2)^{0.5} / 4$ $= \pi(1.0+0.5)(2.0615)/4$ $= 2.42870969$	0.00073469 (0.0302%)
	Y-Z	0.5884430	Circle $A = A_2 - A_1$ $= \pi(r_2^2 - r_1^2)/4$ $= \pi(1.0^2 - 0.5^2)/4$ $= \pi(0.75)/4$ $= 0.58904862$	0.00060562 (0.1028%)
	X-Z	1.5	Trapezium $A = (a+b)h/2$ $= (0.5+1.0)(2.0)/2$ $= 1.5$	0.0 (0.0%)
	X-Y	1.5	Trapezium $A = (a+b)h/2$ $= (0.5+1.0)(2.0)/2$ $= 1.5$	0.0 (0.0%)

Table 4.5 Validation of surface Integration Routine (Quarter Cone).

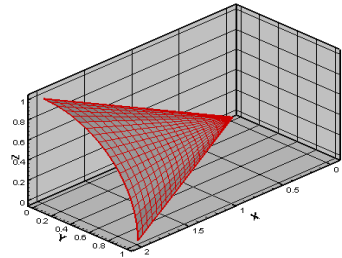
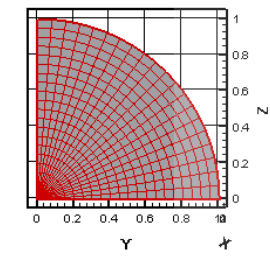
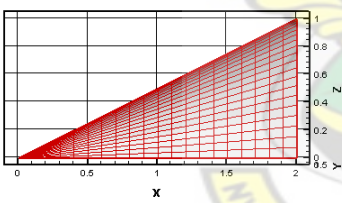
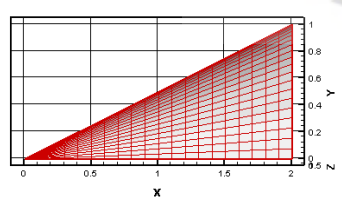
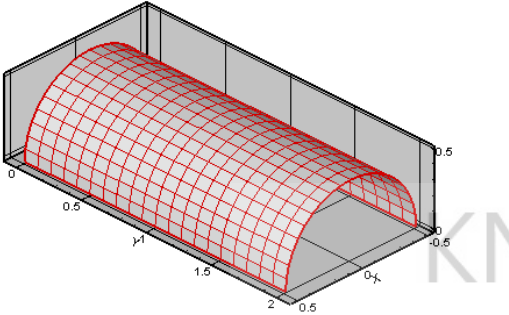
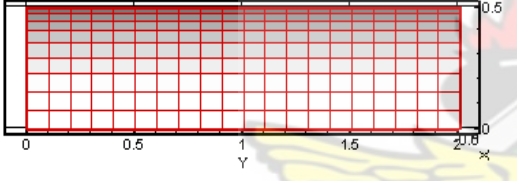
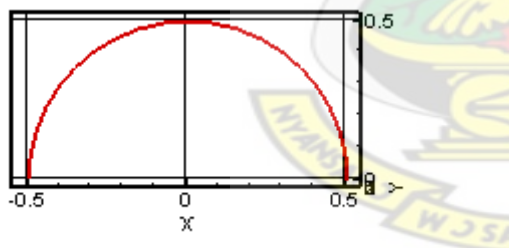
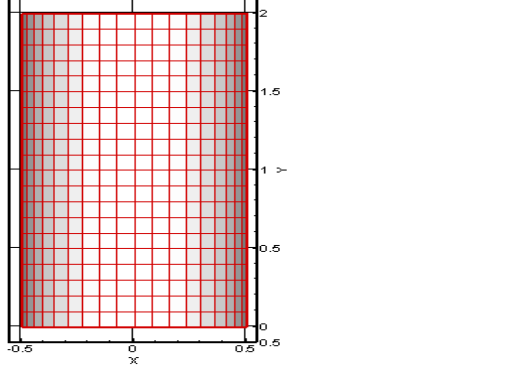
Surface	Plane	Area (Integration)	Area (Exact)	Error
	Surface	1.755482	Cone $A = (\pi r(r^2 + h^2)^{0.5})/4$ $= (\pi(1.0)(1.0^2 + 2^2)^{0.5})/4$ $= 1.756203$	0.000721 (0.041%)
	Y-Z	0.7845909	Circle $A = \pi r^2 / 4$ $= \pi(1.0)^2 / 4$ $= \pi / 4$ $= 0.7853981$	0.0008072 (0.1027%)
	X-Z	1.0	Triangular $A = bh/2$ $= (1.0)(2.0)/2$ $= 1.0$	0.0 (0.0%)
	X-Y	1.0	Triangular $A = bh/2$ $= (1.0)(2.0)/2$ $= 1.0$	0.0 (0.0%)

Table 4.6 Validation of surface Integration Routine (Semi Cylinder).

Surface	Plane	Area (Integration)	Area (Exact)	Error
	Surface	3.138356	$A = 2\pi rh/2$ $= 2\pi$ $(0.5)(2.0)/(2.0)$ $= \pi$ $= 3.141592$	0.003236 (0.103%)
	Y-Z	Front 1.000001 Rear 1.0	Rectangular $A = LB$ $= (1.0)(1.0)$ $= 1.0$	0.000001 (0.0001%) 0.0
	X-Z	0.0	$A = 0.0$	0.0 (0.0%)
	X-Y	2.000001	Rectangular $A = LB$ $= (2.0)(1.0)$ $= 2.0$	0.000001 (0.00005%)

4.7 AERODYNAMIC FORCE ESTIMATION

The inviscid and viscous analyses are conducted using the Euler equation and Boundary layer Equation respectively. The total force acting on the plane surface can be expressed as

$$\vec{F} = f(P, \tau) \quad (4.27)$$

where P is the pressure and τ is the shear stress

The aerodynamic force is obtained through the relation

$$\vec{F} = \left(\sum_s \vec{F}_{xp} + \vec{F}_{x\tau} \right) i + \left(\sum_s \vec{F}_{yp} + \vec{F}_{y\tau} \right) j + \left(\sum_s \vec{F}_{zp} + \vec{F}_{z\tau} \right) k \quad (4.28)$$

The components of the aerodynamic force can be identified such that the Lift is the j component, the Drag the i component, and Side Force the k component.

Lift, Drag, and Side Forces

Each variable in equations 3.46 are now known and thus the forces on the aircraft can be evaluated. Keeping in mind that the Lift is j component, the Drag i component, and Side Force k component, these forces are evaluated as

$$\begin{aligned} L &= \pm P_{avg} A_{xy} \pm \tau_{avg} A_{yz} \pm \tau_{avg} A_{xz} \\ D &= \pm P_{avg} A_{yz} \pm \tau_{avg} A_{xy} \pm \tau_{avg} A_{xz} \end{aligned} \quad (4.29)$$

Where A_{xy} , A_{xz} and A_{yz} are projected areas in the x-y, x-z and y-z planes respectively.

The Side Force is neglected due to the symmetrical design of the aircraft, which causes the Side Forces to cancel each other out.

CHAPTER FIVE

PERFORMANCE ANALYSIS AND RESULTS

5.0 INTRODUCTION

The results of the research are analyzed and presented in this chapter. The results are in two categories. They include overall aircraft performance variation with angle-of-attack and the influence of some of the design parameters on the aerodynamic performance.

5.1 AERODYNAMIC PERFORMANCE

The aerodynamics performance of the aircraft is the Lift and Drag developed as it moves through the air. With the aircraft configuration developed, the numerical wind tunnel developed and validated, it is now possible to perform an aerodynamic performance analysis. The performance analysis will involve the estimation of the lift and drag developed by various object components of the aircraft.

5.2 SAMPLE RESULTS WITH ANGLE OF ATTACK VARIATION

Five sample aircraft geometries are developed with design parameters as illustrated in table 5.1. The performances of these samples are studied with the angle of attack variation. The results are illustrated in figures 5.1 and 5.2 with figures 5.7, 5.10, 5.11, 5.12 and 5.13 showing the configurations of the respective samples. From figure 5.1, the lift performance increases steadily with angle of attack. Sample #2 shows highest lift performance while sample #1 indicates least lift performance. The differences may be attributed to differences in wing profiles used. From figure 5.2, drag

performance shows significant variation. Samples #1 and #3 indicate an increase in drag performance to maximum then followed by a decrease. Samples #2, #4 and #5, however, show decreasing drag performances to minimum then followed by steady increase. The significant differences in the drag performance may be due to wing or fuselage profile differences.

Configurations of samples #1 to #5 were again developed as samples #6 to #10, but with same wing profile of sample #1 (NACA 1412). The design parameter of samples #6 to #10 are shown in Table 5.2. Lift performance results for samples #6 to #10 increase with angle of attack (figures 5.3). Since the wing profiles are the same, the differences in lift may be attributed to contribution from fuselage components shape differences. Drag performance results indicate similar trend as shown in figure 5.4 (compared with samples #1 to #5) but with sample #8 indicating higher drag performances. This infers that the nature of the drag performance is not influenced significantly by the wing (figure 5.4). The magnitude of the drag however, may be affected by different wing profiles. This is illustrated by the case of sample #6 (similar to #1) becoming higher than that of sample #8 (similar to #3 in figure 5.4) which is in contrast with when different wing profiles were used (figure 5.2). Figures 5.16, 5.19, 5.20, 5.21 and 5.22 are the samples #6 - #10 configurations respectively.

Table 5.1 Sample Design Parameters for Samples #1 - #5.

Parameter	#1	#2	#3	#4	#5
Nose Length to Plane Length Ratio	0.100	0.100	0.100	0.100	0.100
Nose End Height to Plane Length Ratio	0.100	0.100	0.100	0.150	0.120
Nose End Width to Plane Length Ratio	0.120	0.120	0.100	0.150	0.130
Nose-Cabin inter Length to Plane Length Ratio	0.100	0.100	0.100	0.100	0.150
Nose-Cabin inter Offset Height to Length Ratio	0.030	0.010	0.000	0.000	0.060
Nose-Cabin End Width to Plane Length Ratio	0.140	0.140	0.100	0.150	0.150
Cabin Length to Plane Length Ratio	0.250	0.250	0.250	0.400	0.300
Luggage Cabin Length to Plane Length Ratio	0.300	0.200	0.200	0.200	0.100
Luggage Cabin End Diameter Plane Length Ratio	0.060	0.020	0.060	0.150	0.050
Tail boom End Diameter to Plane Length Ratio	0.010	0.010	0.010	0.010	0.010
Horizontal tail Root Chord to Plane Length Ratio	0.100	0.100	0.100	0.100	0.100
Horizontal tail Tip to Root Chord Ratio	0.500	0.500	0.500	0.500	0.500
Horizontal tail Span to Plane Length Ratio	0.200	0.200	0.200	0.200	0.300
Vertical tail Root Chord to Plane Length Ratio	0.100	0.100	0.100	0.100	0.100
Vertical Tip to Root Chord Ratio	0.500	0.500	0.500	0.500	0.500
Vertical Span to Plane Length Ratio	0.100	0.100	0.100	0.100	0.100
Wing Root Chord to Plane Length Ratio	0.200	0.300	0.300	0.300	0.300
Wing Tip To Root Chord Ratio	0.500	0.700	1.000	0.300	0.300
Wing Span To Plane Length Ratio	1.500	1.500	1.500	1.500	1.500
Wing Profile	NACA 1412	NACA 2412	NACA 2424	NACA 2410	NACA 2410



Figure 5.1 Lift Performance with different wing profile.

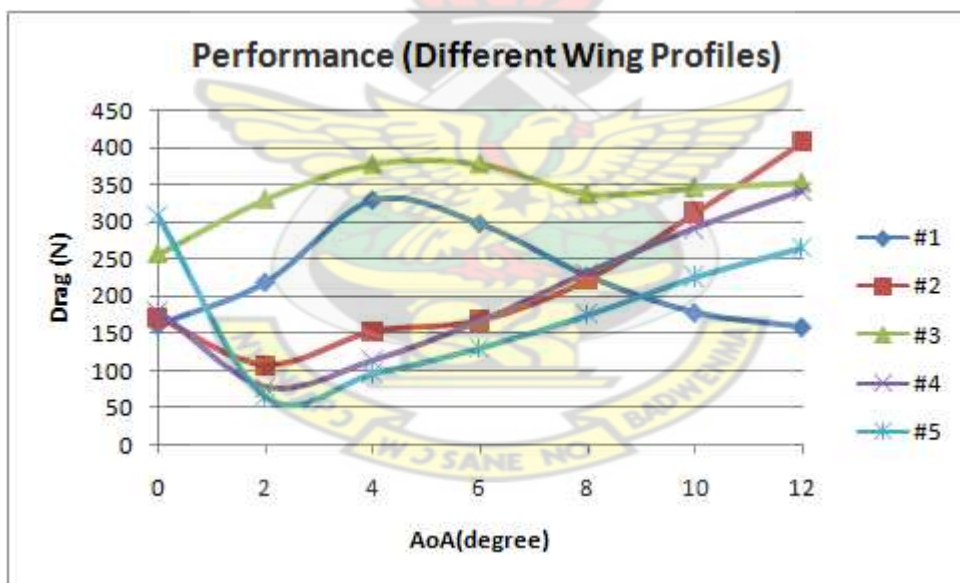


Figure 5.2 Drag Performance with different wing profiles.

Table 5.2 Sample Design Parameters for Samples #6 - #10.

Parameter	#6	#7	#8	#9	#10
Nose Length to Plane Length Ratio	0.100	0.100	0.100	0.100	0.100
Nose End Height to Plane Length Ratio	0.100	0.100	0.100	0.150	0.120
Nose End Width to Plane Length Ratio	0.120	0.120	0.100	0.150	0.130
Nose-Cabin inter Length to Plane Length Ratio	0.100	0.100	0.100	0.100	0.150
Nose-Cabin inter Offset Height to Length Ratio	0.030	0.010	0.000	0.000	0.060
Nose-Cabin End Width to Plane Length Ratio	0.140	0.140	0.100	0.150	0.150
Cabin Length to Plane Length Ratio	0.250	0.250	0.250	0.400	0.300
Luggage Cabin Length to Plane Length Ratio	0.300	0.200	0.200	0.200	0.100
Luggage Cabin End Diameter Plane Length Ratio	0.060	0.020	0.060	0.150	0.050
Tail boom End Diameter to Plane Length Ratio	0.010	0.010	0.010	0.010	0.010
Horizontal tail Root Chord to Plane Length Ratio	0.100	0.100	0.100	0.100	0.100
Horizontal tail Tip to Root Chord Ratio	0.500	0.500	0.500	0.500	0.500
Horizontal tail Span to Plane Length Ratio	0.200	0.200	0.200	0.200	0.200
Vertical tail Root Chord to Plane Length Ratio	0.100	0.100	0.100	0.100	0.100
Vertical Tip to Root Chord Ratio	0.500	0.500	0.500	0.500	0.500
Vertical Span to Plane Length Ratio	0.100	0.100	0.100	0.100	0.100
Wing Root Chord to Plane Length Ratio	0.200	0.200	0.200	0.200	0.200
Wing Tip To Root Chord Ratio	0.500	0.500	0.500	0.500	0.500
Wing Span To Plane Length Ratio	1.500	1.500	1.500	1.500	1.500
Wing Profile	NACA 1412	NACA 1412	NACA 1412	NACA 1412	NACA 1412

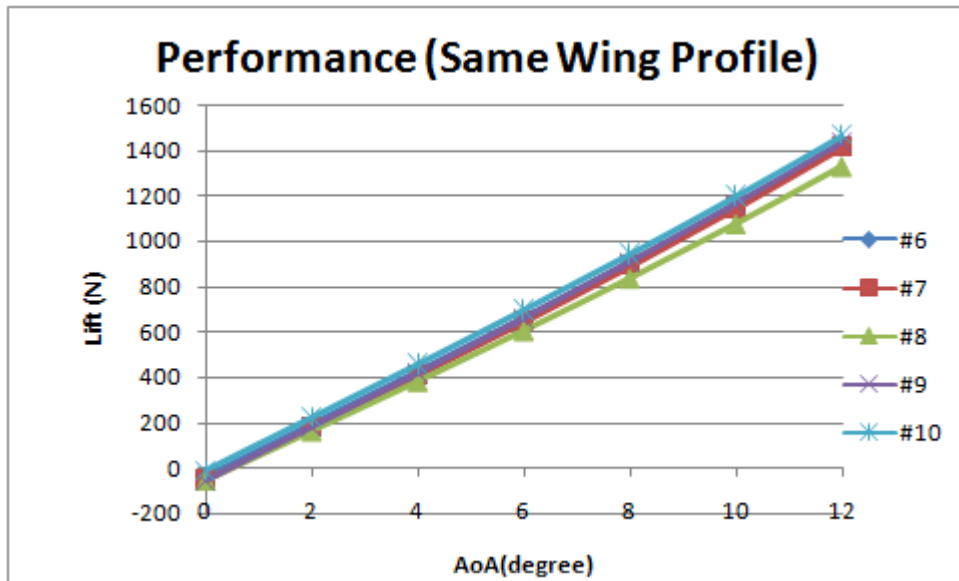


Figure 5.3 Lift Performance with the same wing profile.

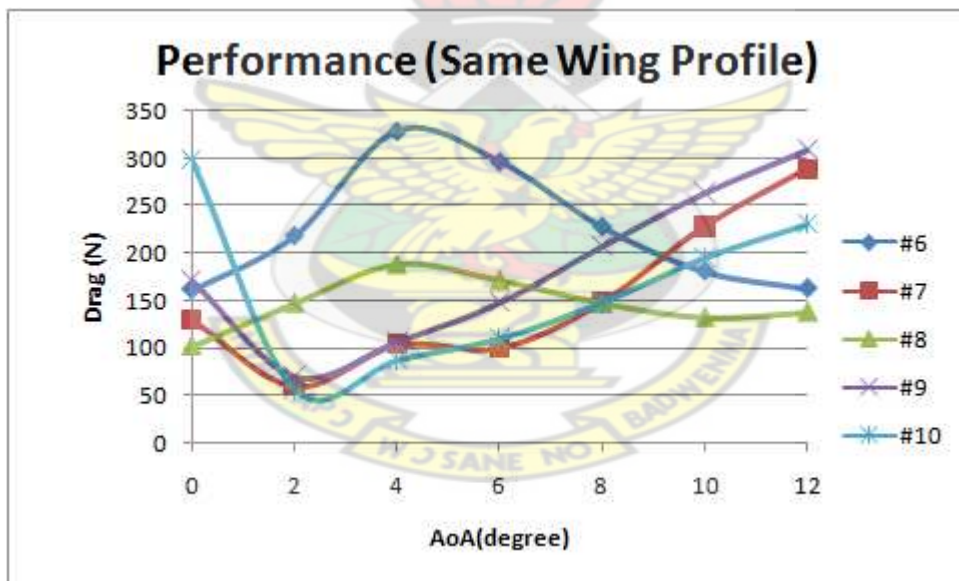


Figure 5.4 Drag Performance with the same wing profile.

The components or objects of the aircraft are expected to contribute to lift and drag performance of the aircraft. Figure 5.5 is the plot of lift performance of each component contributed toward the overall lift performance of the aircraft of sample

#1. The figure shows that major contributor to lift is the wing as expected. It is noted that the contribution by luggage cabin object decreases with increase in angle of attack. Sample #2 also indicates similar trend for the lift performance.

The drag performance contributions from various object components are of varying nature. From figure 5.6, drag performance of the wing increases with increase in angle of attack as expected. Notable component is the luggage cabin drag performance. For sample #1 the drag force of luggage cabin increases to a maximum then decreases. However, for sample #2, luggage cabin drag force increases with angle of attack (figure 5.9). This calls for further studies into influence of luggage cabin object. Results of other samples are provided in appendix B.

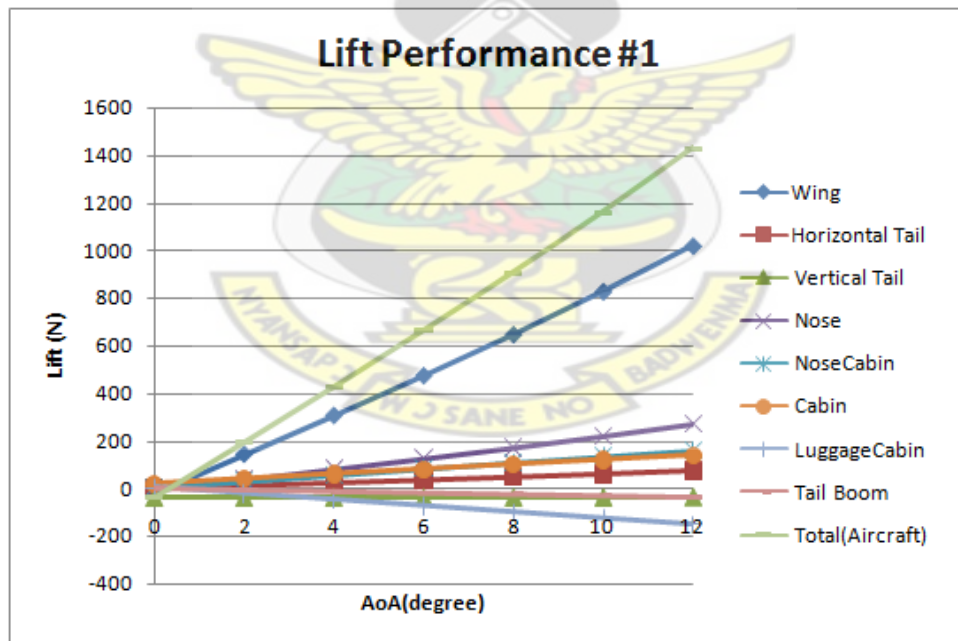


Figure 5.5 Object Lift Performance for Sample #1.

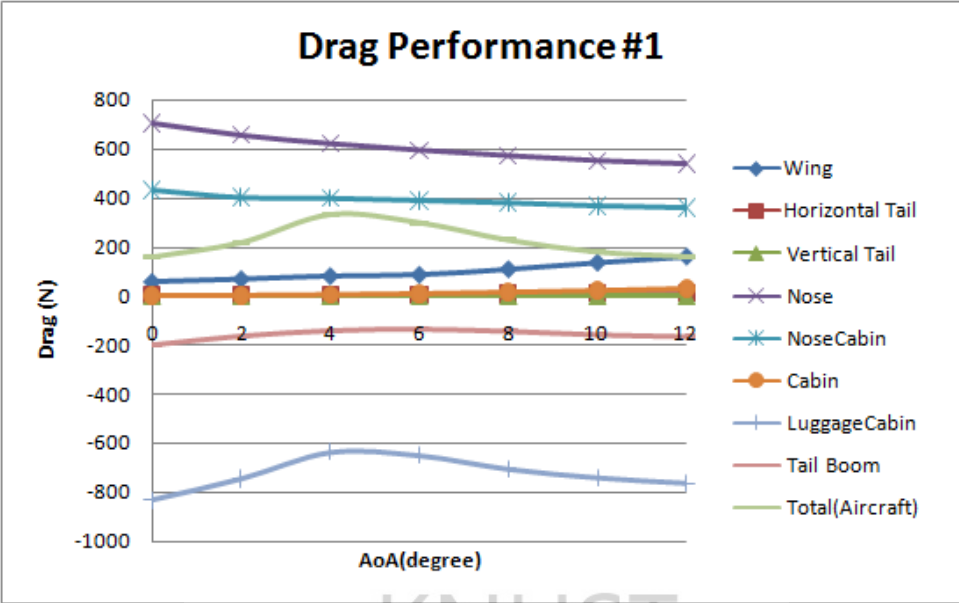


Figure 5.6 Object Drag Performance for Sample #1.

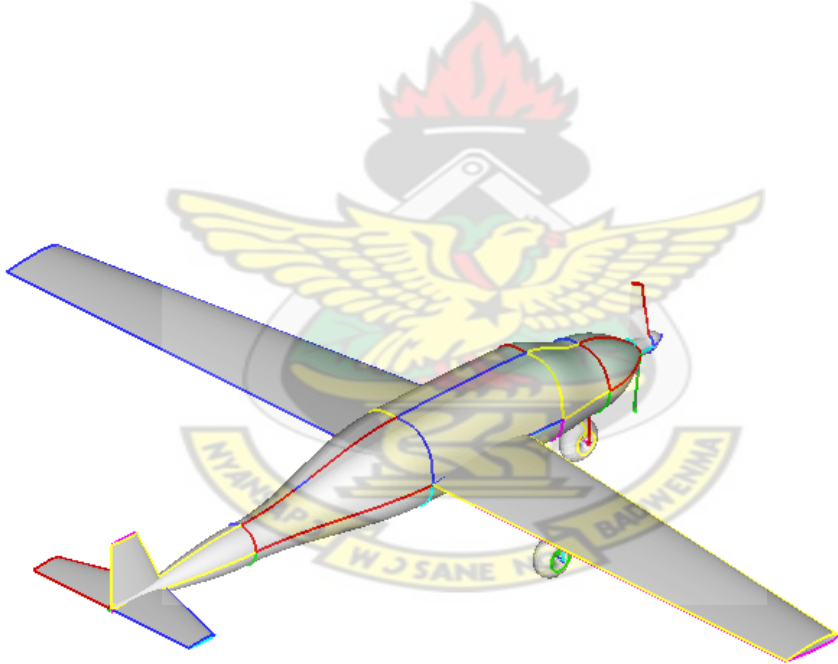


Figure 5.7 Sample #1 Configuration.

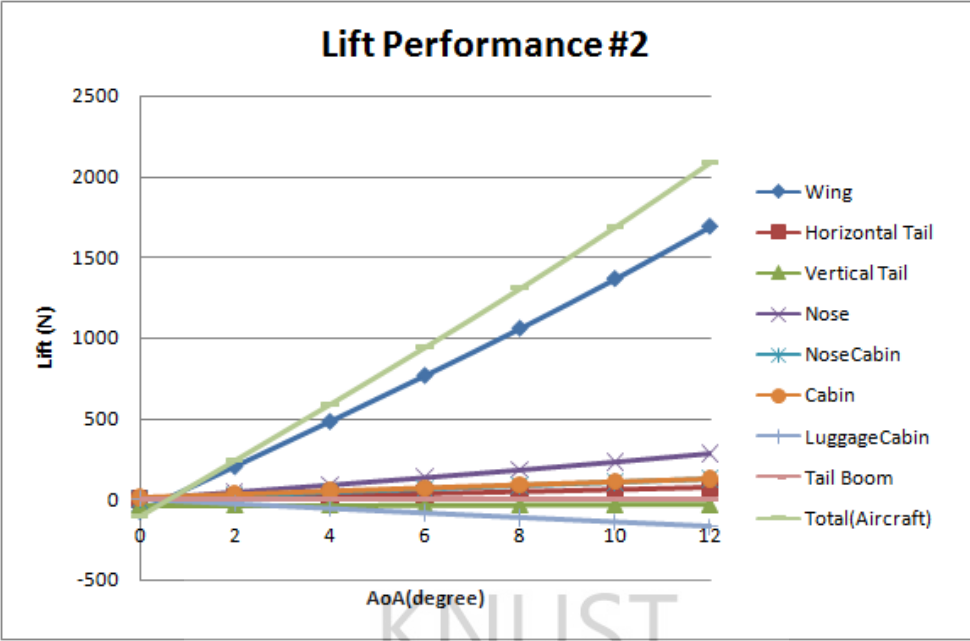


Figure 5.8 Object Lift Performance for Sample #2.

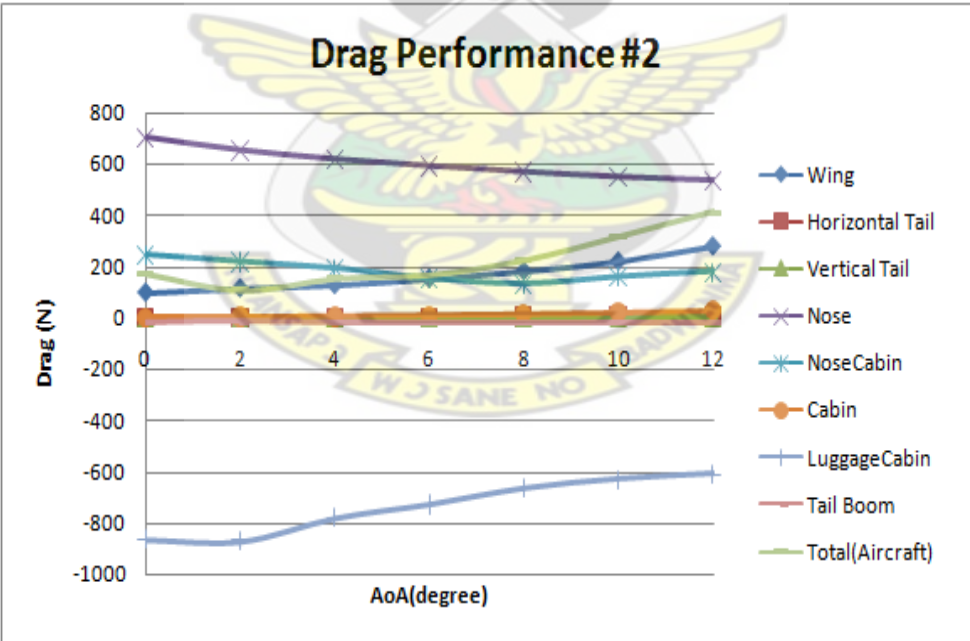


Figure 5.9 Object Drag Performance for Sample #2.

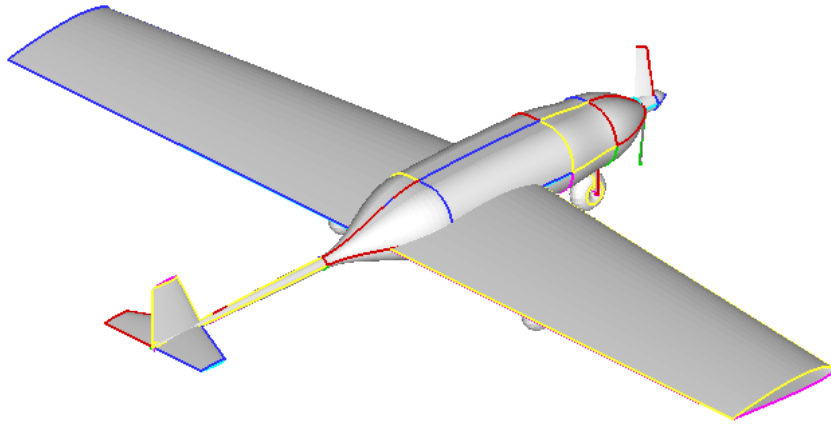


Figure 5.10 Sample #2 Configuration.

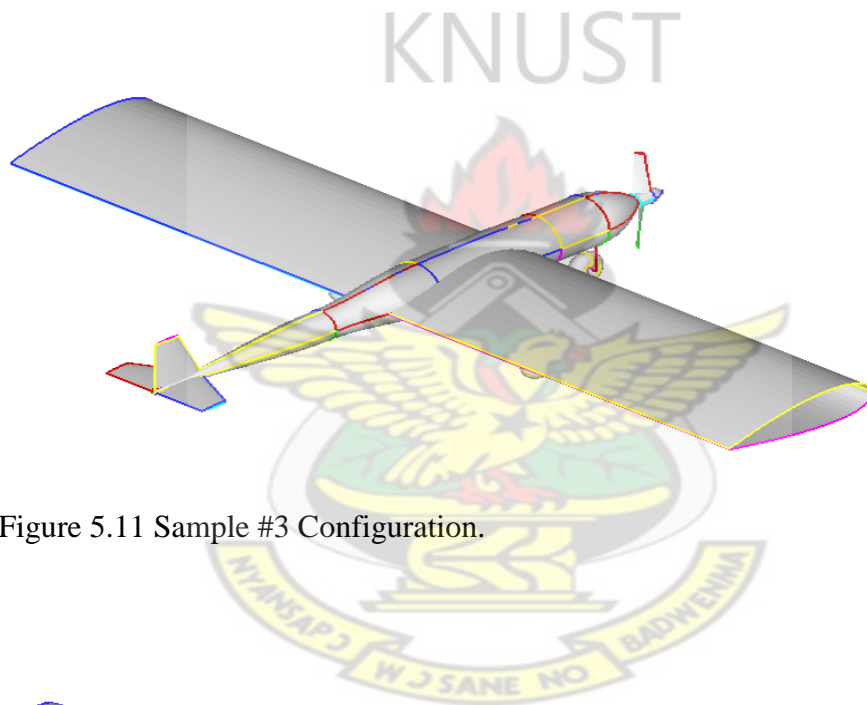


Figure 5.11 Sample #3 Configuration.

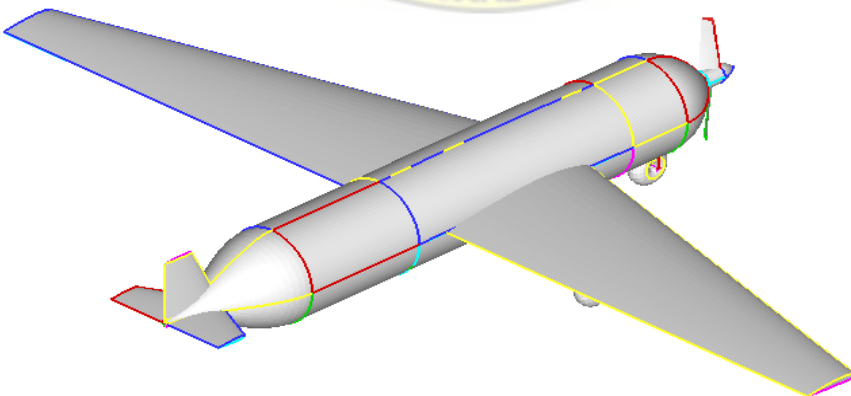


Figure 5.12 Sample #4 Configuration.

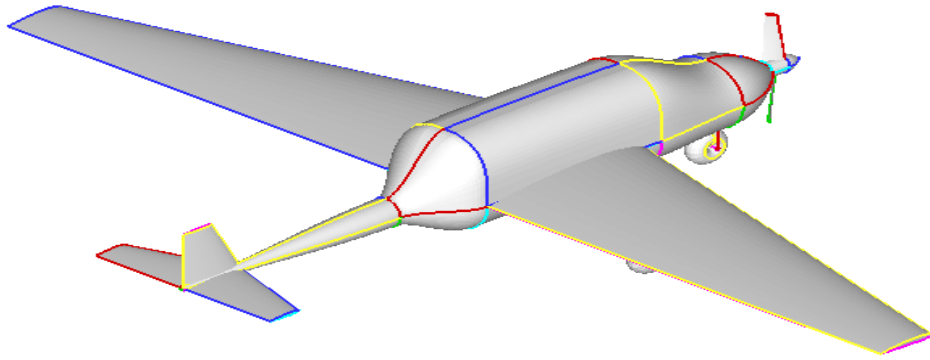


Figure 5.13 Sample #5 Configuration.

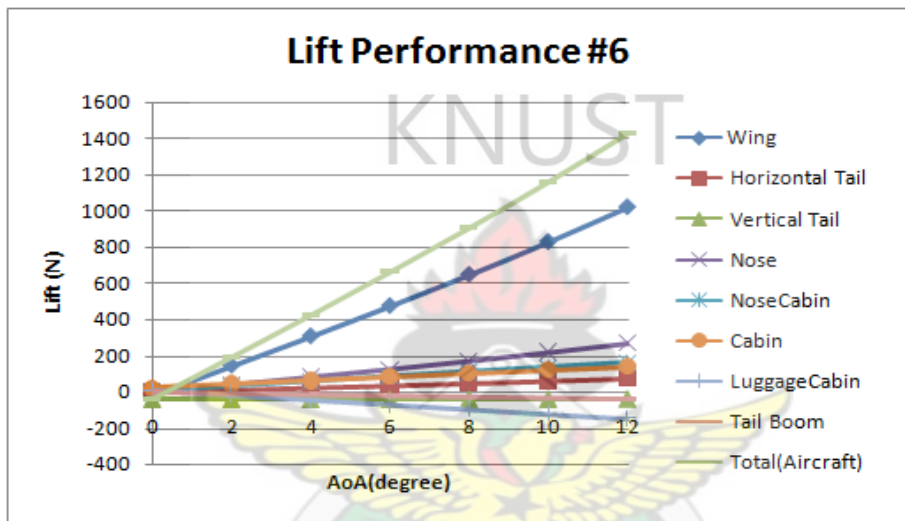


Figure 5.14 Object Lift Performance for Sample #6.

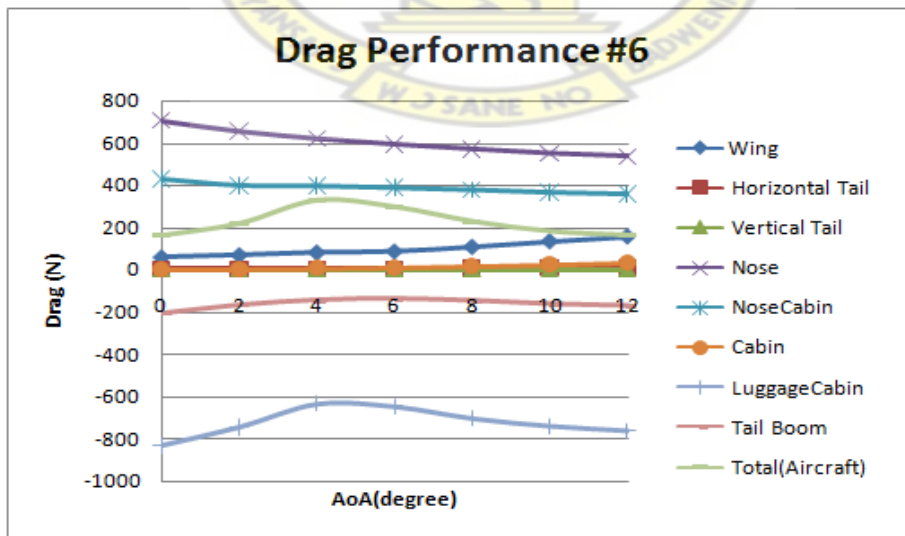


Figure 5.15 Object Drag Performance for Sample #6.

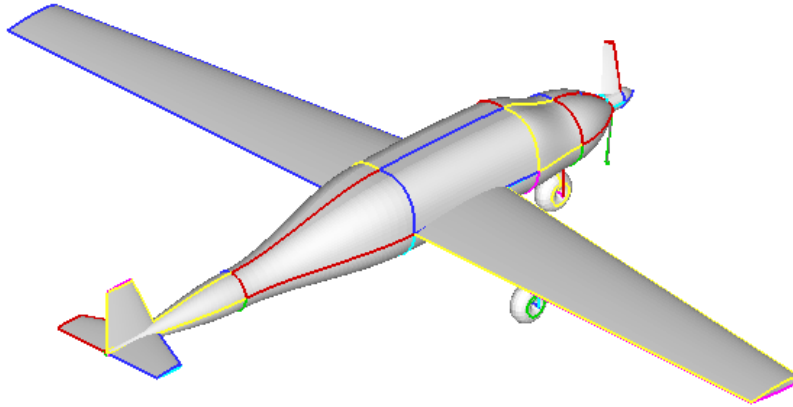


Figure 5.16 Sample #6 Configuration.

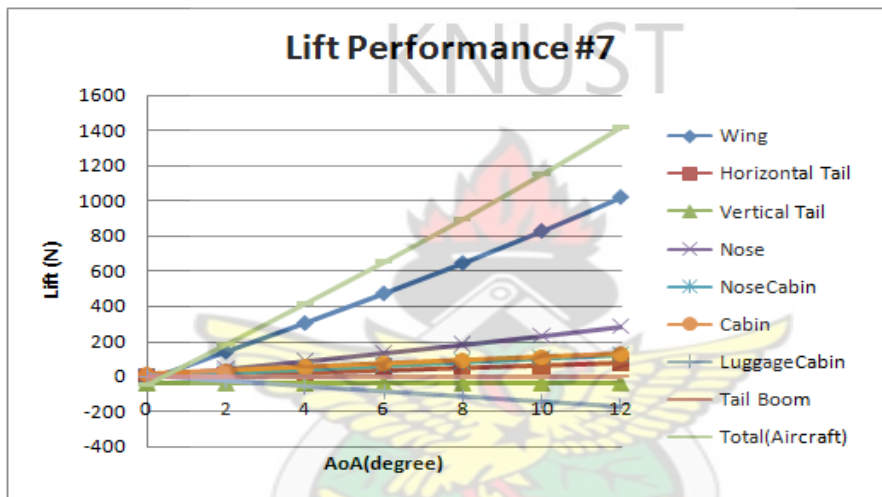


Figure 5.17 Object Lift Performance for Sample #7.

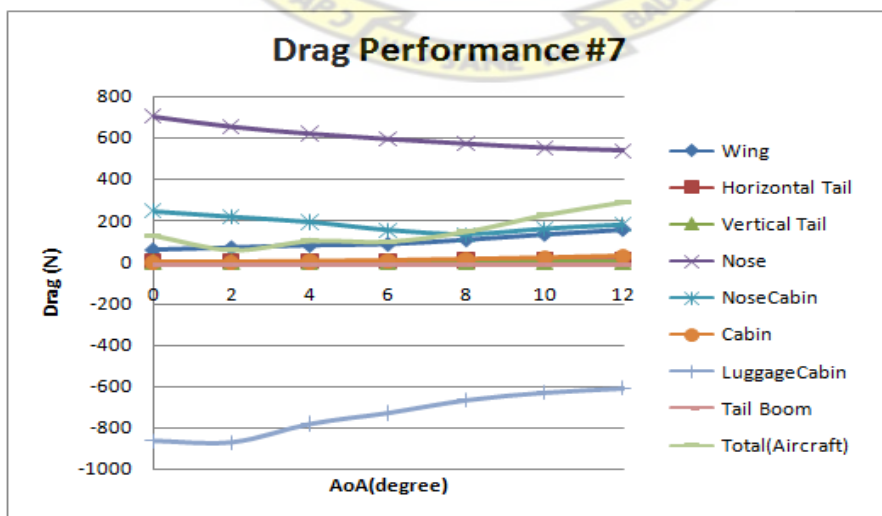


Figure 5.18 Object Drag Performance for Sample #7.

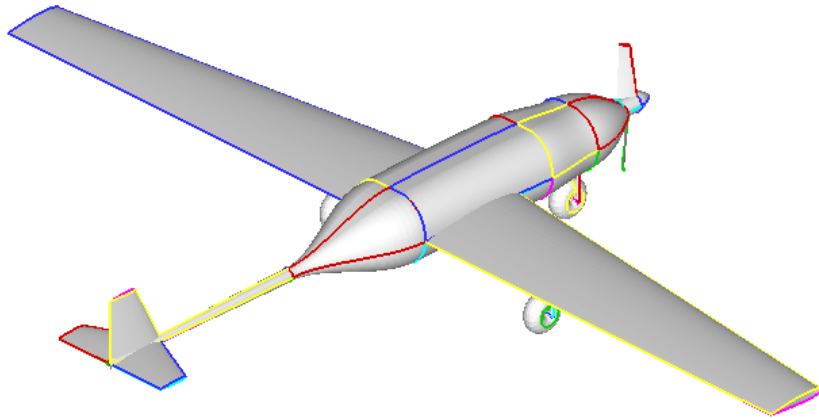


Figure 5.19 Sample #7 Configuration.

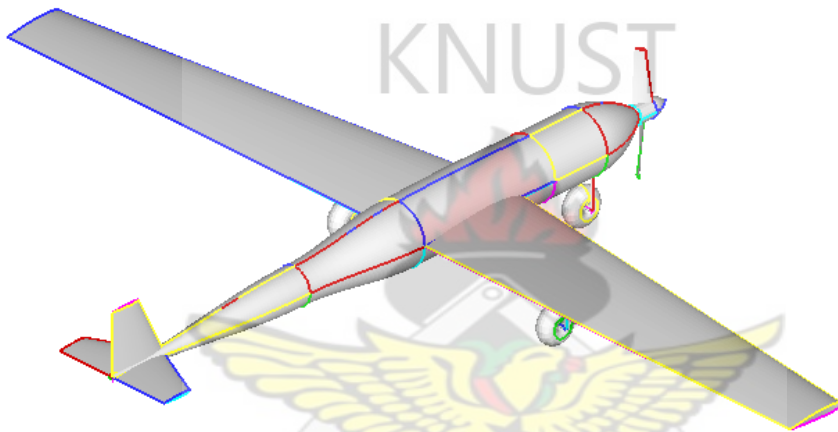


Figure 5.20 Sample #8 Configuration.

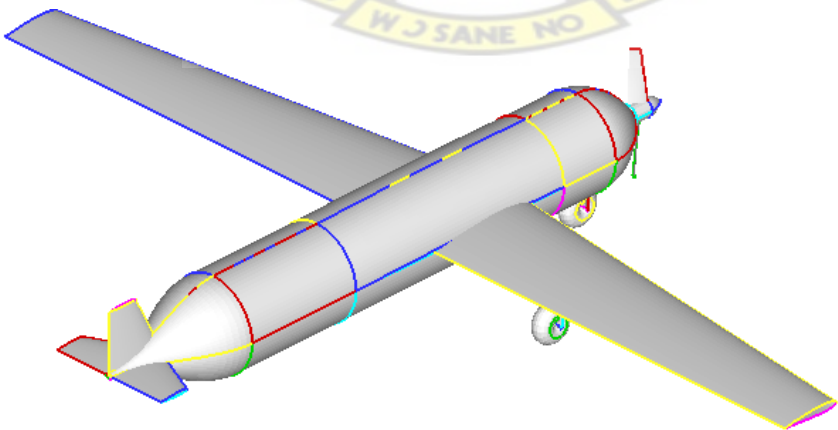


Figure 5.21 Sample #9 Configuration.

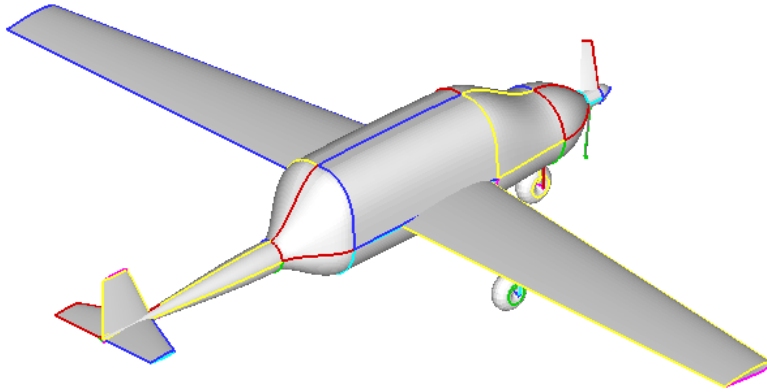


Figure 5.22 Sample #10 Configuration.

KNUST

5.3 DESIGN PARAMETRIC STUDY

The influence of the design parameters on the performance can be studied by holding all parameters constant except a parameter of interest. Studies of the nose-cabin interface offset height (cabin height) results are illustrated in figures 5.23 and 5.24. From figure 5.23, showing the lift performance, the lift increases with increase in the offset height design parameter but decrease for nose and tailboom. For the drag, the nose, cabin and tailboom are not influenced by the offset height design parameter. The study of luggage cabin end diameter (tailboom diameter) influence is shown by figures 5.26 and 5.27.

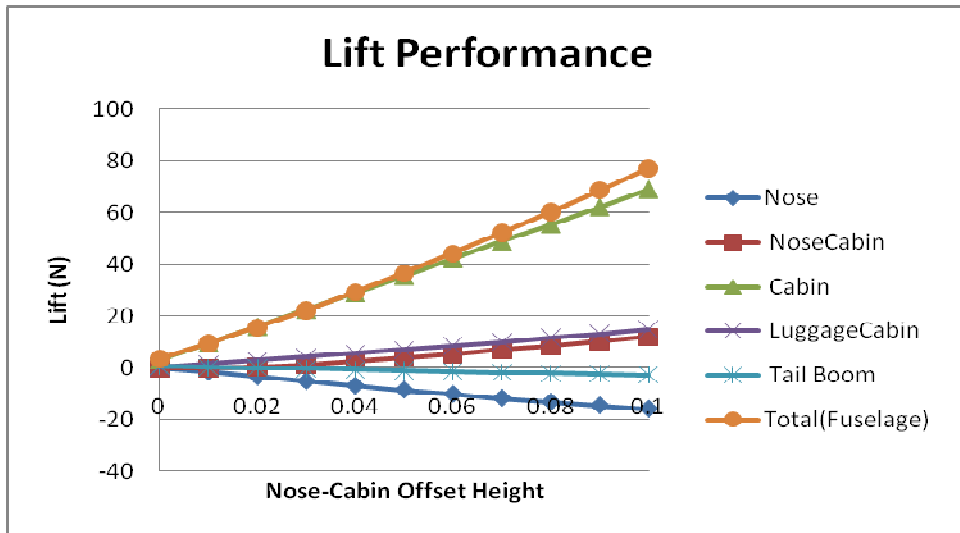


Figure 5.23 Lift Performance for Nose-Cabin Offset height variation.

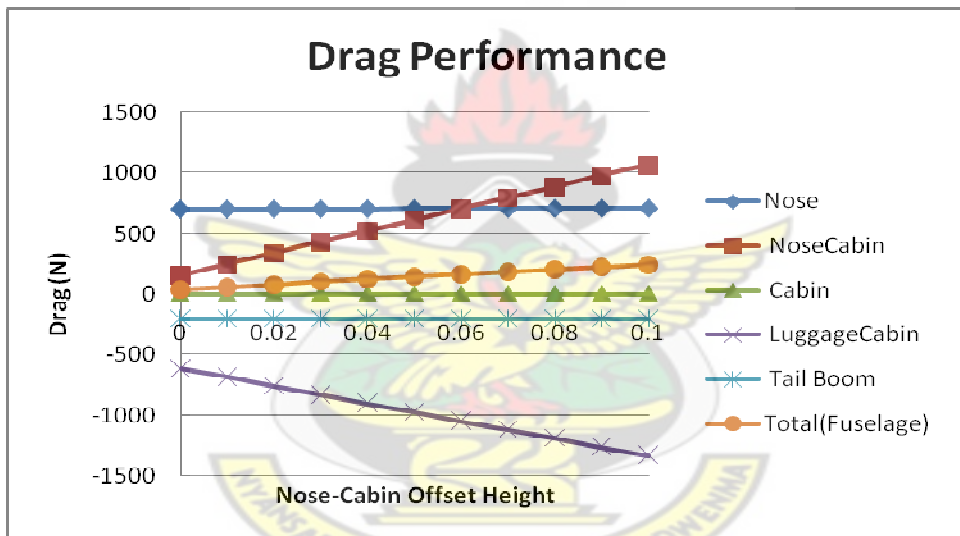


Figure 5.24 Drag Performance for Nose-Cabin Offset height variation.

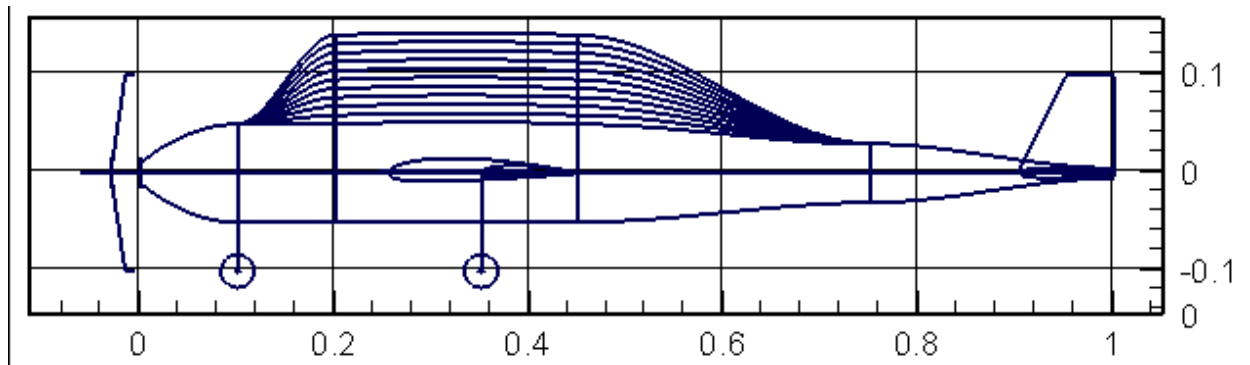


Figure 5.25 Fuselage profile indicating the variation of Cabin height.

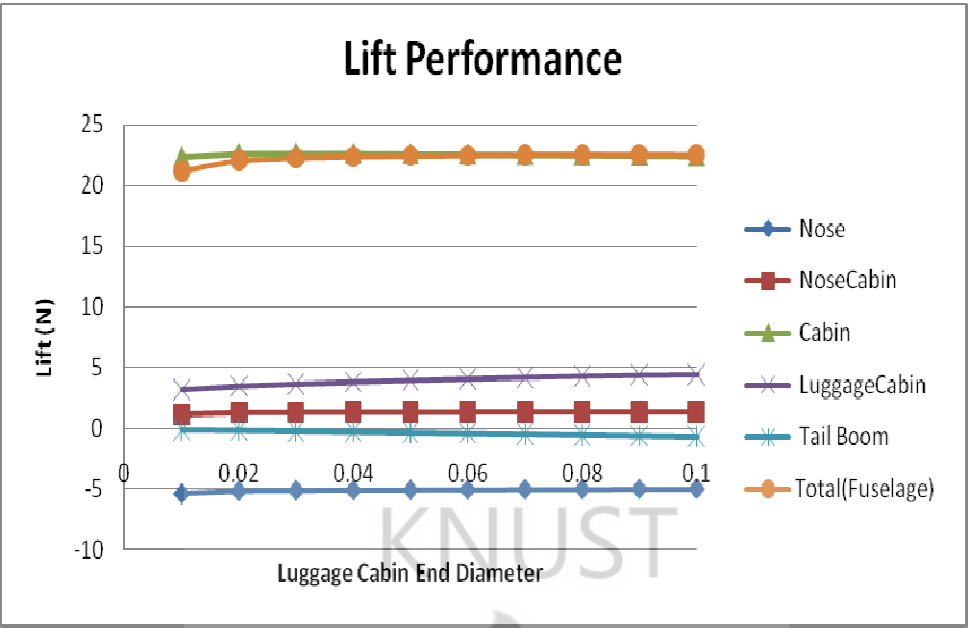


Figure 5.26 Lift Performance for Luggage-cabin end diameter variation.

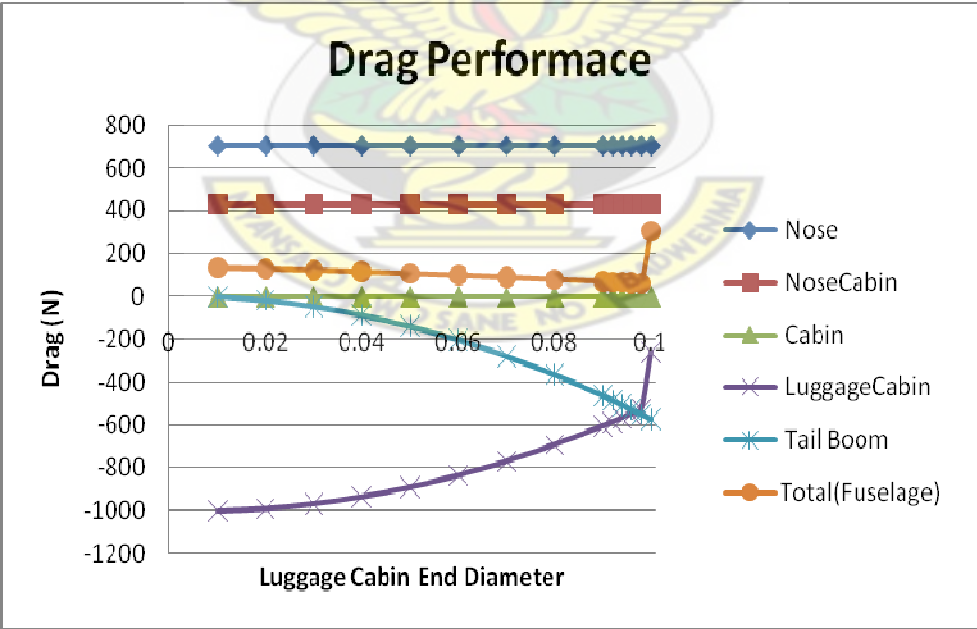


Figure 5.27 Drag Performance for Luggage-cabin end diameter variation.

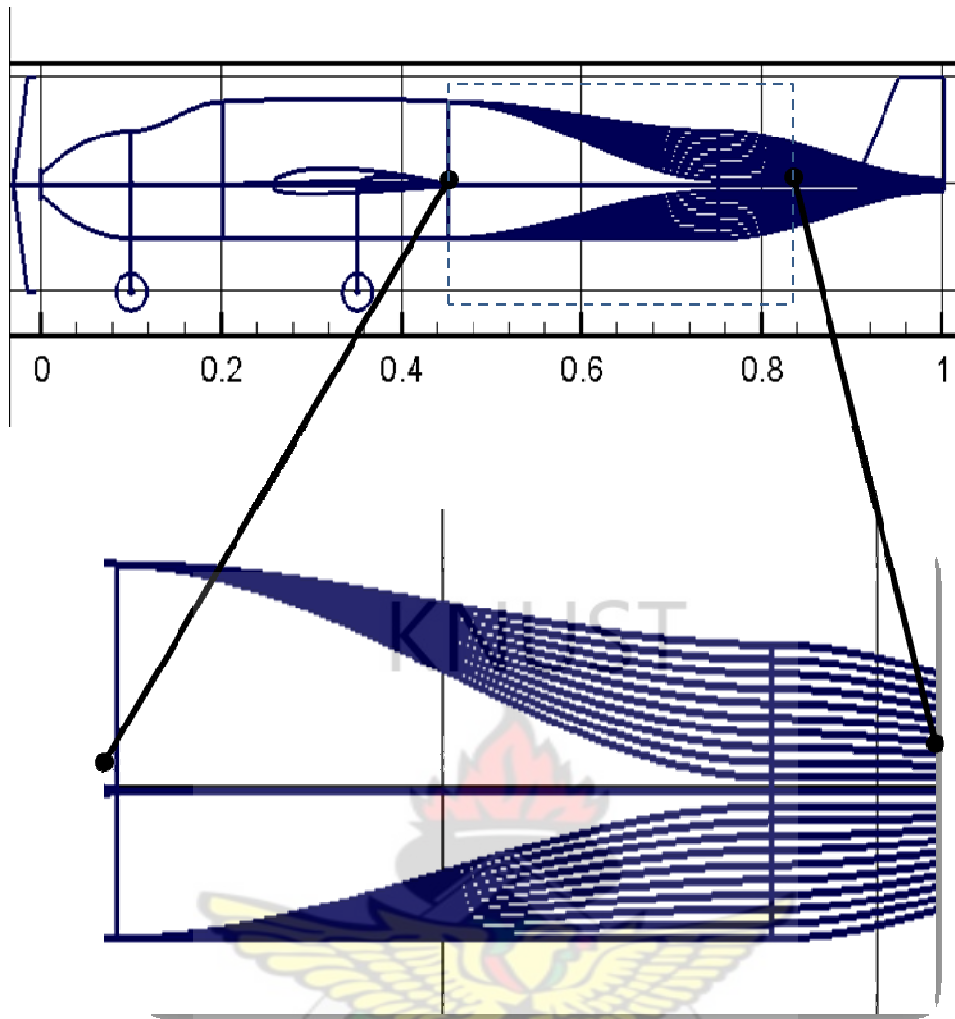


Figure 5.28 Fuselage profile indicating the variation of Luggage Cabin diameter.

5.3.1 Luggage Cabin Influence

The general observation from the performance study indicates possible significant influence of the luggage cabin parameters on drag performance of the aircraft. This calls for closer study with the luggage cabin design parameters. The luggage cabin is defined with two design parameter (length and end diameter). The parametric study of end diameter (figures 5.26 and 5.27) shows no significant influence on the lift performance. For drag performance, the luggage cabin and tailboom interact with

one another such that the overall influence on the aircraft drag performance is insignificant. Luggage cabin length, however, influences the drag performance significantly. The drag decreases with increase in length hyperbolically at zero (0°) angle of attack (figure 5.29). With angle of attack of three degree (3°) the drag force decreases with increase in length to minimum and then increases (figure 5.29). Figure 5.30 is an illustration of the length variation of the luggage cabin object. This indicates that there is an optimum condition for minimum drag performance. Optimum drag performance may therefore be obtained at angle of attack between 2° to 4° and luggage cabin length of from 0.02 to 0.1 of the aircraft length.

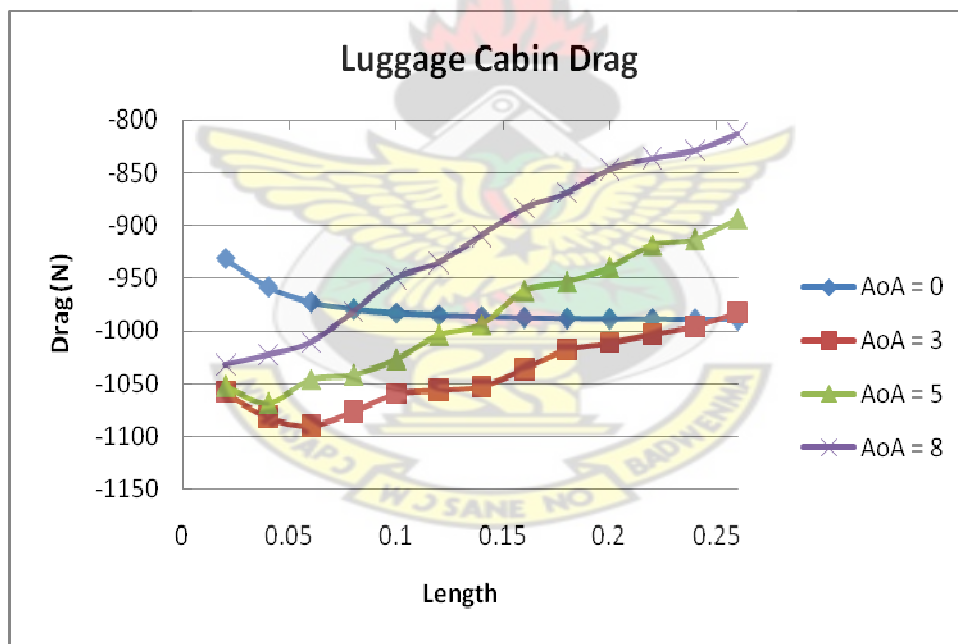


Figure 5.29 Drag Performance for Luggage-cabin length variation.

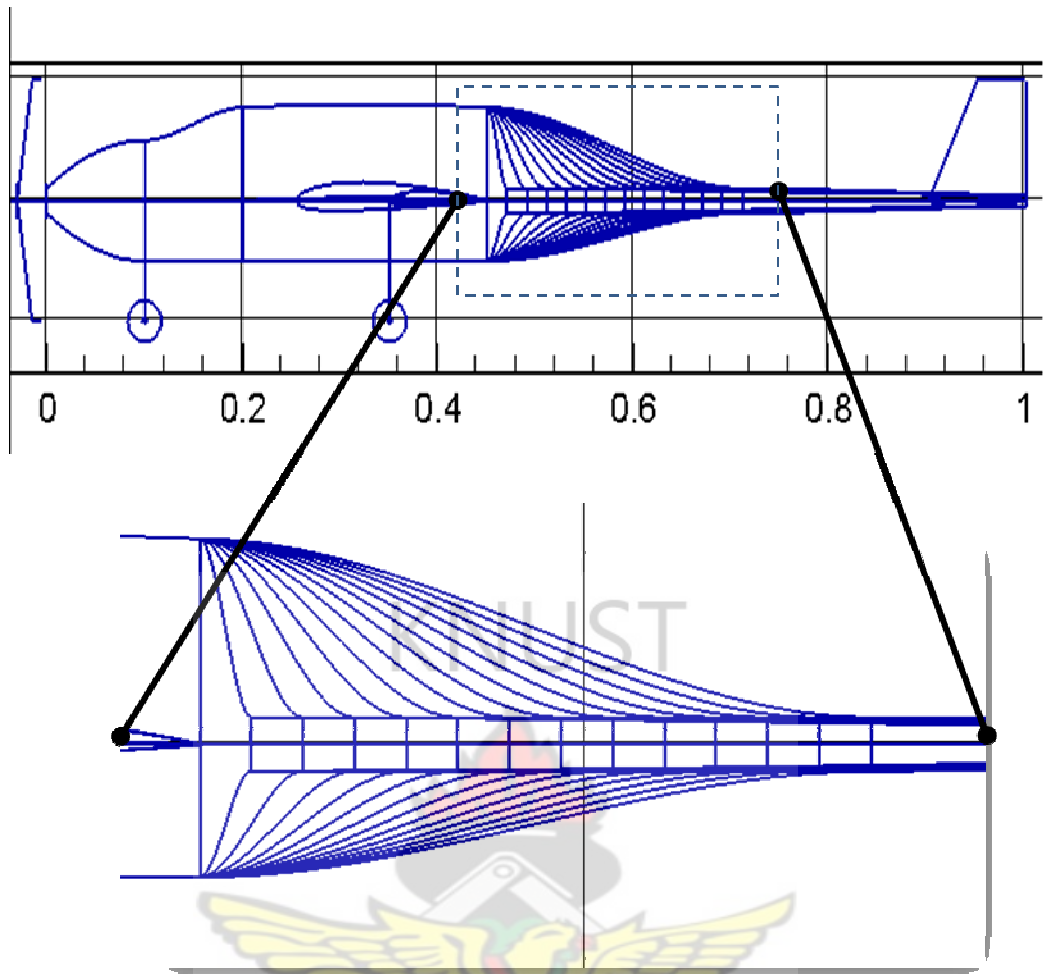


Figure 5.30 Luggage-cabin length variation.

CHAPTER SIX

CONCLUSION AND RECOMMENDATION

6.1 CONCLUSION

The concept of the research is modelled analogous to a mathematical relation with input and output information. The input involves two categories of parameters, fixed and design parameters. The output, also, consist of two kinds, geometry and aerodynamic performance. The aerodynamic performance covers lift and drag developed by the configuration. There were 19 design variables identified that completely define aircraft configuration. The physical aircraft is structured and mapped into Object-Oriented programming environment. Object-oriented technique is implemented by defining the basic primitives like 'point', 'line' and others which are connected to create a desire object. The designed system is developed using FORTRAN 95 programming language and TECPLOT is used for visualization. Components of the system are validated by comparing the respective results with established data and were found to be satisfactory.

Ten sample aircraft geometries have been developed with some chosen design parameters. Five of these samples were of the same wing profile. The aerodynamic performance results of the samples, generally shows increase in lift performance with increase in angle of attack. The drag performance indicates varying results with increase in angle of attack suggesting further studies of the design parameters. The lift performance of the samples with same wing profile show that the components of the fuselage contributed towards the lift force. These contributions indicated higher overall lift force compared to lift force developed by the wing alone (figures 5.5, 5.8, 5.14 and 5.17). Hence, the estimated lift performance is higher when all surfaces are

considered. The total lift and drag estimate of an aircraft using the developed system is more accurate than using estimate from the wing alone.

Small aircrafts in the form of personal aircraft, remote or radio controlled aircrafts usually operate at low speed and are used for different kinds of activities. Since estimation of the aerodynamic forces developed by the configuration forms a significant and challenging part of the design process, the system developed will enhance the process and overcome some of the challenges. With this tool, aerodynamic performance of the aircraft, usually estimated from the lift and drag coefficients obtained as a result of the selected airfoil of the wing geometry, will be better estimated more accurately with contribution from all surfaces. Application of object oriented technique in the conceptual design of the configuration will improve the aerodynamics performance estimate. The developed system or method would significantly influence aircraft design process particularly the conceptual stage.

Results of the research further show that design of small aircraft will have better drag performance at angle of attack between 2° and 4° . Therefore, for small aircraft design, the design should be such that nose to cabin be streamlined and the angle of attack be between 2° to 4° . Also, performance study shows that luggage cabin object significantly influence the drag performance.

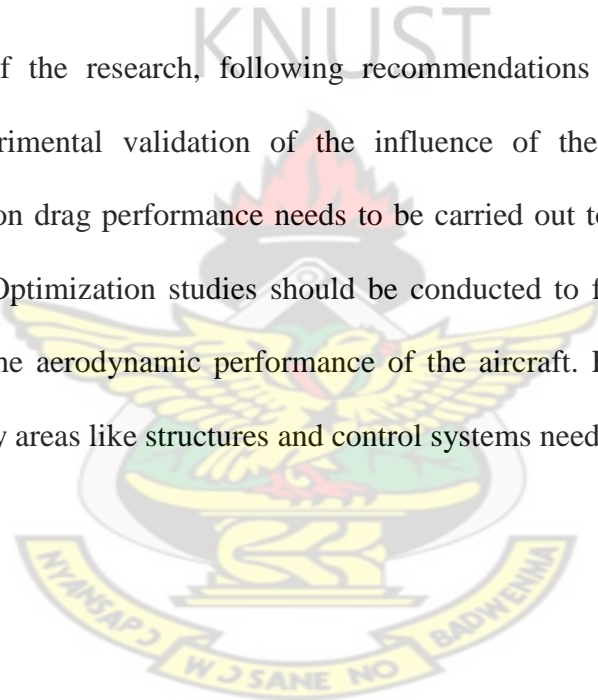
The study of the luggage cabin indicates that the influence of diameter is insignificant but its length, however, significantly influences the drag performance. The drag performance decreases with increase in length to minimum then increases.

Air transportation is becoming very important means of transportation and is expected to continue to contribute a lot to the transportation system throughout the world. The third-world countries need to consider air transportation as a vital tool in

development and get prepared to take tremendous leapfrog in the air transportation system in anticipation of what the trend may be in the near future. In Ghana, encouraging design and production of small aircrafts would be considered as preparatory step to promote air transportation in the country. The developed system or tool will significantly enhance the conceptual design stage of the design process of aircraft and its use will contribute to air transportation system development in Ghana.

6.2 RECOMMENDATIONS

As a result of the research, following recommendations are to be considered: Physical experimental validation of the influence of the luggage cabin object configuration on drag performance needs to be carried out to confirm the results of the research. Optimization studies should be conducted to further identify level of influence on the aerodynamic performance of the aircraft. Further work into other complementary areas like structures and control systems needs to be undertaken.



REFERENCES

1. Abbott, Ira H. and Von Doenhoff, Albert E. (1959), "Theory of Wing Sections including a summary of airfoil data", Dover Publications, Inc, New York.
2. Amadori, Kristian (2008), "On Aircraft Conceptual Design: A Framework for Knowledge Based Engineering and Design Optimization", Linköpings Universitet, SE-581 83, Linköping, Sweden
3. Anderson Jr, John D., (2005), "Fundamentals of Aerodynamics", McGraw-Hill Companies, Inc., New York
4. Anderson Jr, John D., (2007), "Introduction to Flight", McGraw-Hill Companies, Inc., New York
5. Anderson Jr, John D., (1995), "Computational Fluid Dynamics: The Basics with Applications", McGraw-Hill Companies, Inc., New York
6. Antoine, Nicolas E. and Kroo, Ilan M. (2005), "Framework for Aircraft Conceptual Design and Environmental Performance Studies", AIAA JOURNAL, Vol. 43, No. 10, October 2005
7. David L. Rodriguez and Peter Sturdza, (2006), "A rapid Geometry Engine for Preliminary Aircraft Design", 44th AIAA Aerospace Sciences Meeting and Exhibit, 9 – 12 January 2006, Reno, Nevada.
8. Ferguson, Trevor S. (2007), "Design Integration and Analysis of a Remote-Controlled Airplane", Master thesis, North Carolina A&T State University, Greensboro, North Carolina

9. Gloudemans, J. R., Davis, Paul C., and Gelhausen, Paul A., (1996), "A rapid geometry modeler for Conceptual Aircraft", AIAA-1996-0052, January, 1996
10. Grigg, Alan; Audsley, Neil; Fletcher, Martyn and Wake, Allan, "A Method for Design and Analysis of Next Generation Aircraft Computer Systems"
11. Hoffmann, Klaus A. and Chiang, Steve T. (2002), "Computational Fluid Dynamics", Volume 1, Fourth edition, Engineering Education Systems, Wichita, USA
12. Houghton, E.L. and Carpenter, P.W. (2003), "Aerodynamics for Engineering Students", 5th Edition, Butterworth - Heinemann,
13. Jameson, Antony (1989), "Computational Aerodynamics for Aircraft Design", Science, Volume 245, pp. 361-371, 1989
14. Kennedy, Andrew and Russo, Claudio V., "Generalized Algebraic Data Types and Object Oriented Programming", Microsoft Research Ltd, 7JJ Thomson Ave, Cambridge, United Kingdom, <http://research.microsoft.com/~akenn/generics/gadtoop.pdf>, Date accessed: 6th May, 2008
15. Kroo, Ilan; Altus, Steve; Braun, Robert; Gage, Peter and Sobieski, Ian "Multidisciplinary Optimization Methods for Aircraft Preliminary Design", AIAA 94-4325
16. Labrujere, Th.E. and Slooff, J.W. (1993), "Computational Methods for the Aerodynamic Design of Aircraft Components", Annu. Rev. Fluid Mech. 25: 183-214

17. Martínez Martí, Enrique G. (2006), “Flow and Entropy Characteristics around Airfoils in Subsonic and Supersonic Flows”, Master Thesis, University Of Puerto Rico, Mayagüez Campus
18. Moormann, D.; Mosterman, P.J. and Looye, G. (1999), “Object-oriented computational model building of aircraft flight dynamics and systems”. Aerospace Science and Technology, no. 3, Elsevier, Paris
19. Neufeld, Daniel and Chung, Joon (2007), “Development of Aircraft Conceptual Design Optimization Software”, Fifth International Conference on Computational Science and Applications, IEEE
20. Noye, J. (1982), “Numerical Solutions of Partial Differential Equations”, North-holland Publishing Company, Amsterdam.
21. Raymer, Daniel P., (2002), “Enhancing Aircraft Conceptual Design using Multidisciplinary Optimization”, Doctoral Thesis, Swedish Royal Institute of Technology, 2002
22. Stinton, Darrol (1998), “The Anatomy of the Aeroplane”, Blackwell Science Ltd., Oxford
23. Thompson, Joe F., Thames, Frank C. and Mastin, C. Wayne, (1974), “Automatic Numerical Generation of Body-Fitted Curvilinear Coordinate System for Field Containing any number of Arbitrary Two-Dimensional Bodies”, Journal of Computational Physics 15, 299-319
24. Turevskiy, A. Gage, S. and Buhr, C (1999), “Model-Based Design of a new light-weight Aircraft”, American Institute of Aeronautics and Astronautics.

APPENDICES

APPENDIX A: Sample Programme Code

```
PROGRAM Aircraft_Design

USE CartesianBasics_Module
USE Wing_Module
USE Tail_wing_Module
USE Fuselage_Module
USE Aircraft_Data_Module
USE Center_of_Gravity_Module
!USE Airfoil_Transformation_Module
!USE Wind_Tunnel_Module
USE Atmosphere_Module
USE Propeller_Module
USE Landing_Gear_Module
USE Surface_Integration

IMPLICIT NONE

!Declare the Data types
  TYPE (Aircraft_Input_Type)   :: Aircraft_Input
  TYPE (Aircraft_Output_Type)  :: Aircraft_Output

  REAL :: Mach_Number, Flight_Altitude, Plane_Length
  TYPE(AerodynamicDesignPoint_Type) :: AerodynamicDesignPoint
  TYPE(AerodynamicDesignPointData_Type)::
AerodynamicDesignPointData

  TYPE (AtmosphereCdts_Type) :: Atmospheric_data

INTEGER, PARAMETER   :: N=21
INTEGER              :: I, J

  TYPE (QuadCircle_Type) :: QuadCircle

!Declare the Wing_Data types
!Input Related
TYPE(Wing_Inputs_Type)           :: Wing_Input
  TYPE(Wing_DesignParameter_Type) :: Wing_DesignParameter
  REAL                             ::
WingRoot_Chord_PlaneLength_Ratio
  REAL                             :: WingTip_To_RootChord_Ratio
  REAL                             ::
WingSpan_To_PlaneLength_Ratio

  TYPE(Wing_FixedParameter_Type)  :: Wing_FixedParameter
  INTEGER                          :: Wing_Profile
  REAL                             :: Wing_Angle_of_Attack
  REAL                             :: Wing_Dihedral_Angle
  REAL                             :: Wing_Sweep_Angle
  TYPE (POINT_TYPE)               :: Wing_Location

!Output Related
```



```

!CCCCCCCCCCCCCCCCCCCCCCCCCCCCCCCCCCCCCCCCCCCCCCCCCCCCCCCCCCCCCCCC
!Declare the Cabin_Data types
!Input Related
    TYPE(Cabin_Inputs_Type)                :: Cabin_Input
    TYPE(Cabin_DesignParameter_Type)       ::
Cabin_DesignParameter
    REAL  :: CabinLength_PlaneLength_Ratio
    TYPE(Cabin_FixedParameter_Type)       ::
Cabin_FixedParameter

!LLLLLLLLLLLLLLLLLLLLLLLLLLLLLLLLLLLLLLLLLLLLLLLLLLLLLLLLLLLLLLLLL

!Declare the Luggage_Cab_Data types
!Input Related
TYPE(Luggage_Cab_Inputs_Type)            ::
LuggageCabin_Input
    TYPE(Luggage_Cab_DesignParameter_Type) ::
LuggageCabin_DesignParameter
    REAL  :: LuggageCabinLength_PlaneLength_Ratio
    REAL  :: LuggageCabinEndDiameter_PlaneLength_Ratio

    TYPE(Luggage_Cab_FixedParameter_Type) ::
LuggageCabin_FixedParameter

!TTTTTTTTTTTTTTTTTTTTTTTTTTTTTTTTTTTTTTTTTTTTTTTTTTTTTTTTTTTTTTT
T

!Declare the Tail_Data types
!Input Related
TYPE(Tail_Inputs_Type)                   :: Tail_Input
    TYPE(Tail_DesignParameter_Type)       ::
Tail_DesignParameter
    !Put The inner data structure here if/when needed
    REAL  :: TailEndDiameter_PlaneLength_Ratio
    TYPE(Tail_FixedParameter_Type)       ::
Tail_FixedParameter
    !Put The inner data structure here if/when needed

!OOOOOOOOOOOOOOOOOOOOOOOOOOOOOOOOOOOOOOOOOOOOOOOOOOOOOOOOOOOOOO

!Declare the Tail_Data types
!Input Related
TYPE(Propeller_Inputs_Type)              :: Propeller_Input
TYPE(Propeller_DesignParameter_Type)     ::
Propeller_DesignParameter
TYPE(Propeller_FixedParameter_Type)     ::
Propeller_FixedParameter

!Output Related
TYPE(Propeller_Outputs_Type)              :: Propeller_Output
TYPE(Propeller_SurfaceData_Type)         :: Propeller_SurfaceData
!    TYPE(Point_Type)  :: Propeller_points(N, N)

TYPE(Propeller_PerformanceParameter_Type)::
Propeller_PerformanceParameter
!landing gear data

```

```

        TYPE (Landing_Gear_FixedParameter_Type) ::
LandingGear_Input
        REAL                :: Wheel_thickness
        REAL                :: Wheel_Pin_Diameter
        REAL                :: Wheel_Pin_Length
        REAL                :: F_Wheel_Support_Length
        REAL                :: R_Wheel_Support_Length
        TYPE (POINT_TYPE):: F_Wheel_Location
        TYPE (POINT_TYPE):: R_Wheel_Location

!XXXXXXXXXXXXXXXXXXXXXXXXXXXXXXXXXXXXXXXXXXXXXXXXXXXXXXXXXXXXXXXXXXXX
!Other parameters
        REAL :: Temperature, Pressure, Density, Viscosity,
SoundSpeed, Flight_Speed
        REAL :: Fuselage_Lift , Fuselage_Drag, Wing_Lift ,
Wing_Drag
        REAL :: H_TailWing_Lift , H_TailWing_Drag, V_TailWing_Lift
, V_TailWing_Drag
        REAL :: Plane_Lift , Plane_Drag
        REAL :: Fuselage_AoA !Fuselage Angle of Attack

        REAL :: Z_loc, Pi, AoA

!START PROGRAM
!*****

!open(300, file = 'Cl_Cd.dat')
!WRITE(300,*) 'ZONE T = "Cl_cd" ' , I= ',N, ' J = ', N*2-2, 'K=
1, F=POINT'

        !call Create_Surface_Integration_Valitation_1(2.0, 1.0,
2.0) !(Length, Tip_Diameter, End_Diameter)
        !call Create_Surface_Integration_Valitation_2(2.0, 1.0,
0.0) !(Length, Tip_Diameter, End_Diameter)
        !stop

open(301, file = 'Performance.doc')
open(401, file = 'ClCd.doc')
!
WRITE(301,*) 'Component ', ' Lift ', ' ', ' Drag'

open(25, file = 'Aircraft_Geometry.dat') !Output file for
Aircraft Geometry

!*****

Do    AoA = 0.0, 3.0, 3.0
!    AoA = 0.0
Write(*,*) AoA
        pi = 22.0/7.0

!Do    Mach_Number      = 0.02, 0.3, 0.02
        Mach_Number      = 0.2
!Write(*,*) 'Mach_Number = ', Mach_Number
        Flight_Altitude = 2.0
        Plane_Length     = 1.0

        AerodynamicDesignPoint = &

```

```

        Create_AerodynamicDesignPoint_Type(Mach_Number,
Flight_Altitude, Plane_Length)

        AerodynamicDesignPointData = &

        Create_AerodynamicDesignPointData_Type(Mach_Number,
Flight_Altitude, Plane_Length)

        Atmospheric_data =
Create_AtmosphereCdts_Type(Flight_Altitude) !Contains:
                !Altitude, Temperature,           &
                !Pressure, Density, g_Acceleration
                !SoundSpeed,           Viscosity

        Temperature = Atmospheric_data%Temperature
        Pressure     = Atmospheric_data%Pressure
        Density      = Atmospheric_data%Density
        Viscosity    = Atmospheric_data%Viscosity
        SoundSpeed  = Atmospheric_data%SoundSpeed

!       Write(*,*) AerodynamicDesignPoint
        Flight_Speed = Mach_Number*SoundSpeed
!       Write(*,*) Flight_Speed, 'Flight_Speed'

!Nose Design Variables
        Nose_Length_PlaneLength_Ratio           = 0.10
!       Write(*,*) 'Enter NoseLength to PlaneLength Ratio'
!       Read (*,*) Nose_Length_PlaneLength_Ratio
                !Test the validity of input value
                if(Nose_Length_PlaneLength_Ratio<= 0.0 .or.
Nose_Length_PlaneLength_Ratio >= 0.5) Then
                        Write(*,*) 'Nose Length to Plane Length Ratio is
out of range'
                                Write(*,*) 'Enter value between 0.0 and 0.5'
                                Endif
!       stop
        Nose_EndHeight_PlaneLength_Ratio        = 0.10
        Nose_EndWidth_PlaneLength_Ratio        = 0.12
        ! Compare with Nose_EndHeight_PlaneLength_Ratio

!NoseCabin Interface Design Variables
        NoseCabinLength_PlaneLength_Ratio      = 0.10
        NoseCabin_OffsetHeight_Length_Ratio    = 0.05
        NoseCabin_EndWidth_PlaneLength_Ratio   = 0.140 !Compare
with Nose_EndWidth_PlaneLength_Ratio

!Cabin Design Variables
        CabinLength_PlaneLength_Ratio          = 0.250

!Luggage Cabin Design Variables
        LuggageCabinLength_PlaneLength_Ratio   = 0.20
        LuggageCabinEndDiameter_PlaneLength_Ratio = 0.08

!Tail Design Variables
        TailEndDiameter_PlaneLength_Ratio      = 0.01

!Horizontal Tail wing Design Variables
        H_Root_Chord_PlaneLength_Ratio        = 0.10

```

```

H_Tip_To_RootChord_Ratio           = 0.50
H_Span_To_PlaneLength_Ratio        = 0.20

!Vertical Tail wing Design Variables
V_Root_Chord_PlaneLength_Ratio     = 0.10
V_Tip_To_RootChord_Ratio           = 0.50
V_Span_To_PlaneLength_Ratio        = 0.10

!Wing Design Variables
WingRoot_Chord_PlaneLength_Ratio   = 0.30
WingTip_To_RootChord_Ratio         = 0.50
WingSpan_To_PlaneLength_Ratio      = 1.60

!Component Fixed Parameters
!Nose
Nose_Tip_Diameter= 0.02
Nose_Tip_Location= Create_Point_Type(0.0, 0.0, 0.0)
Fuselage_AoA           = AoA

!Wing
Wing_Profile           = 2412
Wing_Angle_of_Attack   = AoA
Wing_Dihedral_Angle   = 0.0
Wing_Sweep_Angle      = 0.0

!Horizontal Tail Wing
H_Wing_Profile         = 0010
H_Angle_of_Attack      = AoA !0.0
H_Dihedral_Angle      = 0.0
H_Sweep_Angle         = 0.0
!Vertical Tail Wing
V_Wing_Profile         = 0010
V_Angle_of_Attack      = 0.0
V_Dihedral_Angle      = 0.0
V_Sweep_Angle         = 0.0

!Write Design variable data to file

!Nose Design Variables
Write(301,*)          'Nose_Length_PlaneLength_Ratio: ',
Nose_Length_PlaneLength_Ratio
Write(301,*)          'Nose_EndHeight_PlaneLength_Ratio: ',
Nose_EndHeight_PlaneLength_Ratio
Write(301,*)          'Nose_EndWidth_PlaneLength_Ratio: ',
Nose_EndWidth_PlaneLength_Ratio           ! Compare with
Nose_EndHeight_PlaneLength_Ratio

!NoseCabin Interface Design Variables
Write(301,*)          'NoseCabinLength_PlaneLength_Ratio: ',
NoseCabinLength_PlaneLength_Ratio
Write(301,*)          'NoseCabin_OffsetHeight_Length_Ratio: ',
NoseCabin_OffsetHeight_Length_Ratio
Write(301,*)          'NoseCabin_EndWidth_PlaneLength_Ratio: ',
NoseCabin_EndWidth_PlaneLength_Ratio     !Compare with
Nose_EndWidth_PlaneLength_Ratio

!Cabin Design Variables

```

```

        Write(301,*)      'CabinLength_PlaneLength_Ratio: ',
CabinLength_PlaneLength_Ratio

!Luggage Cabin Design Variables
        Write(301,*)      'LuggageCabinLength_PlaneLength_Ratio: ',
LuggageCabinLength_PlaneLength_Ratio
        Write(301,*)
        'LuggageCabinEndDiameter_PlaneLength_Ratio: ',
LuggageCabinEndDiameter_PlaneLength_Ratio

!Tail Design Variables
        Write(301,*)      'TailEndDiameter_PlaneLength_Ratio: ',
TailEndDiameter_PlaneLength_Ratio

!Horizontal Tail wing Design Variables
        Write(301,*)      'H_Root_Chord_PlaneLength_Ratio: ',
H_Root_Chord_PlaneLength_Ratio
        Write(301,*)      'H_Tip_To_RootChord_Ratio: ',
H_Tip_To_RootChord_Ratio
        Write(301,*)      'H_Span_To_PlaneLength_Ratio: ',
H_Span_To_PlaneLength_Ratio

!Vertical Tail wing Design Variables
        Write(301,*)      'V_Root_Chord_PlaneLength_Ratio: ',
V_Root_Chord_PlaneLength_Ratio
        Write(301,*)      'V_Tip_To_RootChord_Ratio: ',
V_Tip_To_RootChord_Ratio
        Write(301,*)      'V_Span_To_PlaneLength_Ratio: ',
V_Span_To_PlaneLength_Ratio

!Wing Design Variables
        Write(301,*)      'WingRoot_Chord_PlaneLength_Ratio: ',
WingRoot_Chord_PlaneLength_Ratio
        Write(301,*)      'WingTip_To_RootChord_Ratio: ',
WingTip_To_RootChord_Ratio
        Write(301,*)      'WingSpan_To_PlaneLength_Ratio: ',
WingSpan_To_PlaneLength_Ratio

        Write(*,*)      'Wing Angle of Attack = ',
Wing_Angle_of_Attack
        Write(301,*)      'Wing Angle of Attack = ',
Wing_Angle_of_Attack
        Write(*,*)      'Fuselage Angle of Attack = ',
Fuselage_AoA
        Write(301,*)      'Fuselage Angle of Attack = ',
Fuselage_AoA
        Write(*,*)      'Wing Profile = NACA', Wing_Profile
        Write(301,*)      'Wing Profile = NACA',Wing_Profile
        Write(301,*)      'Mach number: ',Mach_Number
        Write(301,*)      'Flight Velocity:
',AerodynamicDesignPointData%Flight_speed
        Write(301,*)      'Flight Altitude: ',Flight_Altitude

!NOSE
!Use Default FixedParameters Always (ie the Default Values, One
can change this if needed)

```

```

    Nose_DesignParameter = Create_Nose_DesignParameter_Type(
        & Nose_Length_PlaneLength_Ratio,
        Nose_EndHeight_PlaneLength_Ratio,
Nose_EndWidth_PlaneLength_Ratio)

    Nose_FixedParameter = Create_Nose_FixedParameter_Type()
    Nose_Input = Create_Nose_Inputs_Type
(Nose_DesignParameter, Nose_FixedParameter)
    Call Create_Nose(Plane_Length, Nose_Input, Nose_Output)

    Nose_SurfaceData = Nose_Output%SurfaceData

!    Nose_Points = Nose_Output%Nose_SurfaceData%Nose_SurfaceData
!    NoseEnd_Points =
Nose_Output%Nose_SurfaceData%Nose_Surface_EndData
!Stop
! NOSE_CABIN INTERFACE
!Use Default FixedParameters Always (ie the Default Values, One
can change this if needed)
    NoseCabin_DesignParameter =
Create_NoseCabin_Interface_DesignParameter_Type( &
        NoseCabinLength_PlaneLength_Ratio, &
        NoseCabin_OffsetHeight_Length_Ratio, &
        NoseCabin_EndWidth_PlaneLength_Ratio)

    NoseCabin_FixedParameter =
Create_NoseCabin_Interface_FixedParameter_Type(N,
Nose_SurfaceData)

    NoseCabin_Input =
Create_NoseCabin_Interface_Inputs_Type( &
        NoseCabin_DesignParameter, NoseCabin_FixedParameter)

    Call Create_NoseCabin_Interface(Plane_Length,
NoseCabin_Input, NoseCabin_Output)
!STOP

    NoseCabin_SurfaceData = NoseCabin_Output%SurfaceData
!    NoseCabin_Points = NoseCabin_Output%SurfaceData%SurfaceData
!    NoseCabinEnd_Points =
NoseCabin_Output%SurfaceData%Surface_EndData

!CABIN
!Use Default FixedParameters Always (ie the Default Values, One
can change this if needed)
    Cabin_DesignParameter =
Create_Cabin_DesignParameter_Type(CabinLength_PlaneLength_Ratio)
    Cabin_FixedParameter =
Create_Cabin_FixedParameter_Type(N, NoseCabin_SurfaceData)
    Cabin_Input = Create_Cabin_Inputs_Type( &
        Cabin_DesignParameter,
Cabin_FixedParameter)

    Call Create_Cabin(Plane_Length, Cabin_Input, Cabin_Output)
!Stop
    Cabin_SurfaceData = Cabin_Output%SurfaceData
!    CabinEnd_Points = Cabin_Output%SurfaceData%Surface_EndData

```

```

!Luggage_Cab
!Use Default FixedParameters Always (ie the Default Values, One
can change this if needed)
    LuggageCabin_DesignParameter =
Create_Luggage_Cab_DesignParameter_Type(&
    LuggageCabinLength_PlaneLength_Ratio,    &
    LuggageCabinEndDiameter_PlaneLength_Ratio)

    LuggageCabin_FixedParameter =
Create_Luggage_Cab_FixedParameter_Type(N, Cabin_SurfaceData)

    LuggageCabin_Input =
Create_Luggage_Cab_Inputs_Type(    &
    LuggageCabin_DesignParameter, LuggageCabin_FixedParameter)

    Call Create_Luggage_Cabin(Plane_Length, LuggageCabin_Input,
LuggageCabin_Output)

    LuggageCabin_SurfaceData =
LuggageCabin_Output%SurfaceData
!    Luggage_CabEnd_Points =
LuggageCabin_Output%SurfaceData%Surface_EndData
!Stop

!Tail
!Use Default FixedParameters Always (ie the Default Values, One
can change this if needed)
    Tail_DesignParameter =
Create_Tail_DesignParameter_Type(TailEndDiameter_PlaneLength_Rati
o)
    Tail_FixedParameter =
Create_Tail_FixedParameter_Type(N, LuggageCabin_SurfaceData)

    Tail_Input = Create_Tail_Inputs_Type(    &
    Tail_DesignParameter, Tail_FixedParameter)

    Call Create_Tail(Plane_Length, Tail_Input, Tail_Output)

    Tail_SurfaceData = Tail_Output%SurfaceData
!Stop
!WING
!Vertical location of the wing
!Z_loc =
NoseCabin_Output%SurfaceData%LowR_SurfaceData(N,N)%Z_Coordinate
!Low wing
Z_loc =
NoseCabin_Output%SurfaceData%UpR_SurfaceData(1,1)%Z_Coordinate
!Mid wing
!Z_loc =
NoseCabin_Output%SurfaceData%UpR_SurfaceData(N,N)%Z_Coordinate
!High wing

    Wing_Location = Create_Point_Type(0.30*Plane_Length, 0.0,
Z_loc) !The x component will be equal to the Center of gravity
of the

```

! fulage plus tail wings

```

Wing_DesignParameter = Create_Wing_DesignParameter_Type(
    WingRoot_Chord_PlaneLength_Ratio,
    WingTip_To_RootChord_Ratio, &
    WingSpan_To_PlaneLength_Ratio)

Wing_FixedParameter =
Create_Wing_FixedParameter_Type(Wing_Profile, N, &
    Wing_Angle_of_Attack, Wing_Dihedral_Angle,
    Wing_Sweep_Angle, &
    Wing_Location)

Wing_Input = Create_Wing_Inputs_Type(Wing_DesignParameter,
Wing_FixedParameter)

Call Create_Wing(Plane_Length, Wing_Input,
AerodynamicDesignPointData, Wing_Output, Wing_Surface_Property)

!      Wing_Points =
Wing_Output%Wing_SurfaceData%Wing_SurfaceData

!stop
!HORIZONTAL TAIL WING
!Use Default FixedParameters Always (ie the Default Values,
One can change this if needed)
H_Wing_DesignParameter =
Create_Horizontal_TailWing_DesignParameter_Type( &
    H_Root_Chord_PlaneLength_Ratio, H_Tip_To_RootChord_Ratio,
    &
    H_Span_To_PlaneLength_Ratio)

H_Wing_FixedParameter =
Create_Horizontal_TailWing_FixedParameter_Type(H_Wing_Profile,N,
    &
    H_Angle_of_Attack, H_Dihedral_Angle, H_Sweep_Angle,
    H_Wing_Location)

H_Wing_Input =
Create_Horizontal_TailWing_Inputs_Type(H_Wing_DesignParameter, &
    H_Wing_FixedParameter)

Call Create_Horizontal_TailWing(Plane_Length, H_Wing_Input,
Wing_Surface_Property, H_Wing_Output)

!      H_Wing_Points =
H_Wing_Output%Tail_Wing_SurfaceData%Upper_Right_SurfaceData
!Stop
!VERTICAL TAIL WING
!Use Default FixedParameters Always (ie the Default Values,
One can change this if needed)
V_Wing_DesignParameter =
Create_Vertical_TailWing_DesignParameter_Type( &
    V_Root_Chord_PlaneLength_Ratio, V_Tip_To_RootChord_Ratio,
    &
    V_Span_To_PlaneLength_Ratio)

```

```

V_Wing_FixedParameter =
Create_Vertical_TailWing_FixedParameter_Type(V_Wing_Profile, N,
&
V_Angle_of_Attack, V_Dihedral_Angle, V_Sweep_Angle,
V_Wing_Location)

V_Wing_Input =
Create_Vertical_TailWing_Inputs_Type(V_Wing_DesignParameter, &
V_Wing_FixedParameter)

Call Create_Vertical_TailWing(Plane_Length, V_Wing_Input,
Wing_Surface_Property, V_Wing_Output)

! V_Wing_Points =
V_Wing_Output%Tail_Wing_SurfaceData%Upper_Right_SurfaceData

!Stop

Aircraft_Input =
Create_Aircraft_Input_Type(AerodynamicDesignPoint,
Wing_Input, H_Wing_Input, V_Wing_Input, &
Nose_Input, NoseCabin_Input, Cabin_Input, &
LuggageCabin_Input, Tail_Input)

! Aircraft_Output = Create_Aircraft_Output_Type(Wing_Output,
H_Wing_Output, V_Wing_Output, &
!
Nose_Output, NoseCabin_Output, Cabin_Output, &
!
LuggageCabin_Output, Tail_Output)
!print *, Aircraft_Input, 'Aircraft_Input'
!print *, Aircraft_Output, 'Aircraft_Output'
!Develop the fuselage profile

!Enddo

! Call Create_Fuselage_Performance(N, Nose_SurfaceData,
NoseCabin_SurfaceData, &
!
Cabin_SurfaceData, LuggageCabin_SurfaceData, &
!
Tail_SurfaceData, AerodynamicDesignPointData, &
!
Fuselage_AoA, Fuselage_Lift , Fuselage_Drag )

Wing_Lift = Wing_Output%PerformanceParameters%Lift
Wing_Drag = Wing_Output%PerformanceParameters%Drag

H_TailWing_Lift = H_Wing_Output%PerformanceParameters%Lift
H_TailWing_Drag = H_Wing_Output%PerformanceParameters%Drag

V_TailWing_Lift =
V_Wing_Output%Tail_Wing_PerformanceParameters%Lift
V_TailWing_Drag =
V_Wing_Output%Tail_Wing_PerformanceParameters%Drag

```

```
Plane_Lift = Fuselage_Lift + Wing_Lift + H_TailWing_Lift +  
V_TailWing_Lift  
Plane_Drag = Fuselage_Drag + Wing_Drag + H_TailWing_Drag +  
V_TailWing_Drag  
  
Write(*,*)Plane_Lift, 'Plane_Lift'  
Write(*,*)Plane_Drag, 'Plane_Drag'  
  
Write(301,*) 'Total(Aircraft)', Plane_Lift, Plane_Drag  
  
Enddo  
  
END PROGRAM Aircraft_Design
```

KNUST



Appendix B: Sample Results

Table A.1 Specification to Sample Design

Mach number	0.200
Flight Velocity (m/s)	66.649
Flight Altitude (Km)	2.000

Table A.2 Sample #1 - #5 Design Parameters

Parameter	#1	#2	#3	#4	#5
Nose Length to Plane Length Ratio	0.100	0.100	0.100	0.100	0.100
Nose End Height to Plane Length Ratio	0.100	0.100	0.100	0.150	0.120
Nose End Width to Plane Length Ratio	0.120	0.120	0.100	0.150	0.130
Nose-Cabin inter Length to Plane Length Ratio	0.100	0.100	0.100	0.100	0.150
Nose-Cabin inter Offset Height to Length Ratio	0.030	0.010	0.000	0.000	0.060
Nose-Cabin End Width to Plane Length Ratio	0.140	0.140	0.100	0.150	0.150
Cabin Length to Plane Length Ratio	0.250	0.250	0.250	0.400	0.300
Luggage Cabin Length to Plane Length Ratio	0.300	0.200	0.200	0.200	0.100
Luggage Cabin End Diameter Plane Length Ratio	0.060	0.020	0.060	0.150	0.050
Tail boom End Diameter to Plane Length Ratio	0.010	0.010	0.010	0.010	0.010
Horizontal tail Root Chord to Plane Length Ratio	0.100	0.100	0.100	0.100	0.100
Horizontal tail Tip to Root Chord Ratio	0.500	0.500	0.500	0.500	0.500
Horizontal tail Span to Plane Length Ratio	0.200	0.200	0.200	0.200	0.300
Vertical tail Root Chord to Plane Length Ratio	0.100	0.100	0.100	0.100	0.100
Vertical Tip to Root Chord Ratio	0.500	0.500	0.500	0.500	0.500
Vertical Span to Plane Length Ratio	0.100	0.100	0.100	0.100	0.100
Wing Root Chord to Plane Length Ratio	0.200	0.300	0.300	0.300	0.300
Wing Tip To Root Chord Ratio	0.500	0.700	1.000	0.300	0.300
Wing Span To Plane Length Ratio	1.500	1.500	1.500	1.500	1.500
Wing Profile	NACA 1412	NACA 2412	NACA 2424	NACA 2410	NACA 2410

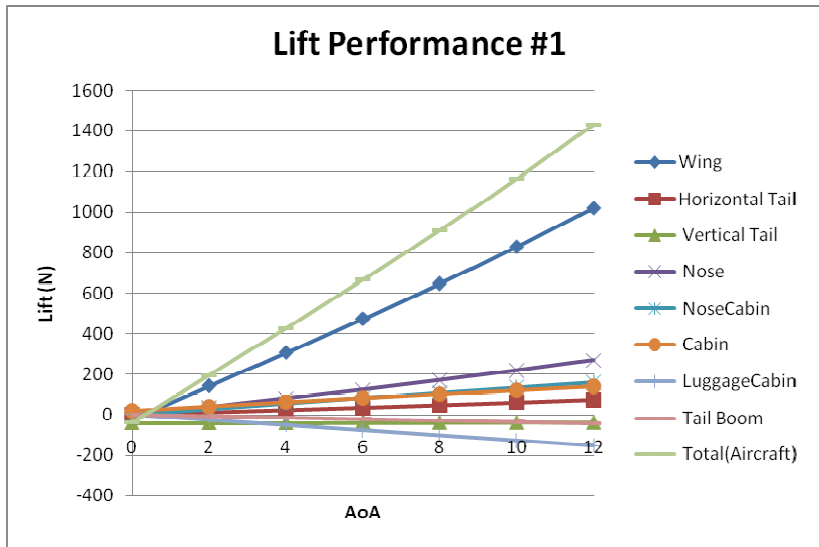


Figure A.1 Object Lift Performance for Sample #1

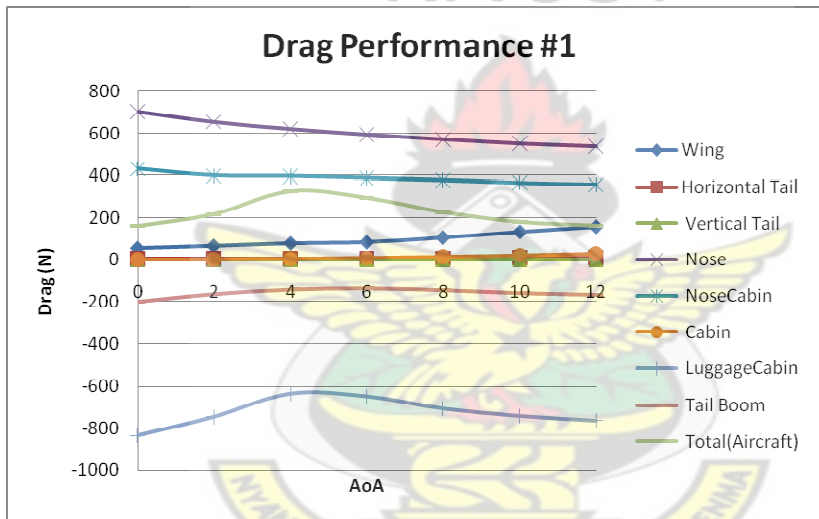


Figure A.2 Object Drag Performance for Sample #1

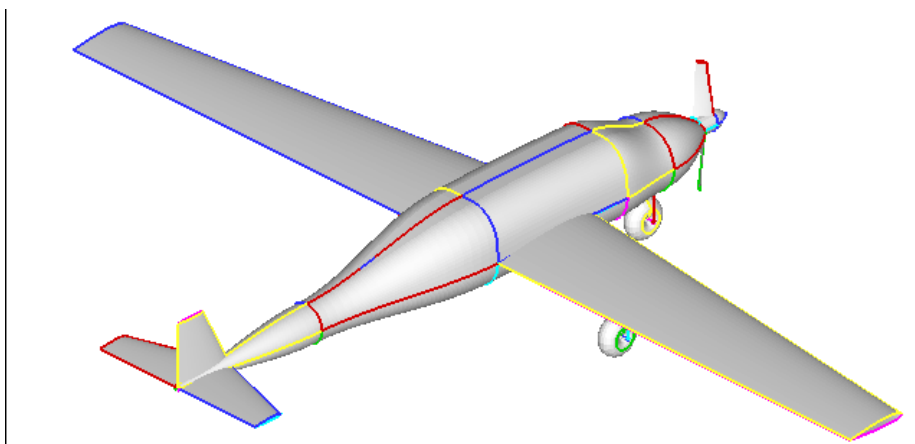


Figure A.3 Sample #1 Configuration

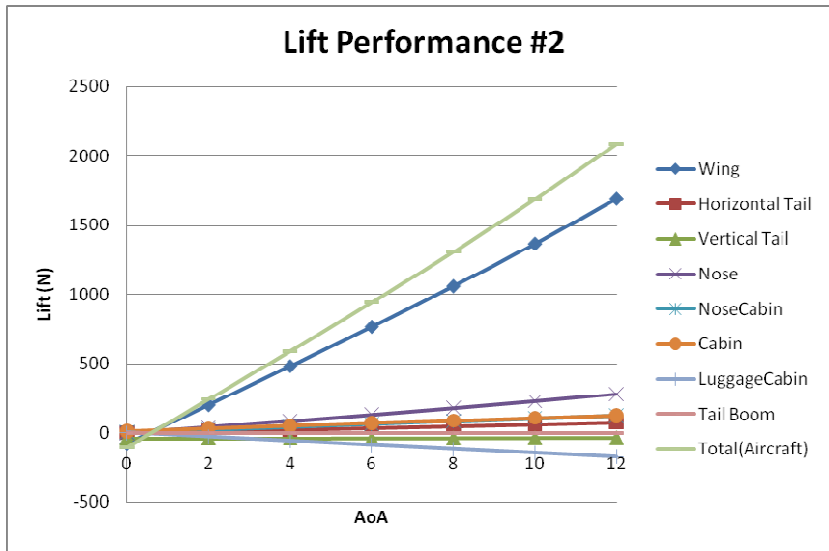


Figure A.4 Object Lift Performance for Sample #2

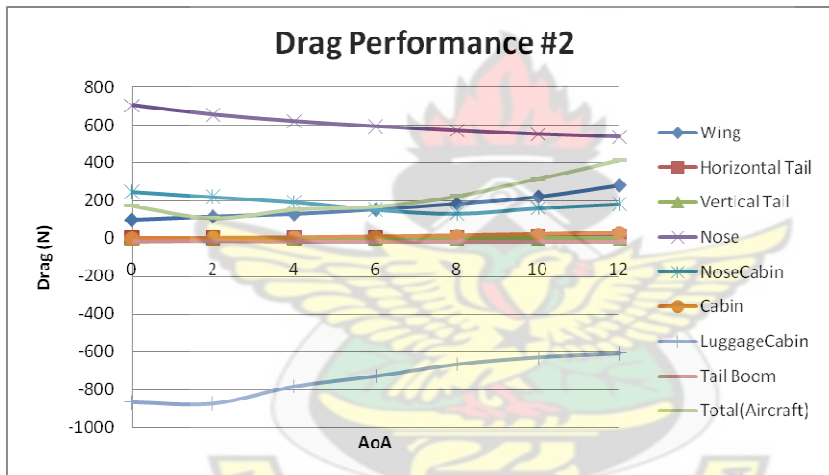


Figure A.5 Object Drag Performance for Sample #2

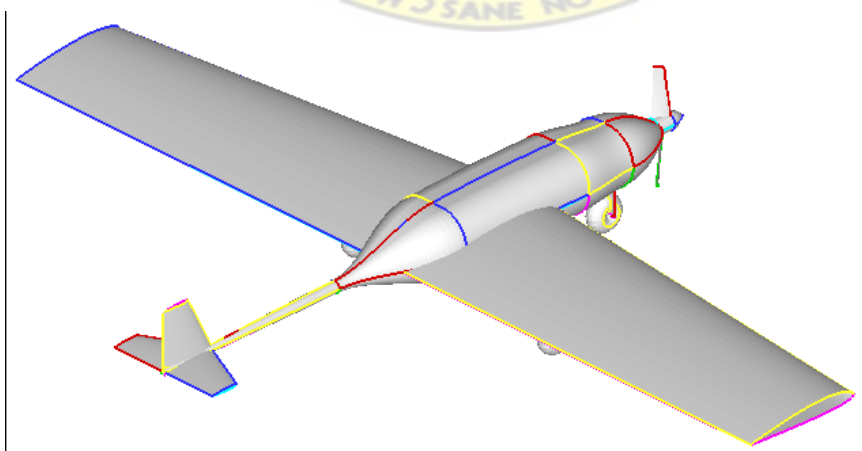


Figure A.6 Sample #2 Configuration

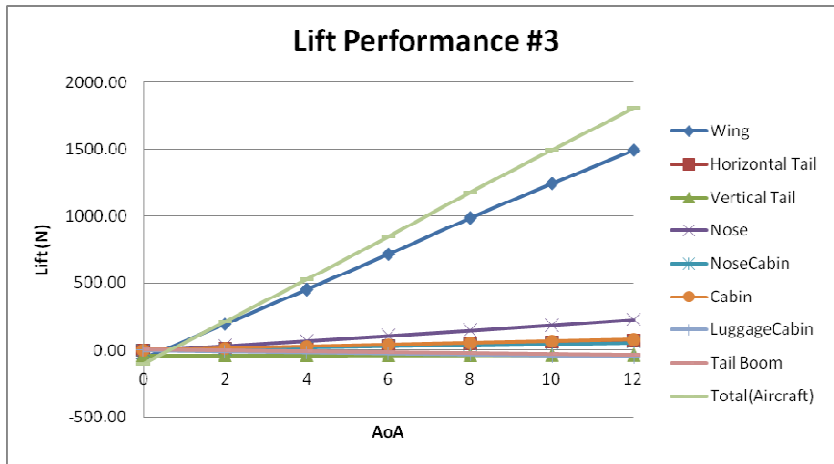


Figure A.7 Object Lift Performance for Sample #3

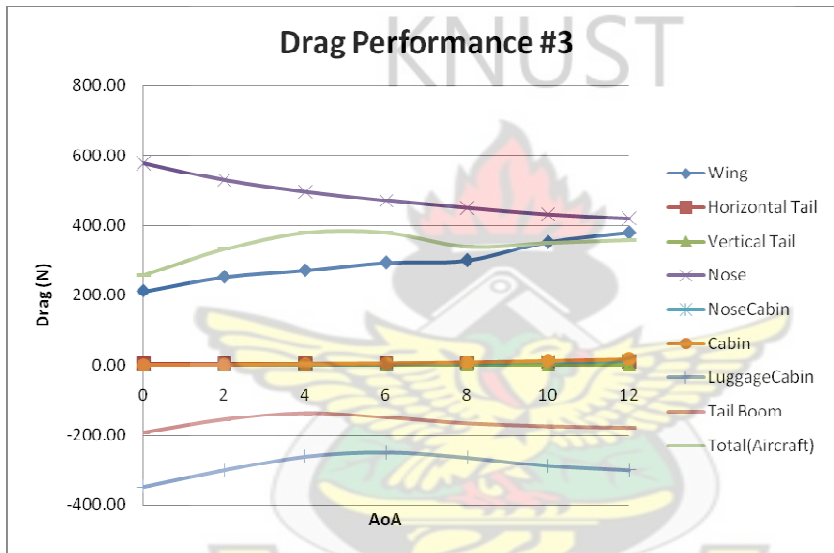


Figure A.8 Object Drag Performance for Sample #3

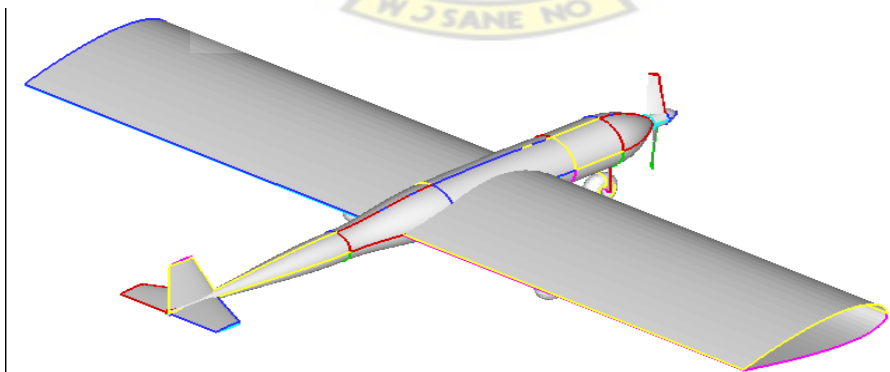


Figure A.9 Sample #3 Configuration

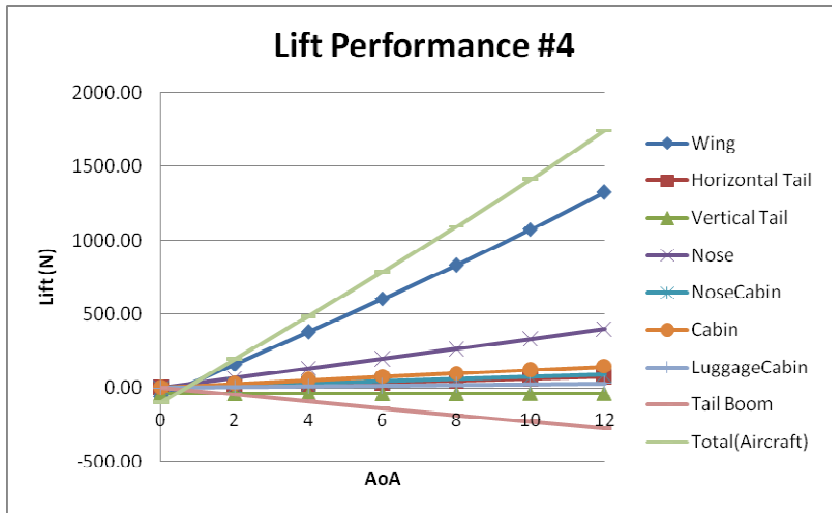


Figure A.10 Object Lift Performance for Sample #4

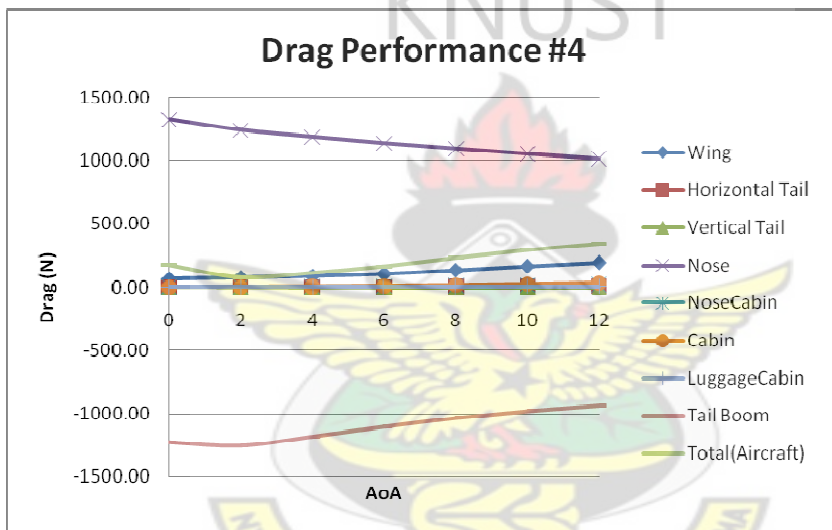


Figure A.11 Object Drag Performance for Sample #4

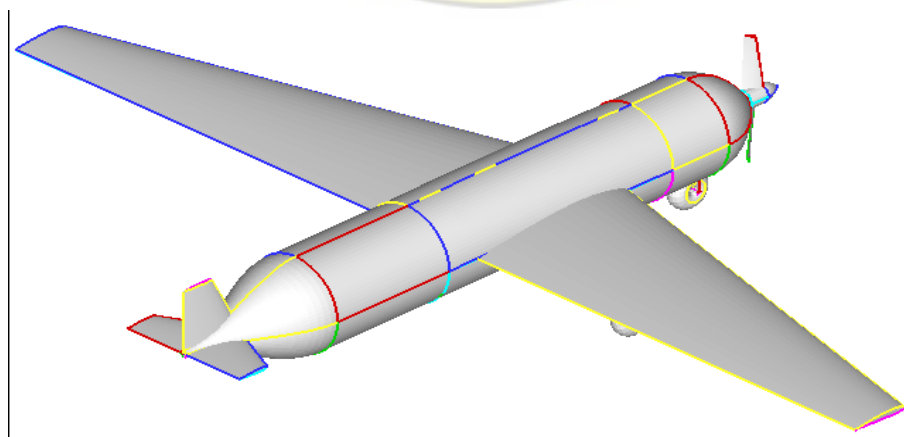


Figure A.12 Sample #4 Configuration

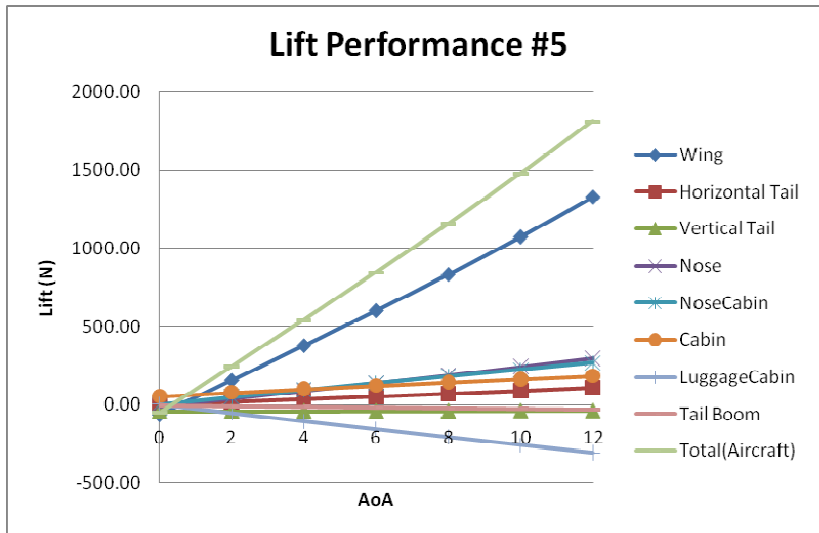


Figure A.13 Object Lift Performance for Sample #5

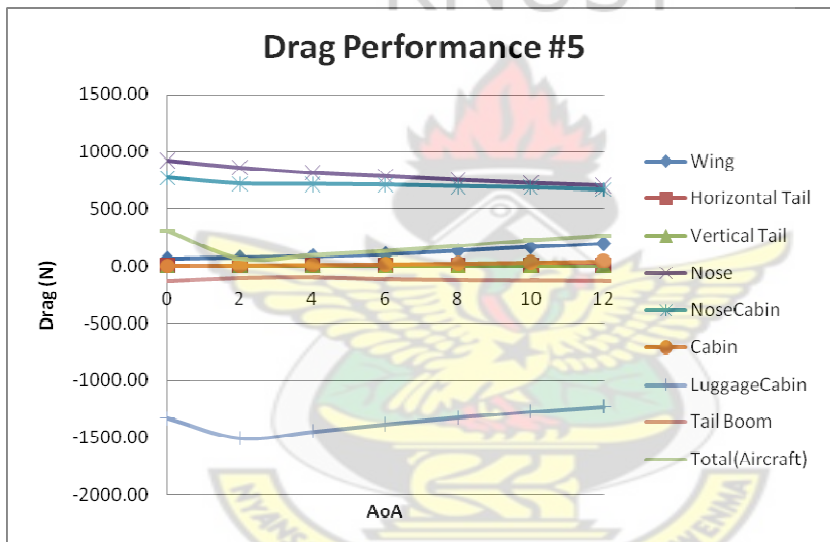


Figure A.14 Object Drag Performance for Sample #5

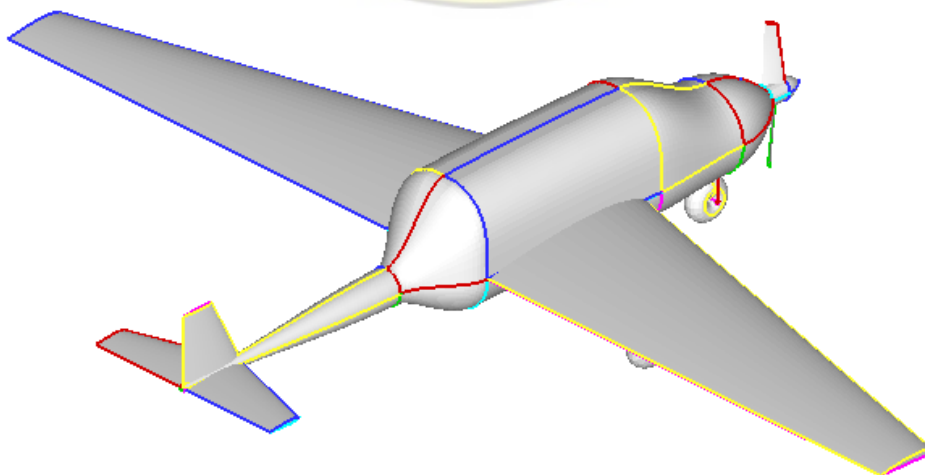


Figure A.15 Sample #5 Configuration

Performance with same wing

Table A.3 Sample #6 - #10 Design Parameters

Parameters	#6	#7	#8	#9	#10
Nose Length to Plane Length Ratio	0.100	0.100	0.100	0.100	0.100
Nose End Height to Plane Length Ratio	0.100	0.100	0.100	0.150	0.120
Nose End Width to Plane Length Ratio	0.120	0.120	0.100	0.150	0.130
Nose-Cabin inter Length to Plane Length Ratio	0.100	0.100	0.100	0.100	0.150
Nose-Cabin inter Offset Height to Length Ratio	0.030	0.010	0.000	0.000	0.060
Nose-Cabin End Width to Plane Length Ratio	0.140	0.140	0.100	0.150	0.150
Cabin Length to Plane Length Ratio	0.250	0.250	0.250	0.400	0.300
Luggage Cabin Length to Plane Length Ratio	0.300	0.200	0.200	0.200	0.100
Luggage Cabin End Diameter Plane Length Ratio	0.060	0.020	0.060	0.150	0.050
Tail boom End Diameter to Plane Length Ratio	0.010	0.010	0.010	0.010	0.010
Horizontal tail Root Chord to Plane Length Ratio	0.100	0.100	0.100	0.100	0.100
Horizontal tail Tip to Root Chord Ratio	0.500	0.500	0.500	0.500	0.500
Horizontal tail Span to Plane Length Ratio	0.200	0.200	0.200	0.200	0.200
Vertical tail Root Chord to Plane Length Ratio	0.100	0.100	0.100	0.100	0.100
Vertical Tip to Root Chord Ratio	0.500	0.500	0.500	0.500	0.500
Vertical Span to Plane Length Ratio	0.100	0.100	0.100	0.100	0.100
Wing Root Chord to Plane Length Ratio	0.200	0.200	0.200	0.200	0.200
Wing Tip To Root Chord Ratio	0.500	0.500	0.500	0.500	0.500
Wing Span To Plane Length Ratio	1.500	1.500	1.500	1.500	1.500
Wing Profile	NACA 1412	NACA 1412	NACA 1412	NACA 1412	NACA 1412

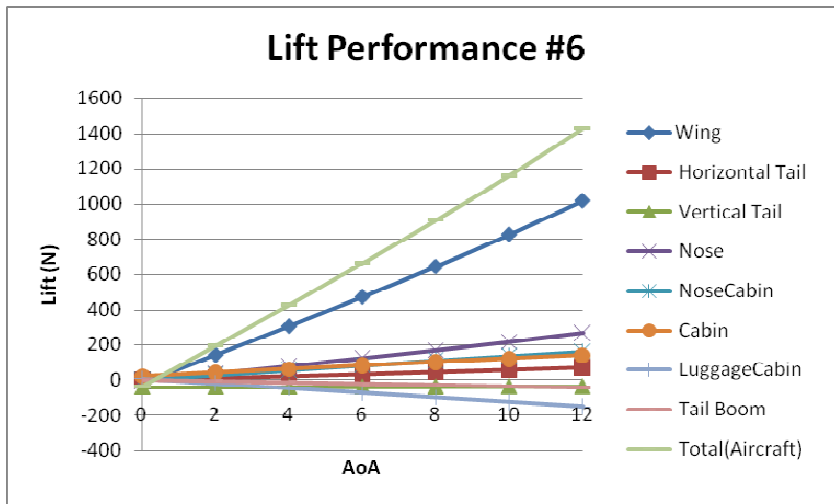


Figure A.16 Object Lift Performance for Sample #6

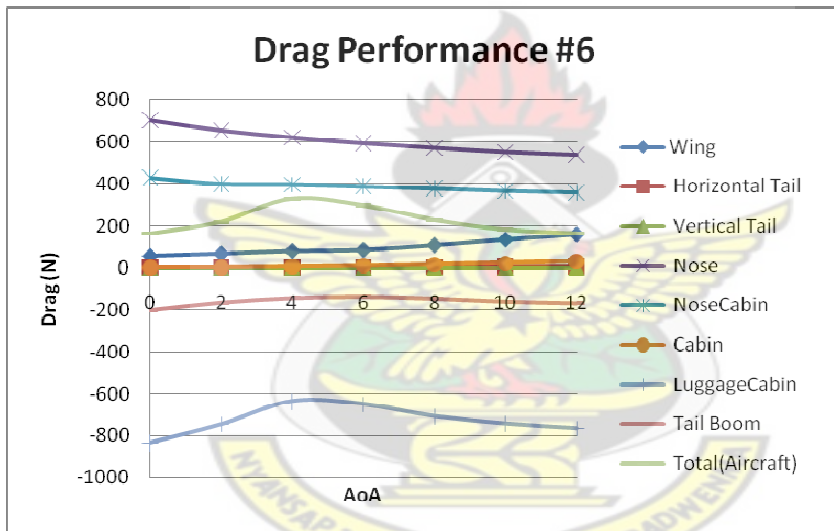


Figure A.17 Object Drag Performance for Sample #6

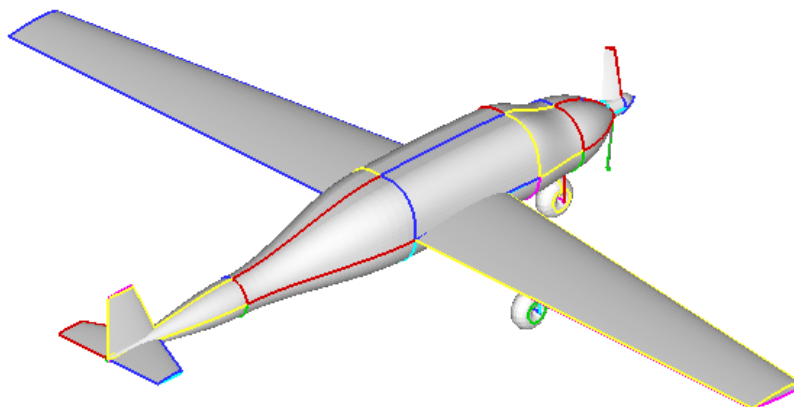


Figure A.18 Sample #6 Configuration

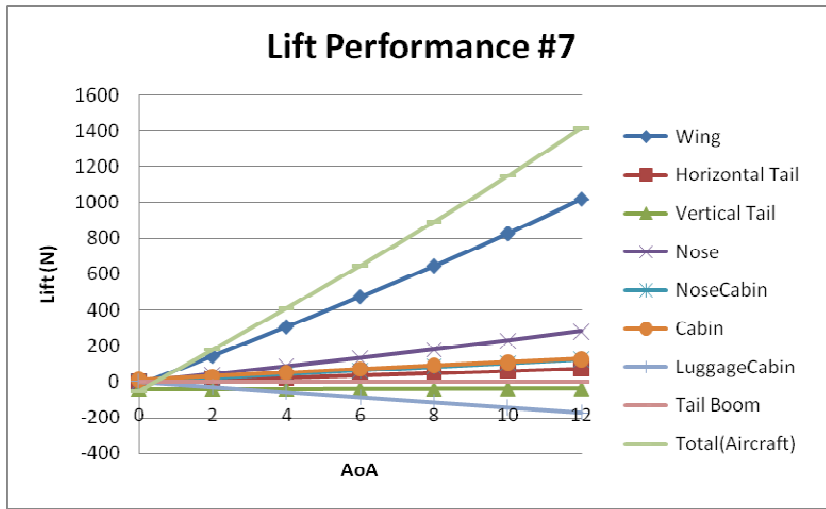


Figure A.19 Object Lift Performance for Sample #7

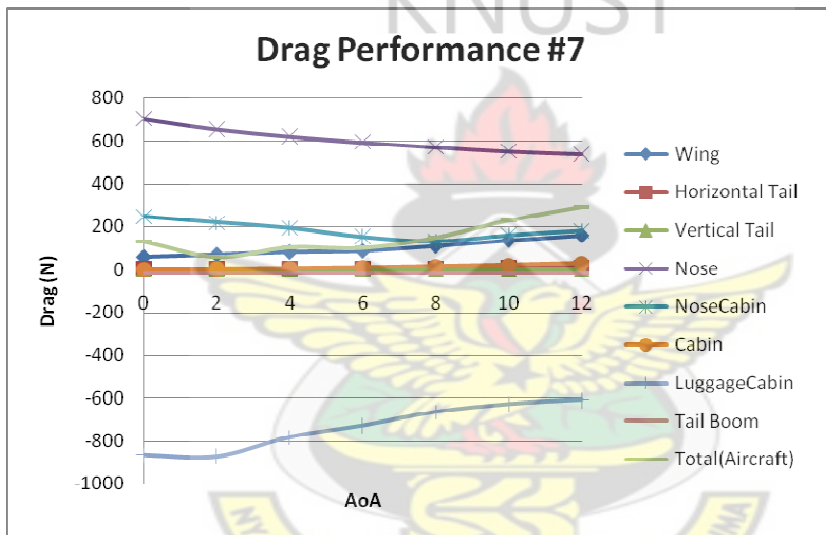


Figure A.20 Object Drag Performance for Sample #7

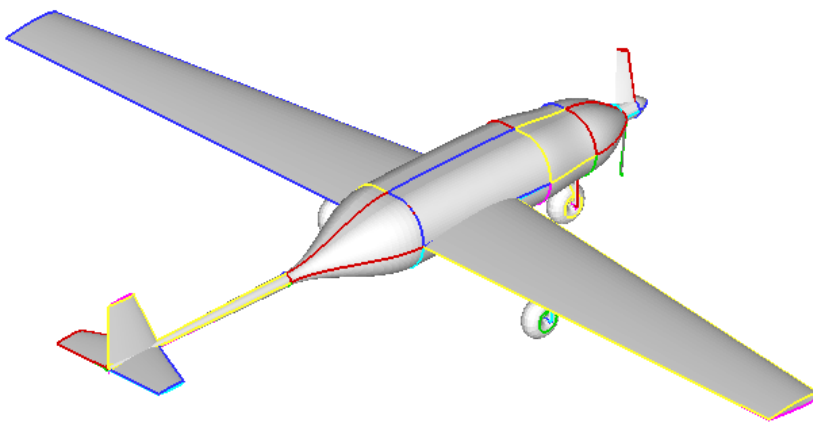


Figure A.21 Sample #7 Configuration

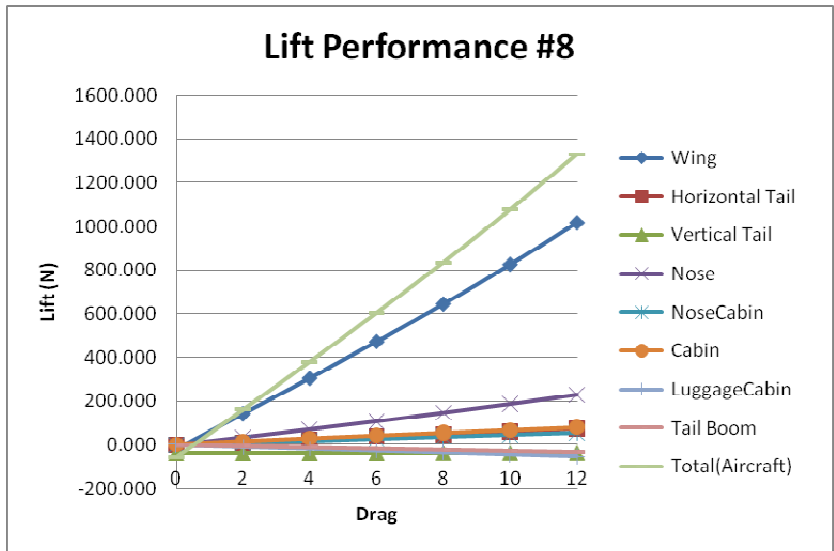


Figure A.22 Object Lift Performance for Sample #8

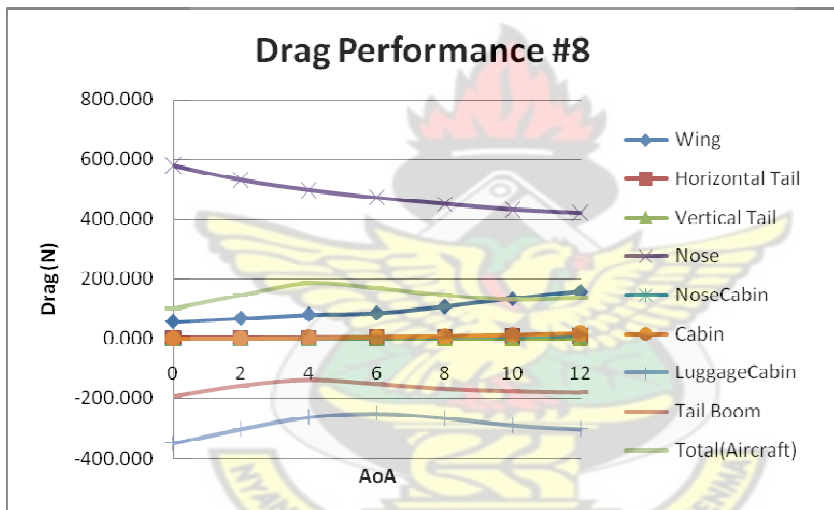


Figure A.23 Object Drag Performance for Sample #8

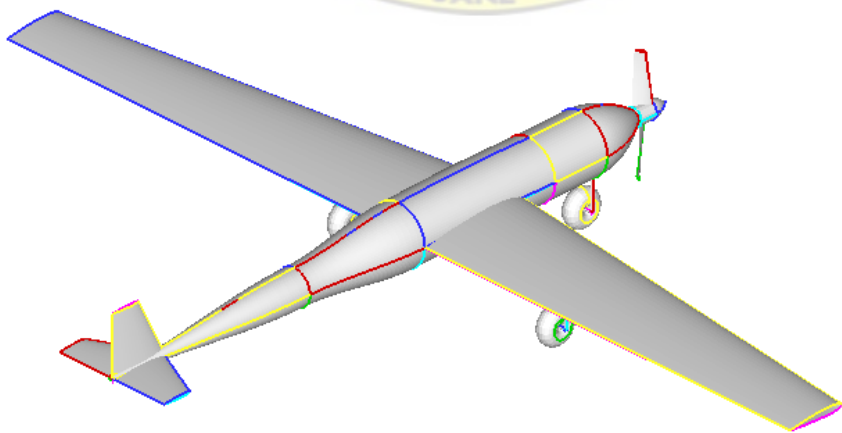


Figure A.24 Sample #8 Configuration

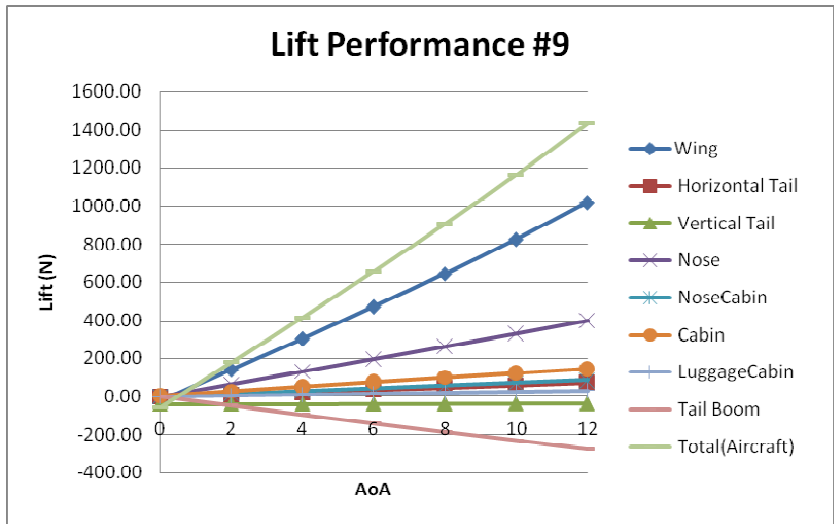


Figure A.25 Object Lift Performance for Sample #9

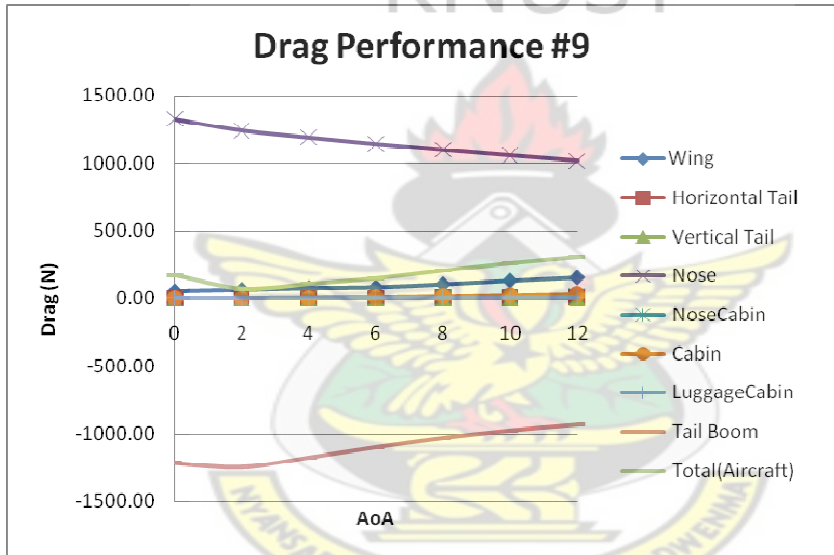


Figure A.26 Object Drag Performance for Sample #9

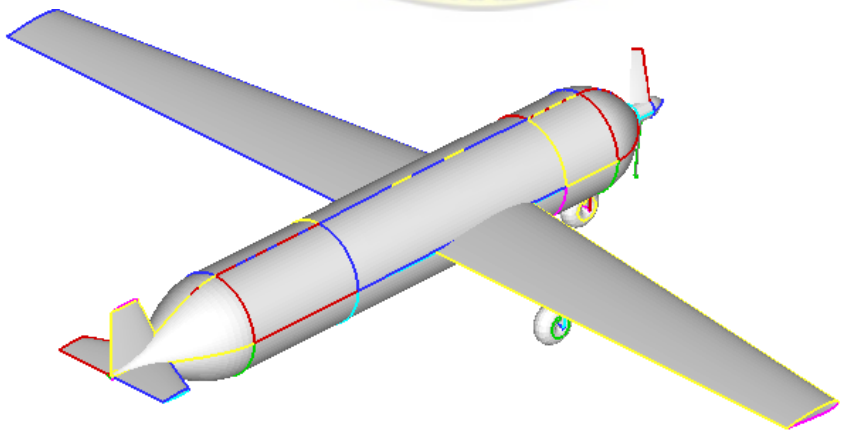


Figure A.27 Sample #9 Configuration

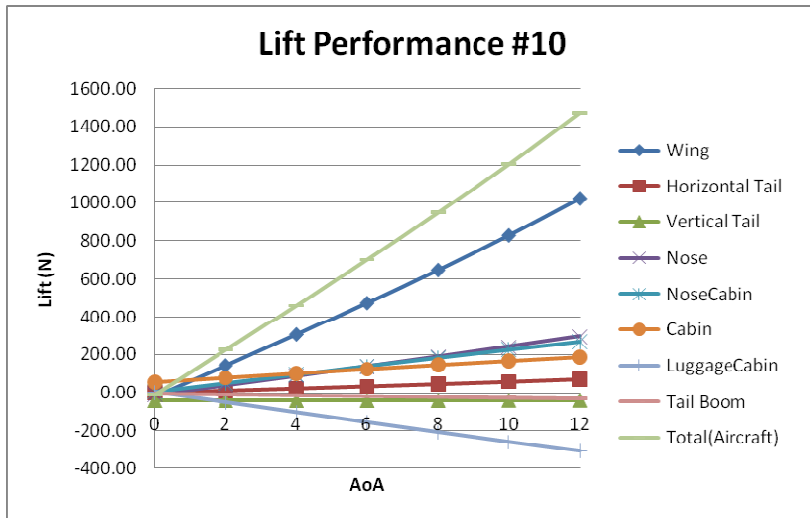


Figure A.28 Object Lift Performance for Sample #10

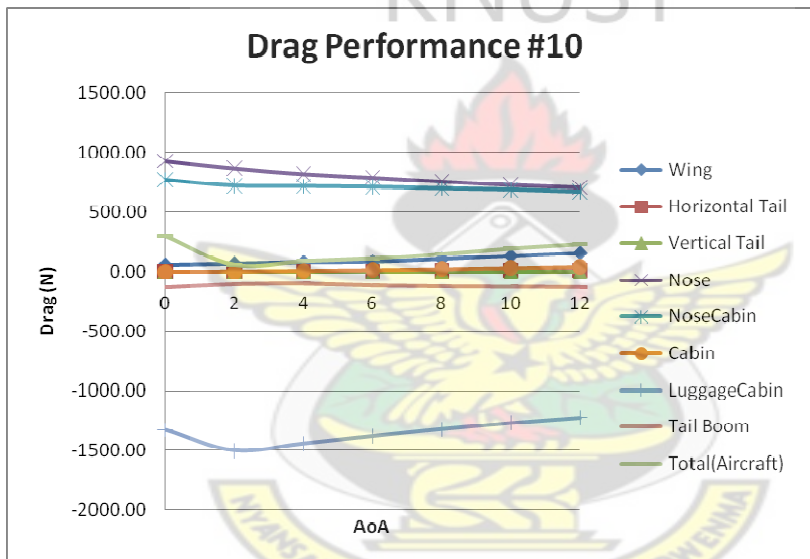


Figure A.29 Object Drag Performance for Sample #10

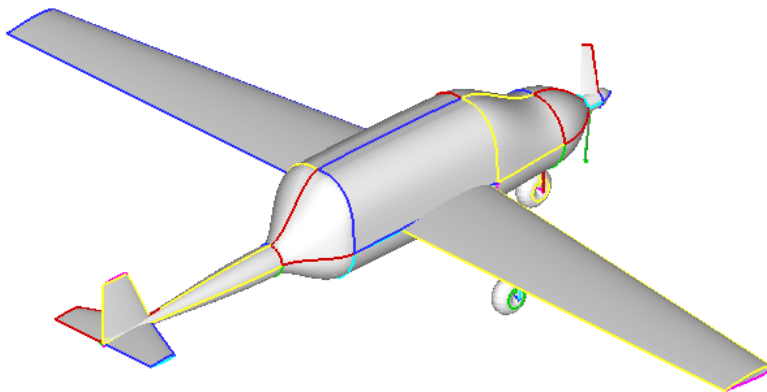


Figure A.30 Sample #10 Configuration